

Design of a Floating Foundation for an HVAC Offshore Substation

Auteur : Jorge Alcantara, Felipe

Promoteur(s) : Rigo, Philippe

Faculté : Faculté des Sciences appliquées

Diplôme : Master : ingénieur civil mécanicien, à finalité spécialisée en "Advanced Ship Design"

Année académique : 2022-2023

URI/URL : <http://hdl.handle.net/2268.2/19338>

Avertissement à l'attention des usagers :

Tous les documents placés en accès ouvert sur le site le site MatheO sont protégés par le droit d'auteur. Conformément aux principes énoncés par la "Budapest Open Access Initiative"(BOAI, 2002), l'utilisateur du site peut lire, télécharger, copier, transmettre, imprimer, chercher ou faire un lien vers le texte intégral de ces documents, les disséquer pour les indexer, s'en servir de données pour un logiciel, ou s'en servir à toute autre fin légale (ou prévue par la réglementation relative au droit d'auteur). Toute utilisation du document à des fins commerciales est strictement interdite.

Par ailleurs, l'utilisateur s'engage à respecter les droits moraux de l'auteur, principalement le droit à l'intégrité de l'oeuvre et le droit de paternité et ce dans toute utilisation que l'utilisateur entreprend. Ainsi, à titre d'exemple, lorsqu'il reproduira un document par extrait ou dans son intégralité, l'utilisateur citera de manière complète les sources telles que mentionnées ci-dessus. Toute utilisation non explicitement autorisée ci-avant (telle que par exemple, la modification du document ou son résumé) nécessite l'autorisation préalable et expresse des auteurs ou de leurs ayants droit.



POLITÉCNICA



Universität
Rostock



Traditio et Innovatio



SOLENT
UNIVERSITY
SOUTHAMPTON



Zachodniopomorski
Uniwersytet
Techniczny
w Szczecinie



With the support of the
Erasmus+ Programme
of the European Union



Design of a Floating Foundation for an HVAC Offshore Substation

submitted on 27 August, 2023

by

JORGE ALCANTARA Felipe | Alonso Heredia 21 | Madrid | felipe.jalcantara@alumnos.upm.es

Student ID No.: s212996

First Reviewer:

Professor, Sascha, Kosleck
Chair of Ocean Engineering at the Uni-
versity of Rostock
Universitätsplatz 1
18055 Rostock
Germany

Second Reviewer:

Antonio, Medina-Manuel
Postgraduate researcher at CEHINAV
Avenida de la Memoria, 4
28040 Madrid
Spain



[This page is intentionally left blank]

Contents

List of Figures	iv
List of Tables	viii
1 INTRODUCTION	1
1.1 Background And Motivation	3
2 HVAC vs HVDC	5
3 WIND FARM	7
3.1 Metocean	7
3.2 Substation Particulars	7
3.2.1 <i>Layout & Equipment</i>	8
3.2.2 <i>Dimensions & Mass</i>	9
3.3 Limiting Operation Conditions	10
3.4 Electric Cables	11
4 FLOATER DESIGN	12
4.1 Qualitative Choice Of Floating Concept	12
4.2 Analytical Modeling Of Geometry	14
4.3 Structural Mass Estimate	15
4.4 Equilibrium Check	16
4.5 Stability Check	16
4.6 Heave Resonance Check	17
4.7 Structural Design	18
4.8 Geometry Optimization	22
4.9 Interface Between Floater And Topside	23
4.10 Results	23
4.10.1 <i>Geometry</i>	24
4.10.2 <i>Scantling</i>	28
4.10.3 <i>Equilibrium & Stability</i>	37
4.10.4 <i>Motion In Heave</i>	39
5 STABILITY	40
5.1 Load Cases	40
5.1.1 <i>Intact Condition</i>	40
5.1.2 <i>Damaged Condition</i>	42
5.2 Heeling Moments	44
5.3 Criteria	46

5.3.1	<i>Intact Stability</i>	46
5.3.2	<i>Damaged Stability</i>	47
5.4	Results	48
5.4.1	<i>Intact Stability</i>	48
5.4.2	<i>Damaged Stability</i>	50
6	PLATFORM MOTIONS	54
7	MOORNING SYSTEM	60
7.1	Load Cases	61
7.1.1	<i>Ultimate Limit State</i>	61
7.1.2	<i>Fatigue Limit State</i>	63
7.1.3	<i>Accidental Limit State</i>	67
7.2	Mooring Pattern	68
7.3	Line Configuration	69
7.4	Mooring System Design Preliminary	70
7.4.1	<i>Results 8 Lines Configuration</i>	72
7.4.2	<i>Results 12 Lines Configuration</i>	73
7.4.3	<i>Conclusion</i>	74
7.5	Mooring System Design OrcaFlex	74
7.5.1	<i>Results 8 Lines Configuration</i>	76
7.5.2	<i>Results 12 Lines Configuration</i>	81
7.5.3	<i>Conclusion</i>	87
8	POWER CABLES	89
8.1	Cable Configuration	94
8.2	Results	94
9	PLATFORM RESPONSE	100
9.1	Results	100
10	CONCLUSION	102
11	ACKNOWLEDGEMENTS	104
	References	105
A	STABILITY	107
B	FATIGUE LOAD CASES	114
C	MATLAB CODE FOR LC FILE GENERATION	128

List of Figures

1	Emissions per sector (Ritchie and Roser n.d.).	1
2	Modern renewable energy generation by source (Data n.d.).	2
3	Cumulative wind power capacity globally (Ruid n.d.).	2
4	Cumulative wind power capacity globally (Council n.d.).	3
5	Common layout of a fully floating wind farm (DNV n.d.).	4
6	Break-even distances by different authors (Thomas 2022).	5
7	Typical fixed offshore wind farm substation (Rasmussen n.d.).	8
8	Simplified Design Approach.	12
9	Floating concepts for OSS (DNV n.d.).	13
10	Substructure topology review (Ellen Jump et al.).	13
11	Floating substation concepts, left to right: Linxon (Linxon n.d.), Nevesbu (Nevesbu n.d.), WIND2GRID (WIND2GRID n.d.).	14
12	Platform dimensions scheme.	15
13	Pontoon isolation illustration	18
14	Column isolation illustration.	19
15	Columns' bulkheads.	20
16	Pontoons' and nodes' bulkheads.	21
17	From left to right: (A), (B) and (C).	23
18	Platform geometry.	24
19	Cable deck arrangement (dimensions in mm).	25
20	Isometric view of the platform without topside.	26
21	Isometric view of the platform with topside.	26
22	Aft to forward view of the platform with topside.	27
23	Bottom view of the platform with topside.	27
24	Pontoon cross-section (dimensions in mm).	29
25	Column cross-section (dimensions in mm).	30
26	Scantling overview.	31
27	Pontoon and node scantling.	32
28	Pontoon and node stiffeners.	32
29	Pontoon and node bulkheads and frames.	33
30	Column scantling.	33
31	Column stiffeners.	34
32	Column bulkheads and frames.	34
33	Deck scantling.	35
34	Deck scantling (detail).	35
35	Transversal Bracings.	36
36	J-tubes.	36

37	Maxsurf model for stability calculation.	42
38	Vertical extent of damage including normal penetration (DNV 2018).	43
39	Horizontal extent of damage in the tangential direction to the outer hull (DNV 2018).	43
40	Damage 1 (left) & 2 (right).	44
41	Heeling moment.	45
42	Heeling moment comparison.	46
43	Righting and heeling moment curve (DNV 2020).	47
44	GZ curve Intact Operational Load Case.	48
45	GZ curve Intact Transit Load Case.	49
46	GZ curve Damage Case 1 Operational Load Case.	50
47	GZ curve Damage Case 2 Operational Load Case.	51
48	GZ curve Damage Case 1 Transit Load Case.	52
49	GZ curve Damage Case 2 Transit Load Case.	53
50	Hydrodynamic mesh.	54
51	Displacement RAO Surge & Sway 0 Degrees.	55
52	Displacement RAO Roll & Pitch 0 Degrees.	55
53	Displacement RAO Heave & Yaw 0 Degrees.	56
54	Displacement RAO Surge & Sway 45 Degrees.	56
55	Displacement RAO Roll & Pitch 45 Degrees.	56
56	Displacement RAO Heave & Yaw 45 Degrees.	57
57	Load RAO Surge & Sway 0 Degrees.	57
58	Load RAO Roll & Pitch 0 Degrees.	57
59	Load RAO Heave & Yaw 0 Degrees.	58
60	Load RAO Surge & Sway 45 Degrees.	58
61	Load RAO Roll & Pitch 45 Degrees.	58
62	Load RAO Heave & Yaw 45 Degrees.	59
63	Design procedure for mooring lines (KIM 2013).	61
64	Wave scatter diagram.	64
65	Wave scatter diagram modified.	65
66	Wave directions.	65
67	Wind directions and speed.	66
68	Current directions.	66
69	Current directions and speed.	67
70	Single failure illustration 8-line configuration.	67
71	Single failure illustration 12-line configuration.	68
72	Catenary anchor leg and taut-leg fiber rope mooring systems (INNOSEA et al.).	69
73	Mooring system idealisation (Faltinsen 1993).	71

74	Preliminary 8 mooring lines layout Side projection view.	72
75	Preliminary 8 mooring lines mooring layout Top view.	73
76	Preliminary 12 mooring lines mooring layout Side projection view.	73
77	Preliminary 12 mooring lines mooring layout Top view.	74
78	ULS Sea Spectrum.	75
79	ULS condition 8 Lines.	76
80	Platform excursion Global X 0° incidence.	76
81	Platform excursion Global Y 0° incidence.	77
82	Platform excursion Global X 45° incidence.	77
83	Platform excursion Global Y 45° incidence.	77
84	Line effective tension at fairlead 0° incidence ULS.	78
85	Anchor vertical force 0° incidence ULS.	78
86	Line effective tension at fairlead 45° incidence ULS.	79
87	Anchor vertical force 45° incidence ULS.	79
88	ALS condition 8 Lines.	79
89	Line effective tension at fairlead 45° incidence ALS.	80
90	Anchor vertical force 45° incidence ALS.	80
91	Line effective tension at fairlead 45° incidence ALS 600m lines.	81
92	Anchor vertical force 45° incidence ALS 600m lines.	81
93	ULS condition 12 Lines.	81
94	Platform excursion Global X 0° incidence.	82
95	Platform excursion Global Y 0° incidence.	82
96	Platform excursion Global X 45° incidence.	82
97	Platform excursion Global Y 45° incidence.	83
98	Line effective tension at fairlead 0° incidence ULS.	84
99	Anchor vertical force 0° incidence ULS.	84
100	Line effective tension at fairlead 45° incidence ULS.	84
101	Anchor vertical force 45° incidence ULS.	85
102	ALS condition 12 Lines.	85
103	Line effective tension at fairlead 45° incidence ALS.	86
104	Anchor vertical force 45° incidence ALS.	86
105	Total fatigue damage over line length.	87
106	Dynamic cable configurations (free hanging, lazy wave and pliant wave) (COREWIND n.d.).	89
107	Pliant wave configuration in detail (Subsea n.d.).	90
108	275 kV cable capacity curve.	91
109	66 kV cable capacity curve	92
110	Buoyancy modules.	92
111	Bell mouth (left) and bend stiffener (right).	93

112	Pliant wave configuration.	94
113	Export cable configurations at SOL and EOL.	95
114	Inter array cable configurations at SOL and EOL.	95
115	EC static results - SOL	96
116	IAC static results - SOL	96
117	Export cable configurations FAR and NEAR at SOL.	97
118	Inter array cable configurations FAR and NEAR at SOL.	97
119	EC static results - EOL	97
120	IAC static results - EOL	98
121	Export cable configurations FAR and NEAR at EOL.	98
122	Inter array cable configurations FAR and NEAR at EOL.	98
123	Cables under transverse current.	99
124	Overview of cable arrangement.	99
125	Complete OrcaFlex model.	100

List of Tables

1	Wind farm Metocean.	7
2	Substation dimensions.	9
3	Substation modified dimensions.	9
4	Substation mass and centre of gravity.	10
5	Substation mass and modified centre of gravity.	10
6	Acceleration and heel operating limit.	10
7	Steel mass per region.	16
8	Pressures for structural design.	21
9	Main Dimensions.	24
10	Pontoon plate and stiffeners.	28
11	Pontoon frame.	28
12	Pontoon cross-section properties.	28
13	Column plate and stiffeners.	29
14	Column frame.	29
15	Column cross-section properties.	30
16	Cable deck scantling.	30
17	Bracings.	31
18	J-Tubes.	31
19	Steel mass properties.	37
20	Masses and centers of gravity.	37
21	Volumes and center of buoyancy.	38
22	Waterline properties.	38
23	Initial GM calculation.	38
24	Masses and centers of gravity from Rhino.	38
25	Initial GM calculation with Rhino input.	39
26	Added mass in heave.	39
27	Motion in Heave.	39
28	Operational load case.	40
29	Hydrostatics Operational Load Case.	41
30	Transit load case.	41
31	Hydrostatics Transit Load Case.	41
32	Downflooding points.	47
33	Criteria evaluation Operational Load Case.	48
34	Criteria evaluation Transit Load Case.	49
35	Hydrostatics Damage Case 1 Operational Load Case.	50
36	Criteria evaluation Damage Case 1 Operational Load Case.	50
37	Hydrostatics Damage Case 2 Operational Load Case.	51

38	Criteria evaluation Damage Case 2 Operational Load Case.	51
39	Hydrostatics Damage Case 1 Transit Load Case.	52
40	Criteria evaluation Damage Case 1 Transit Load Case.	52
41	Hydrostatics Damage Case 2 Transit Load Case.	53
42	Criteria evaluation Damage Case 2 Transit Load Case.	53
43	Platform inertia.	54
44	Platform radius of gyration.	54
45	Wind load.	62
46	Current load for column-based structures.	62
47	ULS Safety factors.	63
48	Wave directions.	65
49	ALS Safety factors.	68
50	Mooring configuration in current projects (INNOSEA et al.).	70
51	Links tested.	72
52	Feasible 8 Lines Configuration.	72
53	Feasible 12-line configurations.	73
54	Links tested OrcaFlex.	75
55	Utilization factor ULS 8 lines 150mm.	78
56	Utilization factor ULS 12 lines 150mm.	83
57	Fatigue results	87
58	Utilization factor ULS 8 lines x 12 lines.	88
59	Utilization factor ALS 8 lines x 12 lines.	88
60	Mooring details	88
61	Cable properties.	91
62	Buoyancy modules' details.	92
63	Cable configuration.	94
64	Cable clearances.	95
65	Points for acceleration measurement.	100
66	Platform response.	101

[This page is intentionally left blank]

DECLARATION OF AUTHORSHIP

I, **Felipe Jorge Alcantara** declare that this thesis and the work presented in it are my own and have been generated by me as the result of my own original research.

Where I have consulted the published work of others, this is always clearly attributed.

Where I have quoted from the work of others, the source is always given. With the exception of such quotations, this thesis is entirely my own work.

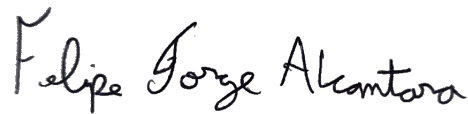
I have acknowledged all main sources of help.

Where the thesis is based on work done by myself jointly with others, I have made clear exactly what was done by others and what I have contributed myself.

This thesis contains no material that has been submitted previously, in whole or in part, for the award of any other academic degree or diploma.

I cede copyright of the thesis in favour of the Polytechnic University of Madrid.

Date: 27 August 2023



Signature:

[This page is intentionally left blank]

ABSTRACT

The offshore energy industry has grown significantly in recent years, specifically the wind energy share. This growth has been happening in areas near shore, due to the reduced complexity of wind farm projects in design, construction, installation, operation & maintenance, and decommissioning. However, the current market trend indicates that wind farms will move further from the coast due to several aspects. These include a current high level of occupation in areas near shore and higher wind resource availability in areas far from the coast.

This change imposes technical challenges such as the swift from fixed to floating foundations due to the increase in water depth. There are already floating wind farms in the experimental and commercial phases. However, these still do not employ floating substations, only floating wind turbines. Therefore, this master thesis proposes the design of a floating foundation for a given offshore wind farm AC substation, which has been designed for a fixed foundation. Initially, a few adjustments are made to the substation, which would be expected if it had been designed for a floating foundation. Following this, the floater dimensions and structure are designed and the stability and seakeeping are assessed, focusing on the electrical equipment's acceleration and heel operation limits. Finally, the mooring system is dimensioned and the tension in the power cables is assessed.

The chosen substation has a 1232 MW capacity and weighs 7000 tons, while the floater mass equals 10000 tons. The floater designed is a four-column semi-submersible made out of steel and its length and breadth are limited by the topside dimensions. Also, the operational draft and depth are defined to ensure compliance with stability and weather conditions, respectively. The mooring system is composed of 12 all-chain 150mm catenary lines with drag anchors. With this configuration, the platform excursion is limited to 17.5% of the water depth and there is enough redundancy to prevent unacceptable consequences due to a single failure. The power cables are distributed on three of the four sides of the floater, leaving one of them as a free cable zone for support vessel approach. A pliant wave cable configuration is employed to mitigate cable movement and avoid cable clashes due to transversal currents.

1. INTRODUCTION

One of the biggest challenges of modern society is addressing the increasing emissions of greenhouse gas (GHG). That is because the sectors that most emit such gas are strategic for any economy. Figure 1 shows that energy is responsible for over 70% of GHG emissions, which involve industrial processes, transportation, and powering buildings. Therefore, reducing GHG emissions would negatively affect any country's economy, unless an alternative energy source is put in place.

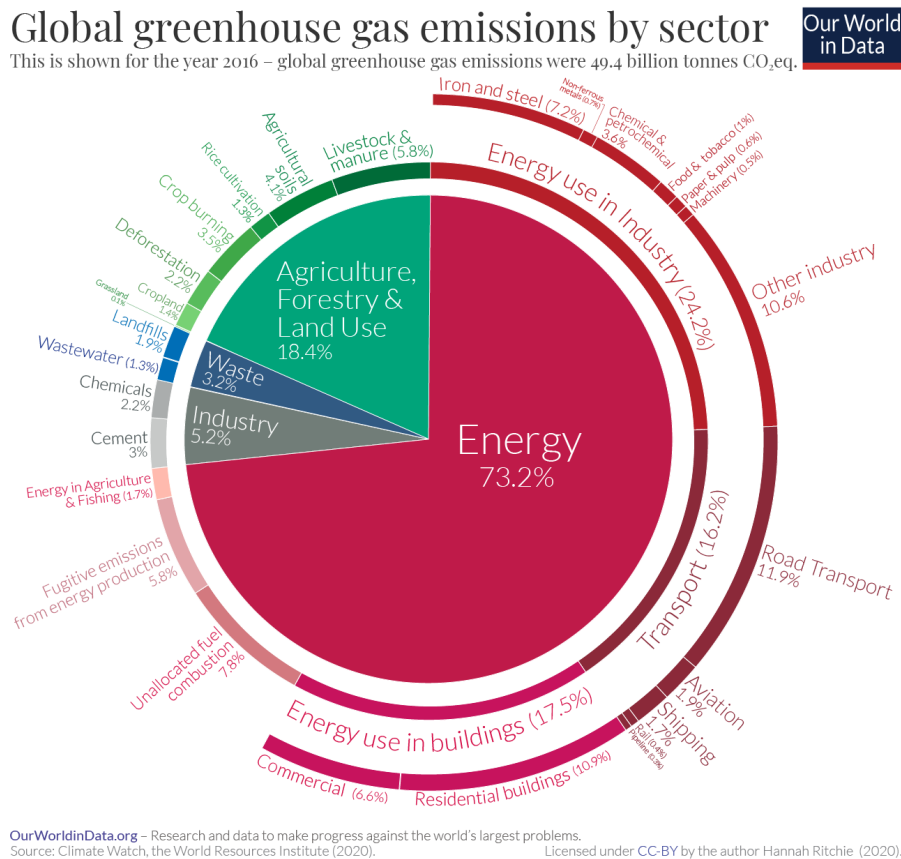


Figure 1. Emissions per sector (Ritchie and Roser n.d.).

To promote a global movement toward a greener future, the Paris Agreement, an international treaty on climate change, was adopted by 196 Parties at the UN Climate Change Conference (COP21) in 2015. Entering into force in 2016, it established that the global average temperature must stay below 2 Celsius degrees above the pre-industrial levels (UNFCCC n.d.).

One way to comply with the target proposed by the Paris Agreement is working to electrify as many sectors as possible (e.g. transportation) and provide clean energy instead of generating it from fossil fuels. Currently, there are several devices under development to harness energy from clean sources, such as wind, waves, sea currents, sun, etc. Figure 2 shows how much renewable energy is produced worldwide by source. Hydropower is

the one contributing the most. However, wind and solar energy have been increasing notoriously in the past ten years and, as technology evolves, this growth is to continue or even increase.

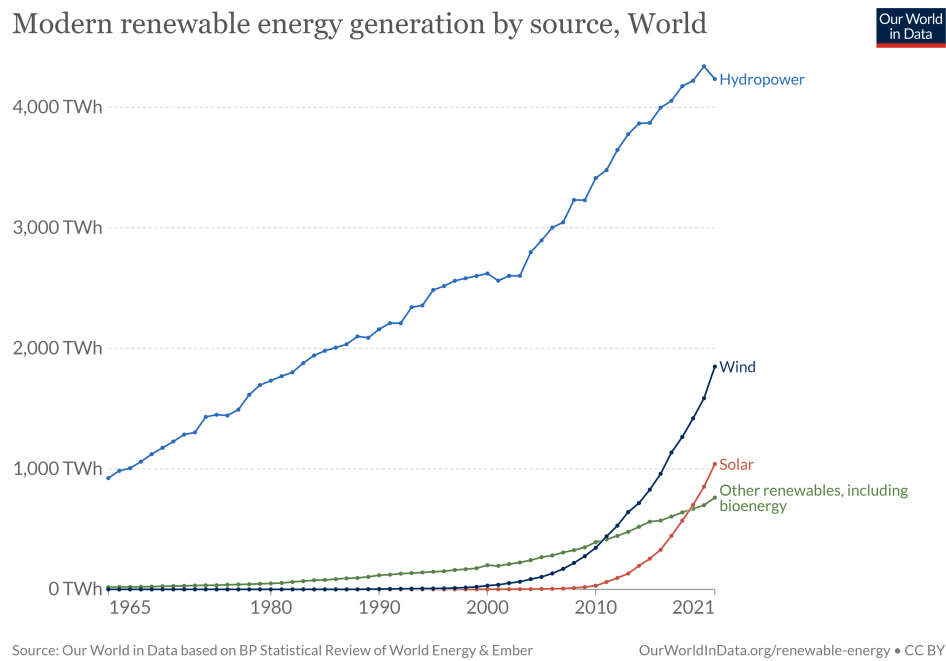


Figure 2. Modern renewable energy generation by source (Data n.d.).

Even though onshore wind energy currently contributes the most to the total energy wind power (Figure 3), there is a big unexplored potential for offshore wind energy. This topic is developed in the following section, where the need for floating wind turbines and substations is tackled.

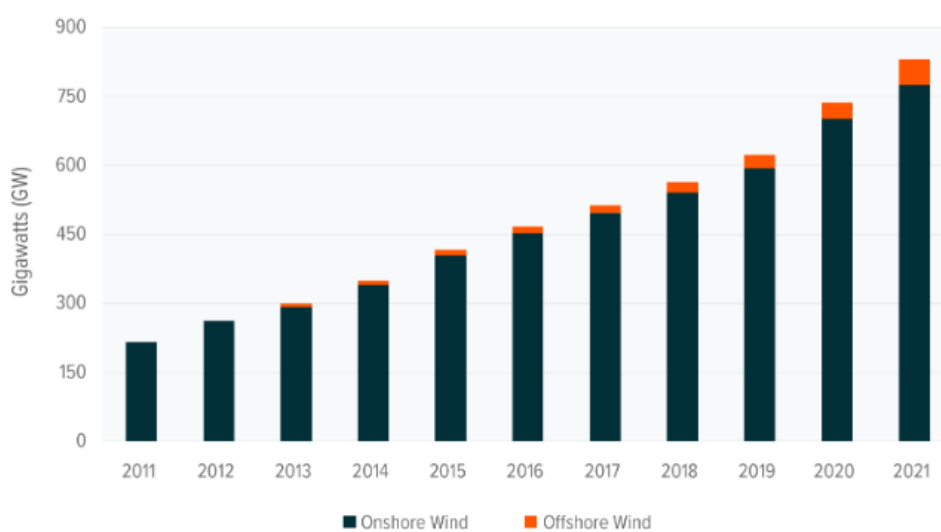


Figure 3. Cumulative wind power capacity globally (Ruid n.d.).

1.1. Background And Motivation

It is known that the further one goes from the coast, the higher the wind resources will be. However, moving to these areas also implies facing technical and economic challenges due to the increase in the water depth. This requires bigger and more complex structures to build and install or floating foundations. Still, this issue must be overcome, due to the enormous energy potential found in these areas. Figure 4 shows the wind speed along the coast of Spain and indicates the offshore wind technical potential for fixed (<50 m depth) and floating (<1000 m depth) foundations. As expected, the potential of floating wind is much higher than that of fixed, and this is the trend all around the globe.

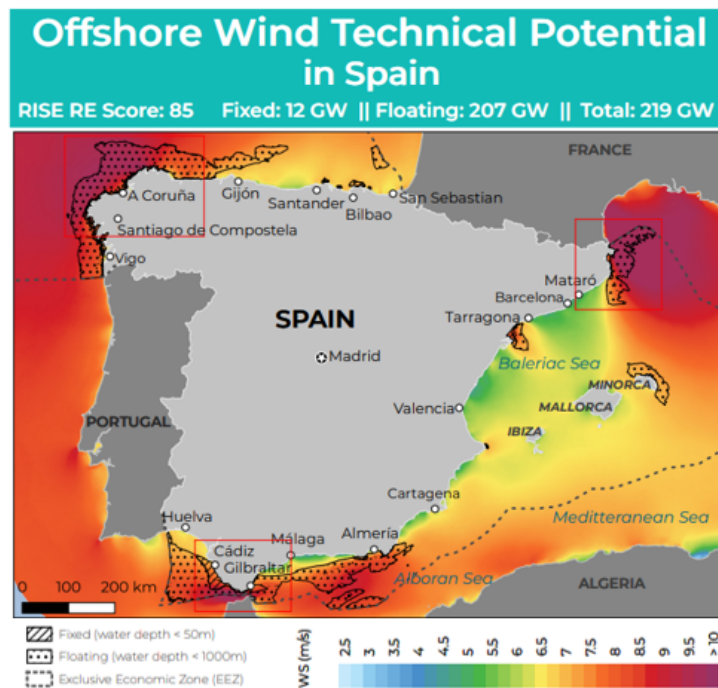


Figure 4. Cumulative wind power capacity globally (Council n.d.).

Different FOWT concepts have been experimented with in several demonstration projects and, in 2017, the first commercial-scale floating wind farm was commissioned (Hywind Scotland). Also, in 2020, the World's first semi-submersible floating offshore wind farm was commissioned (WindFloat Atlantic). This shows a certain level of maturity of this technology, even though it still requires improvements to drive down the costs.

Differently from the FOWT, the offshore substations (OSS) haven't received the same level of investment to boost a transition from fixed to floating foundations. However, this must be addressed if the full offshore wind potential is to be explored. So far, the floating wind turbines are connected to a fixed substation located closer to the shore, which is commonly placed on a jacket-type foundation. Figure 5 illustrates the layout of a fully floating offshore wind farm.

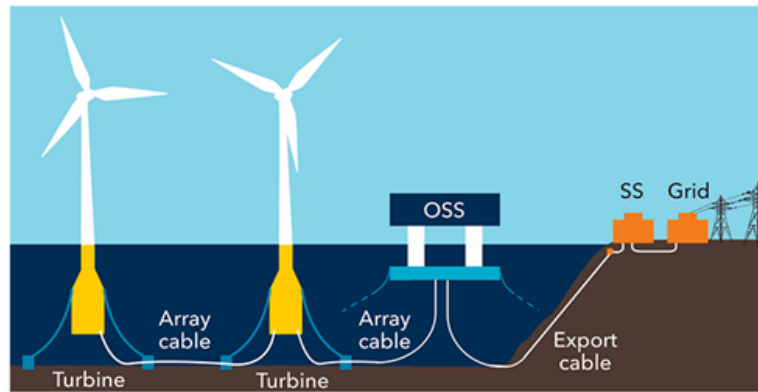


Figure 5. Common layout of a fully floating wind farm (DNV n.d.).

The OSS foundations to come will probably be different from the wind turbines' foundations. That is mainly due to the significant difference in weight and centre of gravity between a wind turbine and a substation. Also, an OSS is connected to many more cables than a wind turbine (DNV n.d.). The major challenges in a floating OSS are related to the equipment it carries and to the electrical cables connected to it. Both were initially designed for fixed structures and the movements of the foundation impose detrimental effects on these components.

The main power transformer and gas-insulated switchgear (GIS) are not suitable to be installed in a floating foundation. That is because oil sloshing might happen in the transformer's compensator tank or the HV GIS seal might deteriorate. These two situations would be caused by the platform's movement (DNV n.d.).

The cables connecting the wind turbines and the OSS are dynamic 66kV cables and were designed to be constantly in motion. However, the export cables have a much higher voltage and are not conceived to operate under constant movement. That is because the lead sheaths surrounding each cable core have poor fatigue resistance (DNV n.d.). Therefore an alternative would be necessary, possibly made of aluminium or copper, but this is still under development. Currently, dynamic export cables of 132kV are available in the market, but cables with higher voltages are still under development.

Lastly, the dynamic behaviour of dynamic cables and mooring lines should be studied to avoid clash (Ellen Jump et al.). Under extreme weather conditions, this scenario could damage the cables and, ultimately, cause the disconnection of the whole wind farm, since the OSS is a single-point failure. Unless there is more than one OSS in the wind farm.

In this thesis, an OSS floating foundation is designed. It includes the definitions of the main dimensions, scantling, and mooring system while complying with the stability and seakeeping requirements. Also, the power cables are studied for their ultimate strength.

2. HVAC vs HVDC

The wind turbines deployed in modern wind farms generate energy at a voltage of 66 KV (Energy n.d.), in contrast to the voltage of 33 KV used in the past. However, to prevent significant losses and unnecessary high currents, the voltage must be increased in high-voltage substations before the energy is sent onshore. During this process, the current can be changed to direct current (HVDC) or remain as alternating current (HVAC).

HVAC substations can be chosen as the preferable option due to the availability of standardized transformers and the simpler design of protection systems when compared to HVDC (Thomas 2022). However, switching to direct current brings a series of advantages, such as no limit on cable length, no need for an intermediate station, no increase of capacitance in the AC network, and lower losses. Additionally, DC cables are cheaper than AC ones.

Nevertheless, a significant drawback of HVDC substations is the higher fixed cost, when compared to HVAC substations. Therefore, there is a break-even point at which HVDC is more advantageous than HVAC. Considering only the wind farm distance from shore, this point occurs at around 50 km (Thomas 2022). However, if the wind farm rating power is considered, a new perspective can be observed. As shown in Figure 6, the higher the rating power is, the farthest from the coast the break-even occurs.

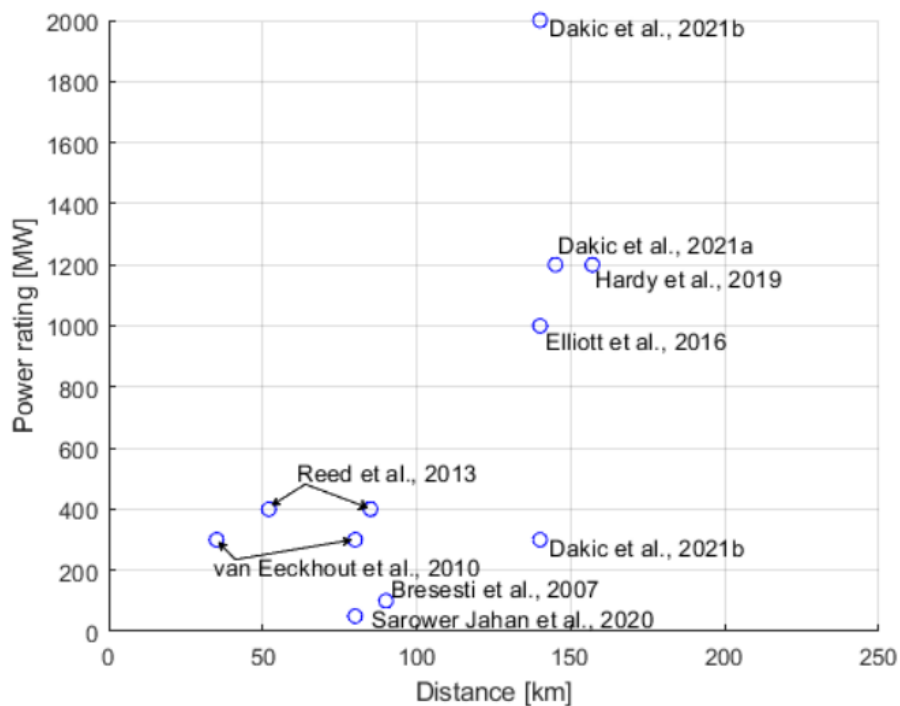


Figure 6. Break-even distances by different authors (Thomas 2022).

It is indeed challenging to create a general rule regarding when to use HVAC or HVDC. That is due to the complexity and diversity of factors involved in this decision. Some of the aspects to be considered are listed below:

- Wind farm size.
- Wind farm location.
- Wind resources.
- Ground conditions, water depth, metocean conditions, and burial requirements.
- Current equipment technology and market CAPEX and OPEX prices impact LCOE.
- Financial assumptions, e.g. discount rate.

It is logical to conclude that each wind farm should be analyzed on a case-by-case basis for which substation technology to employ. However, when it comes to floating offshore wind farms, there is a trend to move into deeper waters due to the presence of stronger and steadier winds. At the first moment, HVAC could still be employed due to the movement of the break-even point shown in the previous figure. However, bigger distances from shore would lead to HVDC substations.

Having said that, the floating foundation developed in this report comports a high-power AC substation, whose dimensions are close to those of a low-power rating DC substation. This way, the foundation can be adapted for both technologies, up to a certain limit.

3. WIND FARM

Currently, there are no floating offshore substations in operation. Therefore, a fixed substation is used as a reference for this work. In Section 3.2, it is discussed how the substation's dimensions should be adjusted so it becomes a better fit for a floating foundation. This includes the construction method, floater stability, and motions.

Since the substation is taken from a fixed wind farm, it wouldn't be interesting to design the floating foundation for the same site. Therefore, the substation is designed to operate in a location where a floating wind farm is under development. This site is located off the coast of Scotland, where the water depth is 100 meters.

3.1. Metocean

In addition to the water depth, the design of an offshore structure should consider the influence of waves, currents, wind, snow & ice, and temperature (DNV 2021c). However, the current work does not consider the action of temperature, snow, and ice. The extreme environmental conditions are summarized in Table 1. The operational environmental conditions are detailed in Section 7.1.2, where a discussion is developed on how the wave, wind, and current can be combined to define the fatigue load cases for the mooring system design.

Table 1. Wind farm Metocean.

Return Period	1-year	10-year	100-year
Sea State			
H_s [m]	8.10	9.90	11.50
T_p [s]	12.40	13.40	14.10
H_{max} [m]	14.50	17.50	20.30
Current [m/s]			
Depth average	0.67	0.76	0.87
Water Level [m\MSL]			
Surge	0.72	0.96	1.22
Wind Speed [m/s]			
1-hr mean wind speed at 10m	25.3	30.5	35.7

3.2. Substation Particulars

In this section, the equipment present in the substation and its layout are provided. This information is used in Section 4 as a parameter to set the dimensions of the floating foundation. Figure 7 illustrates a typical offshore wind farm AC substation.



Figure 7. Typical fixed offshore wind farm substation (Rasmussen n.d.).

3.2.1. *Layout & Equipment*

The substation comprises all the necessary equipment for the wind farm operation and the safety of the personnel onboard. These include electrical, automation, HVAC, mechanical, safety, and HV equipment. Its capacity is 1232 MW and it has a vertical arrangement composed of the following decks, from the lowest to the highest:

- Cable Deck.
- Cellar Deck.
- Main Deck.
- Utility Deck.
- Roof Deck.

The Cable Deck is a part of the floating foundation. It contains the Pull-in device and the access for the export and inter-array cables to reach the substation equipment. Also, it is through this deck that the access from and to a CTV via ladders takes place.

The Cellar Deck includes all the installations necessary to assist the temporary permanence personnel, while providing access to work landing, davit-launched and overboard life rafts. The sump tank is also included in this deck.

The Main Deck houses the MV (66 kV) and HV (275 kV) Gas Insulated Switchgears (GISs), firefighting system, main transformers, radiators, and workshop.

The Utility Deck accommodates the control and LV rooms, the auxiliary transformers, the shunt reactor, and radiators.

The Roof Deck houses the main crane, evacuation heli-winch, HVAC equipment, diesel generator, communication antennas, and 'cut away' hatched for removing major equipment in case of need for repair.

3.2.2. *Dimensions & Mass*

Table 2 presents the overall original dimensions of a substation provided by Iberdrola.

Table 2. Substation dimensions.

Length [m]	61.15
Breadth [m]	24.30
Height [m]	33.30
Cable Deck Length [m]	31.05
Cable Deck Breadth [m]	24.30

Currently, a significant share of an offshore substation cost comes from its installation, due to the necessity of employing expensive large crane vessels. Therefore, the substations are designed with a rectangular shape to reduce this cost. This way, the crane required outreach is reduced and a smaller crane can be used. In Table 2, it can be seen that the substation's length is almost three times its breadth. However, if the substation foundation is a floating structure, the foundation and topside are built all at once, making it unnecessary to install the topside separately. Consequently, the substation can have a square shape, which would optimize the pipping and cable arrangement and better fit a symmetric floating foundation.

For the same lifting restrictions mentioned above, substations are currently much more vertical than horizontal. If these are installed on a floating foundation, achieving a stable configuration would require a very large foundation, due to the elevated centre of gravity. Also, the equipment in the higher decks would experience severe longitudinal and transversal accelerations due to the pitch and roll motions, respectively. For these reasons, this kind of design is not suitable for a floating foundation. Therefore, the substation height is reduced in half and the length and breadth are modified in a way that the total area doesn't change and that the substation is square. Table 3 shows the new dimensions.

Table 3. Substation modified dimensions.

Length [m]	52.00
Breadth [m]	52.00
Height [m]	16.65
Cable Deck Length [m]	28.00
Cable Deck Breadth [m]	28.00

Even though the cable deck is not a part of the substation, its dimensions are manipulated the same way as those of the topside. The cable deck to be built in the floater has the dimensions shown in Table 3.

Table 4 provides the substation's original mass and centre of gravity. The LCG is referenced in the centre of the substation, the TCG in the centre line, and the VCG in the cable deck.

Table 4. Substation mass and centre of gravity.

LCG [m]	1.805
TCG [m]	-0.063
VCG [m]	17.662
Mass [tons]	6960.9

To achieve the substation dimensions proposed, the equipment is rearranged and it is assumed that the final LCG and TCG are exactly in the centre of the topside. Also, the VCG is reduced in half to account for the reduction of the topside height. Table 5 shows the new centre of gravity.

Table 5. Substation mass and modified centre of gravity.

LCG [m]	0.000
TCG [m]	0.000
VCG [m]	8.831
Mass [tons]	6960.9

3.3. Limiting Operation Conditions

Table 6 provides the limiting acceleration and inclination of the electrical equipment under extreme and operational conditions. These values are used for the stability and motions analysis further in this report.

Table 6. Acceleration and heel operating limit.

Condition	Extreme	Operational
a_x [m/s ²]	0.30g	0.25g
a_y [m/s ²]	0.30g	0.25g
a_z [m/s ²]	0.25g	0.10g
Inclination [deg]	13	7

3.4. Electric Cables

The substation employed in this work is connected by fourteen 66 kV inter-array cables (IAC) and three 275 kV export cables (EC). All of them are static cables since the WTs and OSS are originally fixed. However, these are changed by dynamic cables to comport the motions induced by the WTs and OSS foundation.

As mentioned in Section 1.1, dynamic IACs are already a reality, due to the development of FOWTs. However, dynamic ECs are still under development. Therefore, assumptions are made later in this report to address the analysis of these cables.

4. FLOATER DESIGN

The design process of an offshore platform is intrinsically iterative. Therefore, a simplified method is developed to assist in the initial design stages, in which the main dimensions and weight must be defined quickly to allow the assessment of several configurations. Furthermore, these configurations are checked for their equilibrium, stability, and dynamic behaviour through key parameters that can easily be estimated.

Later on, the chosen configuration is analyzed in depth, when the hull structure is modelled in Rhinoceros for an accurate definition of the mass and centre of gravity. Also, the large angle stability and motion analysis are performed with Maxsurf and OrcaFlex, respectively. The simplified method proposed is based on the steps shown in Figure 8.

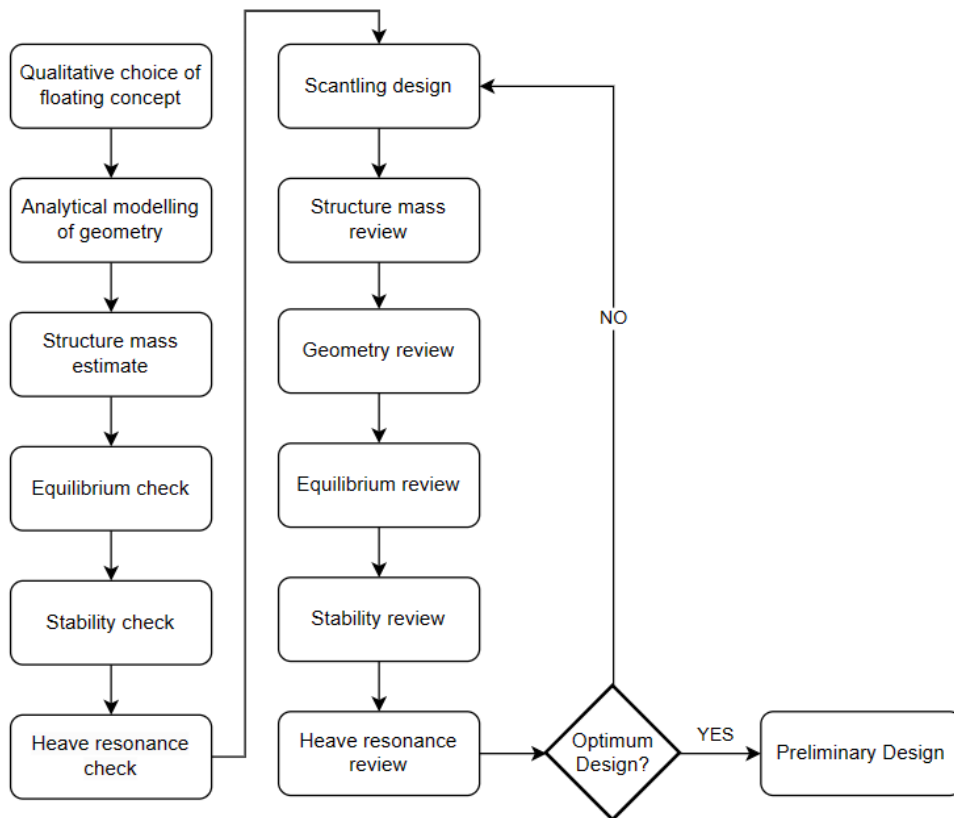


Figure 8. Simplified Design Approach.

4.1. Qualitative Choice Of Floating Concept

The floating concepts used for OSSs are the same as those employed for WTs. Figure 9 illustrates the different configurations available for floating platforms.

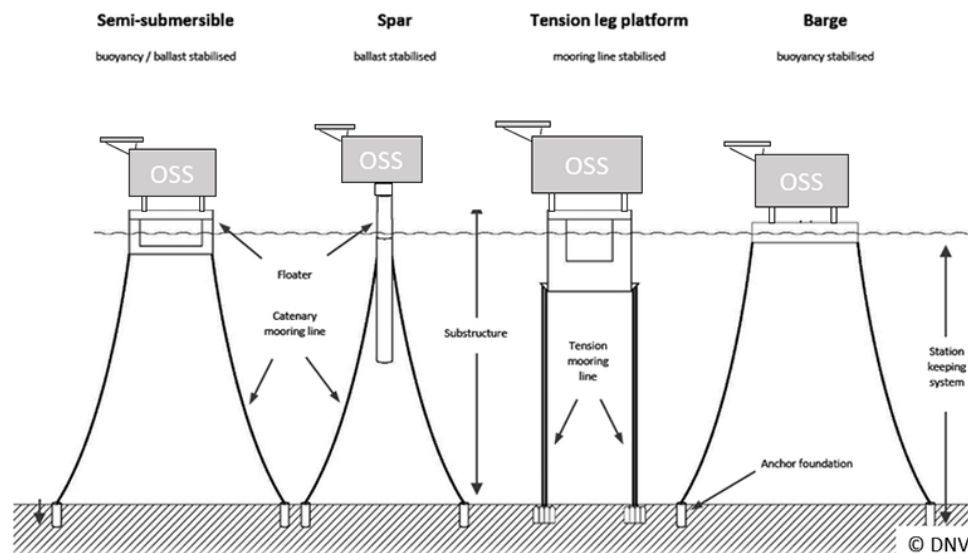


Figure 9. Floating concepts for OSS (DNV n.d.).

The barge concept presents a relatively large waterplane area, resulting in considerably high motions when excited by waves. Since the platform will be connected to several energy cables, a very important aspect of the current design is minimizing the platform motions. Therefore, this concept is discarded. The remaining ones are compared according to the table shown in Figure 10.

Substructure Type	Advantages	Disadvantages
Spar	<ul style="list-style-type: none"> Suitable for higher sea states Relatively low steel weight Low operational risk 	<ul style="list-style-type: none"> Large draft – limits ports and transportation routes Attachment of top mass to substructure can be complex Heavy lift likely to be needed
Semi-submersible	<ul style="list-style-type: none"> Low overall risk (most proven for FOWT) Onshore or drydock assembly Shallow draft Well understood supply chain Suitable for heavy payloads 	<ul style="list-style-type: none"> Large and heavy structure – higher build costs Columns likely to need inspection every 10 years by rope access technician
TLP	<ul style="list-style-type: none"> High stability, low motions Lower steel weight Onshore or drydock assembly Suitable for deeper waters 	<ul style="list-style-type: none"> Sensitive to waves and strong tidal currents Potentially not self-stable during towing Mooring system likely to be expensive
Shortened Spar	<ul style="list-style-type: none"> Moderate draft Onshore or drydock assembly Reduced maintenance 	<ul style="list-style-type: none"> Lower stability compared to spar Lack of operational platforms in floating wind and O&G

Figure 10. Substructure topology review (Ellen Jump et al.).

Even though the spar concept behaves well under high sea states and demands relatively less steel, it requires a large draft. Therefore, its construction and transport become extremely challenging and can represent a logistical bottleneck for the advance of a wind farm project. For this reason, this concept is rejected.

The TLP concept works on the principle of buoyancy excess while tensioning the tendons attached to the seabed. This mechanism provides high stability and low motions, which are desired characteristics. However, the mooring system is likely to be expensive. That would be because the tendons' installation is complex and they require anchors with vertical force resistance (piles, suction buckets), which are costly and time-consuming to install.

The shortened spar concept is not an option due to the lack of experience both in the floating wind and O&G industry. Therefore, the most suitable concept is the semi-submersible. It requires a shallow draft and is suitable for heavy payloads, which is the case of the OSS chosen (nearly 7000 tons). Also, depending on the design, the foundation behaviour in waves can be good enough to accommodate the accelerations and movement amplitude tolerances of the energy cables and equipment onboard.

Throughout the development of the O&G and floating wind industries, various types of semi-submersible foundations were conceived. When it comes to the topology of these foundations, they can be triangular or rectangular with a ring-pontoon or two-pontoon design and have from 3 to 10 columns. After revising a few of the floating OSSs under development, it was found that the most common configuration consists of a quadrangular shape with four columns and a ring-pontoon, as shown in Figure 11. Therefore, this layout is chosen for the following design steps.



Figure 11. Floating substation concepts, left to right: Linxon (Linxon n.d.), Nevesbu (Nevesbu n.d.), WIND2GRID (WIND2GRID n.d.).

4.2. Analytical Modeling Of Geometry

As mentioned in the previous section, the floating foundation is designed as a rectangular semi-submersible platform with four columns and a ring pontoon. Therefore, four pontoons and four columns are modelled based on their length, breadth, and height. Some of these

dimensions are interconnected, such as the pontoons and columns' width. Also, the four pontoons are set to have the same height. To govern the columns' height and pontoons' length, the overall length, beam, and depth of the platform are defined. Figure 12 illustrates how these dimensions are applied to the platform.

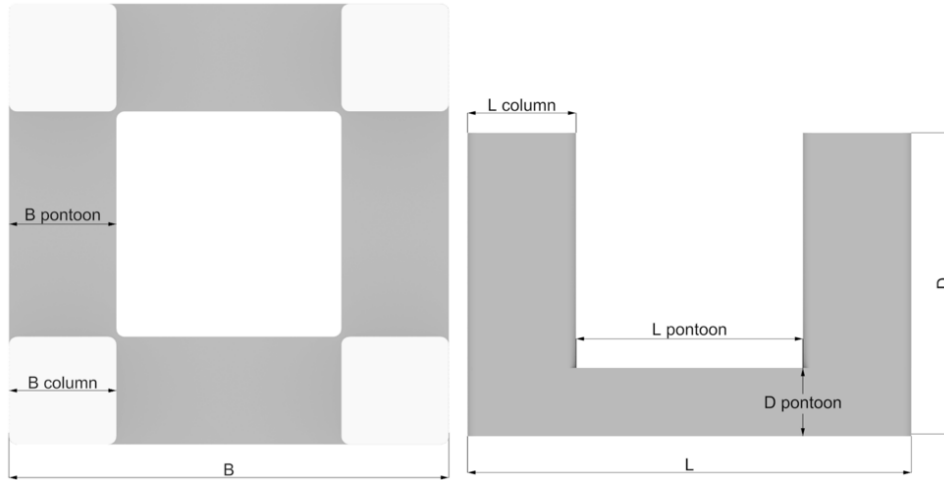


Figure 12. Platform dimensions scheme.

Using the substation dimensions provided in Section 3.2.2, a first estimate of the platform horizontal dimensions (B and L) is performed. Also, the platform depth is defined by setting an initial draft and minimum air gap. With this information, the volume of each member is computed and added for a first estimate of the platform volume and displacement. Equations 1, 2, 3 and 4 detail these calculations.

$$V_{pont.} = L_{pont.} \cdot B_{pont.} \cdot D_{pont.} [m^3] \quad (1)$$

$$V_{col.} = B_{col.}^2 \cdot (T - D_{pont.}) [m^3] \quad (2)$$

$$V_{node} = B_{col.}^2 \cdot D_{pont.} [m^3] \quad (3)$$

$$Displacement = 4 \cdot (V_{pont.} + V_{col.} + V_{node}) \cdot \rho_{water} [tons] \quad (4)$$

4.3. Structural Mass Estimate

Initially, the structural mass is defined from the pontoon, column, and node volume by applying a factor that translates these volumes to steel mass. These factors are shown in Table 7. At this moment, the cable deck mass is disregarded due to its small share of the total platform mass.

Table 7. Steel mass per region.

Region	Factor [tons/m ³]
Node	0.25
Pontoons	0.20
Columns	0.15

Based on the initial geometry, the structure is designed according to the process described in Section 4.7, and the mass is retrieved from each structural member, including the cable deck.

4.4. Equilibrium Check

Once the platform displacement and structural mass are obtained, the OSS mass can be introduced for the verification of the equilibrium condition with the proposed draft. It is known that semi-submersible platforms need to carry ballast to be stable. Therefore, to prevent stability issues, the difference between buoyancy and mass is met with the introduction of ballast in the pontoons and nodes.

To check if the required ballast mass fits in the pontoons, the ballast volume is compared with that of the pontoons and nodes, assuming a permeability of 90%. The ballast considered is seawater, with a density of 1.025 tons/m³.

$$Mass_{ballast} = Displacement - (Mass_{structure} + Mass_{substation}) [tons] \quad (5)$$

4.5. Stability Check

When designing a floater, reducing its initial metacentric height (GM) to the lowest practical value is of interest because it (Limited 2006):

- Reduces the unit's cost.
- Improves its dynamic behaviour (longer natural roll and pitch periods).
- Increases its carrying capacity.

However, the GM must be at least positive, so the floater stays upright when floating in still water with no action of environmental factors. DNV requires the GM to be at least 1 meter in operating, transit, and survival conditions and not less than 0.3 meters during temporary conditions (DNV 2020). Therefore, at this stage, the stability analysis checks compliance with a minimum GM of 2.5 meters, where the 1.5-meter excess is to account for possible CG changes further in the design process and to improve the chance

of complying with the large angle stability criteria.

To calculate the GM, the total centre of gravity and buoyancy are assessed (Equations 6 and 7). Following that, the waterplane inertia is computed (Equation 8) so the metacentric radius (BM) can be calculated (Equation 9). With this information, the initial GM is obtained in Equation 10.

$$KG = \frac{\sum_i^n Mass_i \cdot KG_i}{Mass_{total}} [m] \quad (6)$$

$$KB = \frac{\sum_i^n Volume_i \cdot KB_i}{Volume_{total}} [m] \quad (7)$$

$$WP_{inertia} = 4 \cdot \left(\frac{B_{col.} \cdot B_{col.}^3}{12} + B_{col.}^2 \cdot \left(\frac{B_{plat.}}{2} - \frac{B_{col.}}{2} \right)^2 \right) [m^4] \quad (8)$$

$$BM = \frac{WP_{inertia}}{Volume_{total}} [m] \quad (9)$$

$$GM = KB + BM - KG [m] \quad (10)$$

4.6. Heave Resonance Check

The natural period in heave is compared with the typical period of semi-submersible platforms, so resonance is avoided. This phenomenon would lead to excessive vertical motion and excitation of the power cables. To calculate this parameter, the restoration coefficient in heave is estimated according to Equations 11. Also, the added mass in heave is obtained after DNV-RP-C205, where a 2D rectangular added mass coefficient is used to define the added mass per length (Equation 12). Then, the natural period is obtained from the natural frequency given by Equation 13.

$$C = 4 \cdot g \cdot \rho_{water} \cdot B_{col.}^2 [kN/m] \quad (11)$$

$$m_A = \rho \cdot C_A \cdot A_R [kg/m] \quad (12)$$

$$\omega_0 = \sqrt{\frac{C}{Mass_{total} + A}} [rad/s] \quad (13)$$

$$T_0 = \frac{2 \cdot \pi}{\omega_0} [s] \quad (14)$$

4.7. Structural Design

The structural design is based on the DNV recommended practices and offshore standards for steel columns-stabilized units. The documents followed are listed below:

- DNV-OS-C101 | Design of Offshore Steel Structures, General - LRFD method
- DNV-OS-C103 | Structural Design of Column Stabilised Units - LRFD method
- DNV-RP-C103 | Column-stabilised Units
- DNV-RP-C201 | Buckling Strength of Plated Structures

The formulations provided by DNV require the stresses to which each structural member is subjected. Therefore, equations derived from Euler–Bernoulli beam theory (classical beam theory) are used to obtain these stresses. The pontoons, columns, and cable deck are assessed separately and the connection between these parts is approximated by suitable boundary conditions.

The global strength of each pontoon is analyzed assuming they are beams simply supported at the connection with the nodes (Figure 13). Regarding the global loads, a uniformly distributed load is assumed, where its magnitude is the difference between the pressure acting on the upper and lower part of the pontoon. These pressures are obtained after DNV. Once this configuration is defined, the pontoon cross-section properties are calculated (area, centre, inertia, and section modulus) and the traction, compression, and shear stresses are computed. Equations 15 to 23 are used in this calculation.

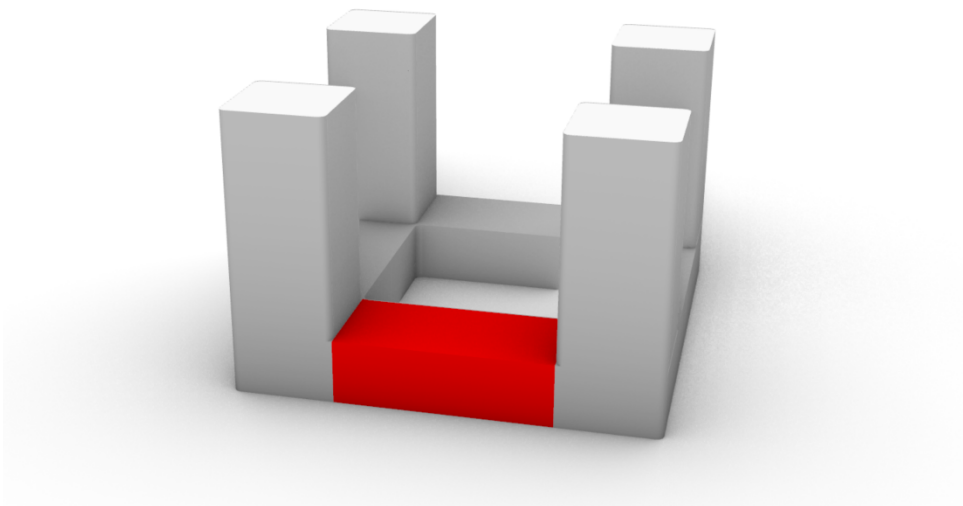


Figure 13. Pontoon isolation illustration

$$M_{pontoon} = \frac{q_{pressure} \cdot L_{pontoon}^2}{8} [kNm] \quad (15)$$

$$z_g = \frac{\sum_i^n A_i \cdot z_i}{\sum A_i} [m] \quad (16)$$

$$I_{pontoon} = \sum_i^n (I_i + A_i \cdot (z_i - z_g)^2) [m^4] \quad (17)$$

$$W_{deck} = \frac{I_{section}}{z_{deck} - z_g} [m^3] \quad (18)$$

$$W_{bottom} = \frac{I_{section}}{z_{bottom}} [m^3] \quad (19)$$

$$\sigma = \frac{M_{pontoon}}{W} [MPa] \quad (20)$$

$$SF_{pontoon} = \frac{q \cdot L_{pontoon}}{2} [kN] \quad (21)$$

$$SA_{pontoon} = D_{pontoon} \cdot B_{column} [m^2] \quad (22)$$

$$\tau = \frac{SF_{pontoon}}{SA_{section}} [MPa] \quad (23)$$

For the columns' global strength assessment, compression load due to the topside weight and bending load resulting from the topside lateral acceleration are assumed. Also, the columns are assumed to be fixed at the connection with the nodes (Figure 14). The lateral and vertical acceleration used is the maximum that the electric equipment can be subjected to. (Table 6). The compression force and bending moment are divided by four to be applied in each column individually. The pontoon cross-section properties are calculated following the same procedure used for the pontoons.

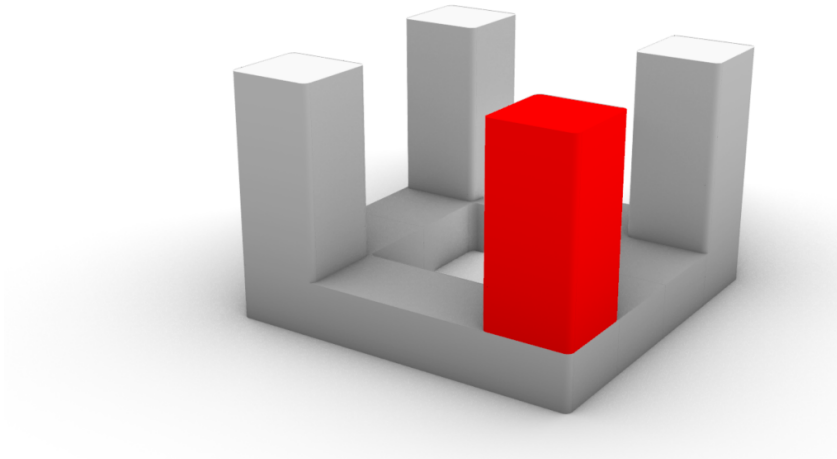


Figure 14. Column isolation illustration.

The cable deck is designed as an open grid deck to save weight. Currently, open grid decks are composed of galvanized steel or polymers combined with glass fibre. The latter is a lighter solution and can be as strong as steel. However, it cannot be placed in escape routes because of its low resistance to fire. Since these routes are not defined at this point of the project, the galvanized steel is chosen. Further modifications can be made in the detail design phase to reduce the cable deck weight by applying polymers combined with glass fibre in suitable areas.

At this moment, only the intact stability of the platform is assessed through the initial GM and no considerations are made regarding the damaged stability and the required level of hull subdivision. Therefore, a transversal and longitudinal bulkhead arrangement is proposed here and verified in Section 5.

Due to their relatively small water plane area, semi-submersible platforms are sensitive to significant loss of buoyancy. Therefore, the columns are fitted with two perpendicular longitudinal bulkheads and transversal bulkheads spaced by two frame spacing. Similarly, the pontoons include a longitudinal vertical bulkhead, and transversal bulkheads, one in the middle and one more on each side with the same spacing as the columns' bulkheads. The nodes are divided into four compartments by two vertical bulkheads. Figures 16 and 15 illustrate the bulkhead arrangement. The pontoons' and nodes' compartments are ballast tanks whereas those in the columns are watertight compartments to limit the hull flooding.

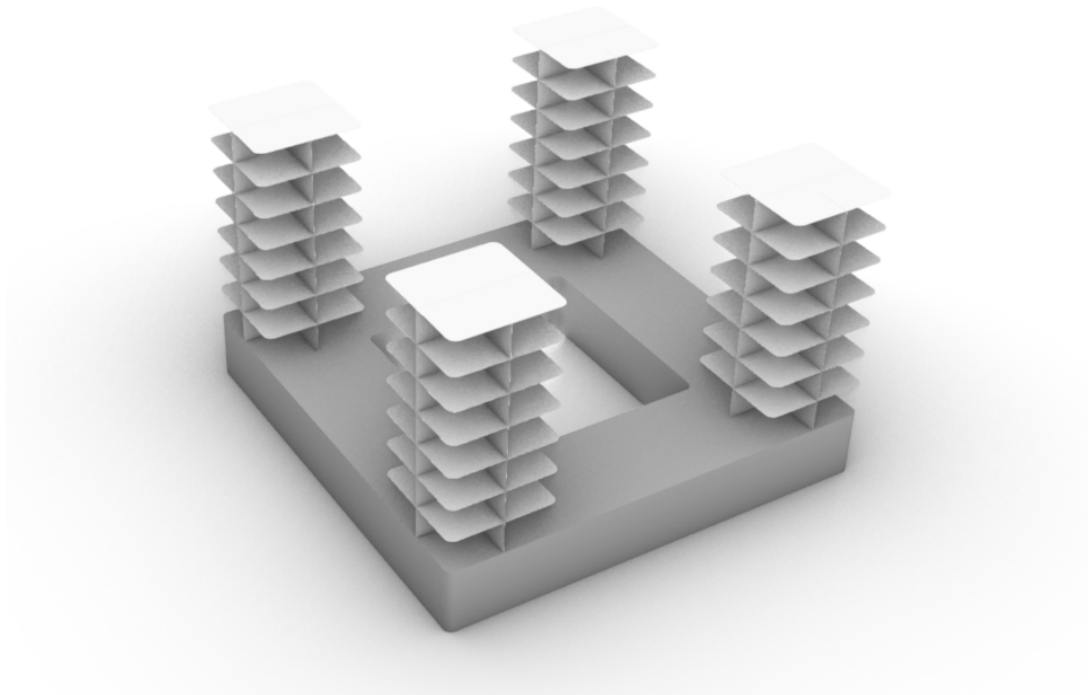


Figure 15. Columns' bulkheads.

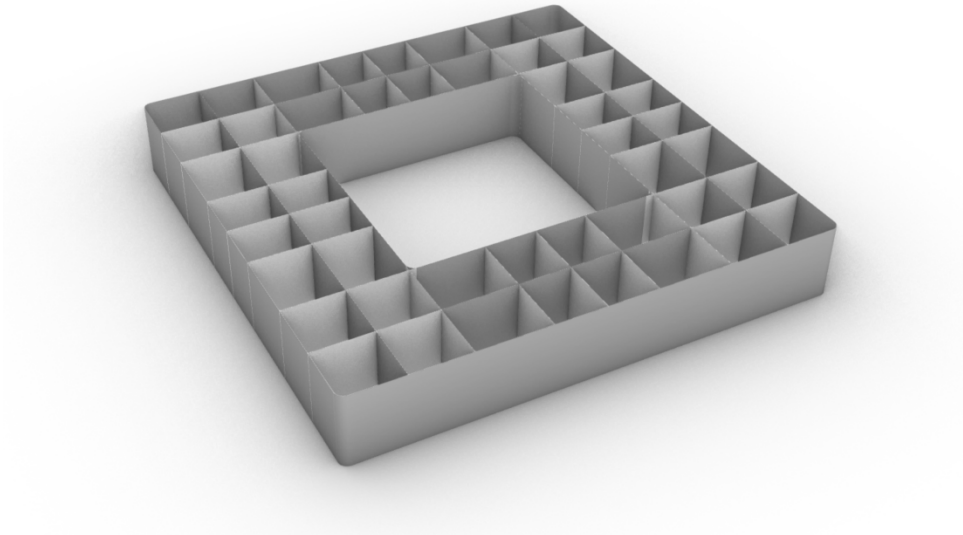


Figure 16. Pontoons' and nodes' bulkheads.

Following this, the bending and shear of stiffeners, frames, and plates due to hydrodynamic pressure are analyzed. A longitudinal framing system is chosen and the frame spacing is defined as four times the stiffener spacing. Also, the transversal bracings that support the J-tubes are designed according to the pressure for components with a negative air gap and the J-tubes' thickness is defined using the same design pressure since the outer diameter is given. Table 8 provides the pressures used during the calculations.

Table 8. Pressures for structural design.

Description	Pressure [kN/m ²]
Cable Deck	70.00
Trans. Bracings & J-Tubes	150.00
Column	233.30
Pontoon Deck	233.30
Pontoon Side	271.31
Pontoon Bottom	309.32
Pontoon Bhd	216.23
Column Bhd	106.05

Once the global and local stresses are computed, they are combined using the Von Mises equivalent stress, described by Equation 24.

$$VM = \sqrt{\sigma_x^2 + \sigma_y^2 - \sigma_x \cdot \sigma_y + 3 \cdot \tau_{xy}^2} \quad (24)$$

Lastly, a corrosion allowance is added to the net scantling. DNV recommends that a minimum of 0.1 mm of thickness per year of operation should be included to account for corrosion (DNV 2021a). Therefore, assuming 25 years of operation, 2.5 mm are added

to all structural members, since they will be constantly exposed to seawater and humid atmosphere.

4.8. Geometry Optimization

The geometry optimization is performed using the Excel GRG Nonlinear Solver engine. This algorithm is based on the gradient optimization method, in which the objective function gradient is computed for each combination of the design variables to indicate where is the function minimum. At this point, the partial derivatives equal zero, indicating that the optimum configuration has been found. When constraints are included, the algorithm follows the same strategy to look for the objective function minimum value, but it stops when it cannot obtain a better configuration due to imposed constraints. This method is recommended for smooth nonlinear problems.

The optimization objective, variables, and constraints are listed below:

- Objective
 - Minimize the structural mass of the floater
- Variables:
 - Pontoon Depth
 - Pontoon Breadth
 - Floater Length
 - Floater Depth
- Constraints:
 - $GM_0 \geq 2.50$ meters
 - $T_0 \geq 19$ seconds (typical semi-submersible platform heave natural period (DNV 2014))
 - $5.00 \text{ meters} \leq \text{Pontoon Depth} \leq 10.00 \text{ meters}$
 - $5.00 \text{ meters} \leq \text{Pontoon Breadth} \leq 15.00 \text{ meters}$
 - Floater Length ≥ 52.00 meters (topside length)
 - Air Gap ≥ 12.00 meters (100-year return period maximum wave height)
 - Distance between columns ≥ 28.00 meters (minimum to fit cable deck)

The scantling design is not a direct part of the optimization. It adjusts to the new geometry, but manual modifications are made in case the new geometry results in the collapse of a structural member. In that case, the optimization is run again and the tendency is for the geometry to change less and less after each cycle until a satisfactory scantling is found.

Furthermore, once the optimal geometry is found, small adjustments are made so it becomes a multiple of the stiffener and frame spacing defined. During this process, there is a slight modification of the GM and heave natural period.

4.9. Interface Between Floater And Topside

For the definition of the interface between floater and topside, research on the strategies applied in the oil & gas industry is carried out and three options are identified. These are illustrated in Figure 17.



Figure 17. From left to right: (A), (B) and (C).

These strategies are identified as follows:

- Topside integrated with a box-type deck (A)
- Topside supported by a truss structure (B)
- Topside supported by columns (C)

As mentioned in Section 3.2.2, the floater and substation are planned to be built together. For this reason, configuration "B" would not be applicable, since it implies that the substation is built separately and then lifted to be placed on the truss structure. Therefore, for the building strategy assumed, configurations "A" or "C" could be chosen. However, the full integration of the topside with a box-type deck would result in an unnecessary increase in the steel weight. For this reason, the configuration "C" would be the best one to be employed.

4.10. Results

In this section, the results obtained after the analysis described are shown. In the following sections, the obtained design is validated with detailed stability and motion calculations.

4.10.1. Geometry

The platform geometry and final dimensions are shown in Figure 18 and Table 9.

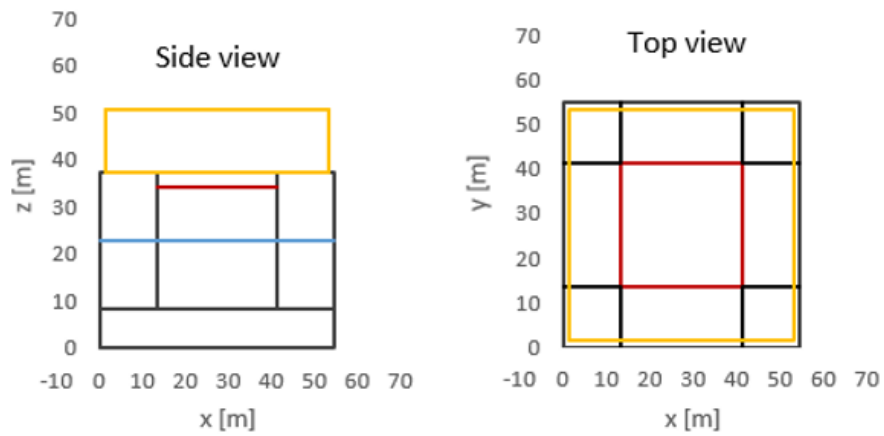


Figure 18. Platform geometry.

Table 9. Main Dimensions.

Platform L [m]	54.78
Platform B [m]	54.78
Platform D [m]	37.30
Draft [m]	22.00
Cable deck height [m]	34.00
Air gap [m]	12.00
Column L [m]	13.39
Column D [m]	28.90
Pontoon L [m]	28.00
Pontoon B [m]	13.39
Pontoon D [m]	8.40
Displacement [tons]	29084

The J-tubes' arrangement is shown in Figure 19. It was developed in a way that the tubes coincide with the relevant structural members and that the space between them avoids possible interference between the power cables.

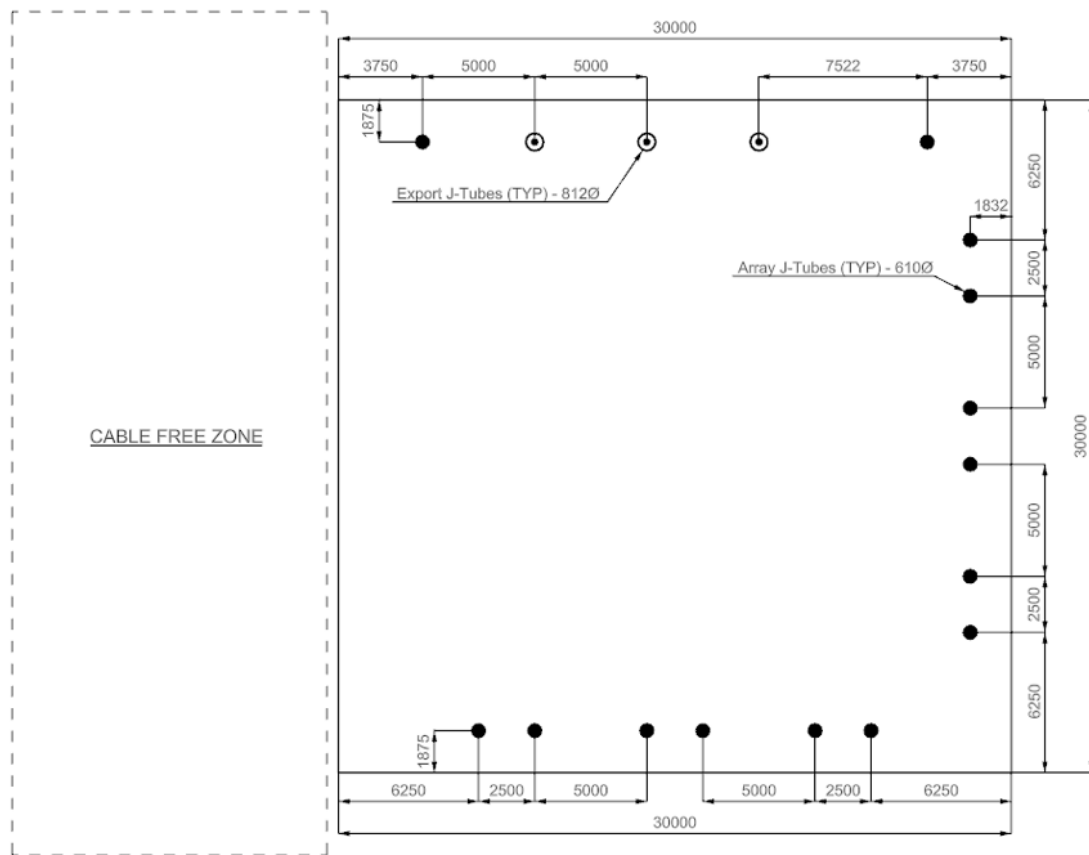


Figure 19. Cable deck arrangement (dimensions in mm).

Figures 20 to 23 show the 3D model built in Rhino. Small adjustments are made to the geometry defined above, consisting in rounding the columns' and nodes' vertical edges with a 1-meter radius. The J-tubes in blue refer to the inter-array cables and the ones in red to the export cables. The aft is a cable-free zone and the substation is represented by a green block with the main dimensions provided in Table 3.

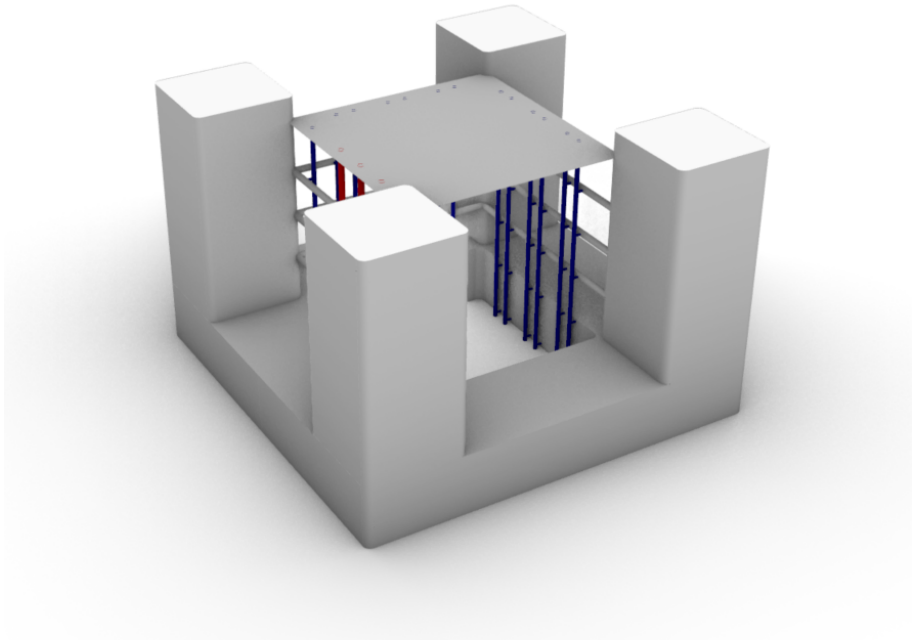


Figure 20. Isometric view of the platform without topside.

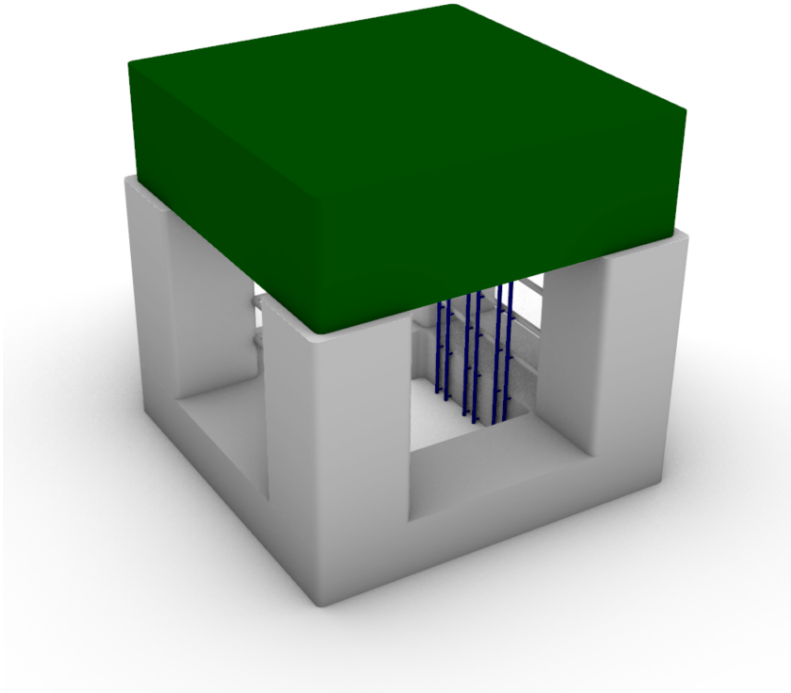


Figure 21. Isometric view of the platform with topside.

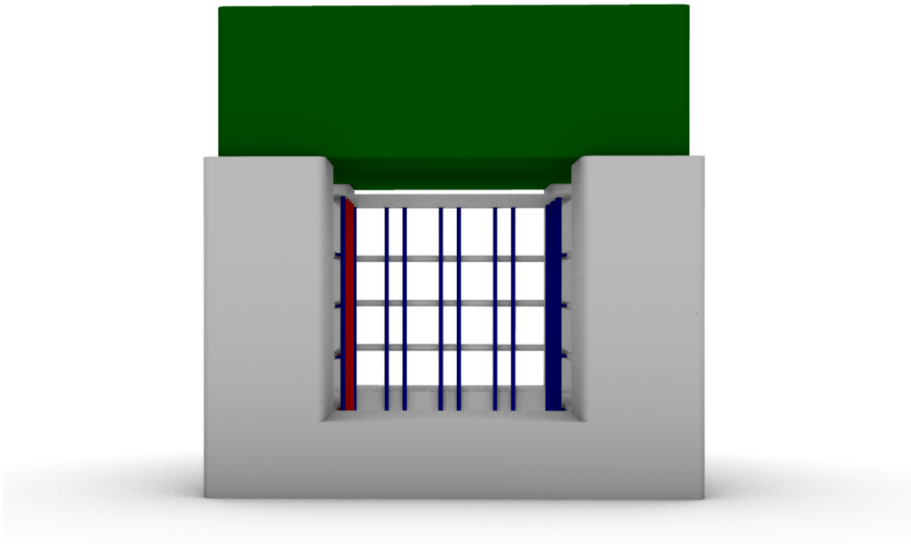


Figure 22. Aft to forward view of the platform with topside.

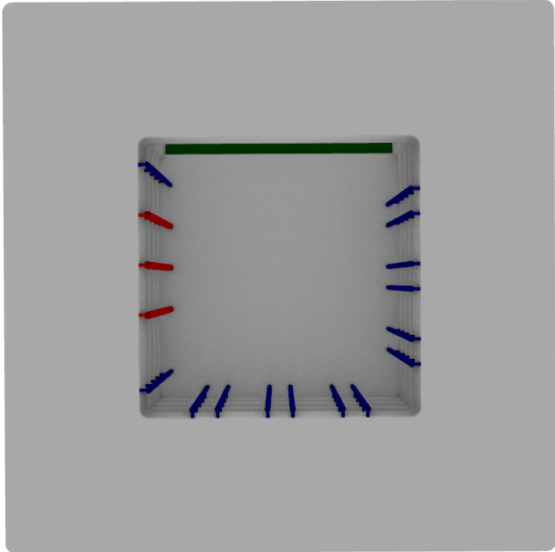


Figure 23. Bottom view of the platform with topside.

4.10.2. Scantling

Tables 10 to 11 provide the dimensions of the pontoons' scantling designed. All stiffeners and frames have a "T" profile.

Table 10. Pontoon plate and stiffeners.

Region	t_{plate} [mm]	S_{stiff} [mm]	t_{web} [mm]	b_{web} [mm]	t_{flange} [mm]	b_{flange} [mm]
Bottom	23.5	515	22.5	180	23.5	120
Side	23.5	525	22.5	180	23.5	120
Deck	23.5	515	22.5	180	23.5	120
Trans. Bulkhead	21.5	515	21.5	160	22.5	100
Long. Bulkhead	21.5	525	21.5	160	22.5	100

Table 11. Pontoon frame.

Region	S_{frame} [mm]	t_{web} [mm]	b_{web} [mm]	t_{flange} [mm]	b_{flange} [mm]
Bottom	2060	32.5	800	37.5	400
Side	2060	32.5	800	44.5	400
Deck	2060	32.5	800	37.5	400
Trans. Bulkhead	2625	32.5	800	37.5	400
Long. Bulkhead	2060	32.5	800	37.5	400

Table 12 provides the pontoon cross-section properties and Figure 24 shows the cross-section.

Table 12. Pontoon cross-section properties.

$\sum (Ai)$ [m ²]	1.63
$\sum (Ai*Zi)$ [m ³]	6.84
Inertia [m ⁴]	38.06
Zg [m]	4.20
Section Modulus - Deck [m ³]	9.09
Section Modulus - Bottom [m ³]	9.08

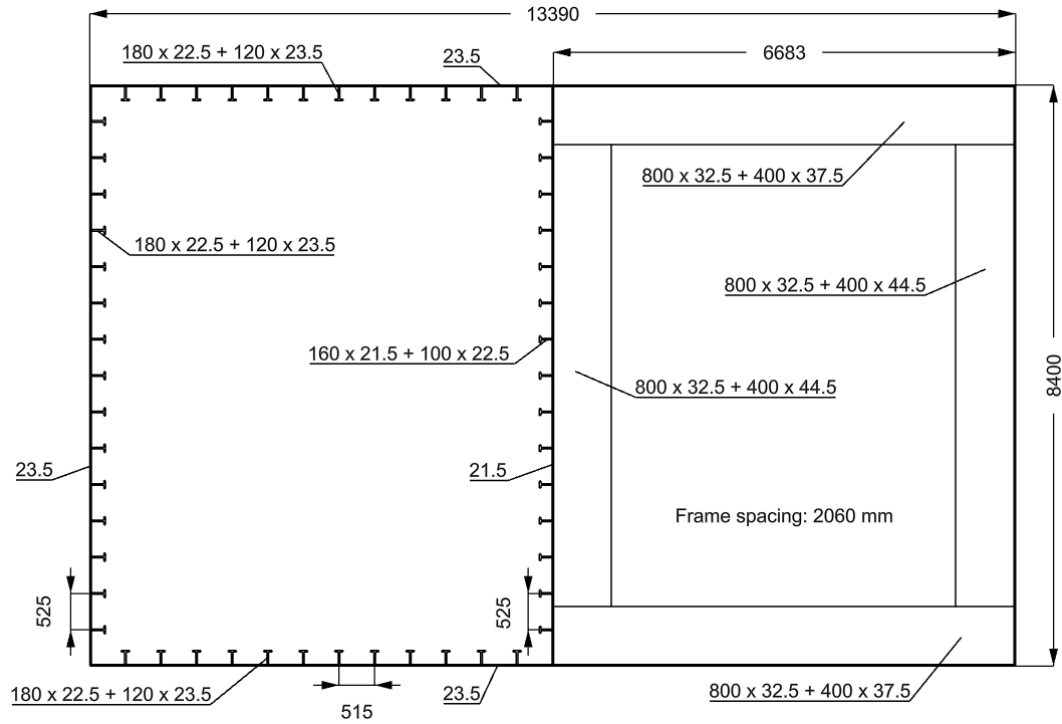


Figure 24. Pontoon cross-section (dimensions in mm).

Tables 13 to 14 provide the dimensions of the columns' scantling designed. All stiffeners and frames have a "T" profile.

Table 13. Column plate and stiffeners.

Region	t_{plate} [mm]	S_{stiff} [mm]	t_{web} [mm]	b_{web} [mm]	t_{flange} [mm]	b_{flange} [mm]
Side	20.5	515	23.5	150	23.5	100
Trans. Bulkhead	19.5	515	22.5	150	22.5	100
Long. Bulkhead	19.5	515	22.5	150	22.5	100

Table 14. Column frame.

Region	S_{frame} [mm]	t_{web} [mm]	b_{web} [mm]	t_{flange} [mm]	b_{flange} [mm]
Side	2060	37.5	850	42.5	350
Trans. Bulkhead	2232	32.5	600	42.5	350
Long. Bulkhead	2060	32.5	600	42.5	350

Table 15 provides the column cross-section properties and Figure 25 shows the cross-section.

Table 15. Column cross-section properties.

$\Sigma (A_i)$ [m ²]	2.17
$\Sigma (A_i * Z_i)$ [m ³]	14.57
Inertia [m ⁴]	96.74
Zg [m]	6.70
Section Modulus [m ³]	14.48

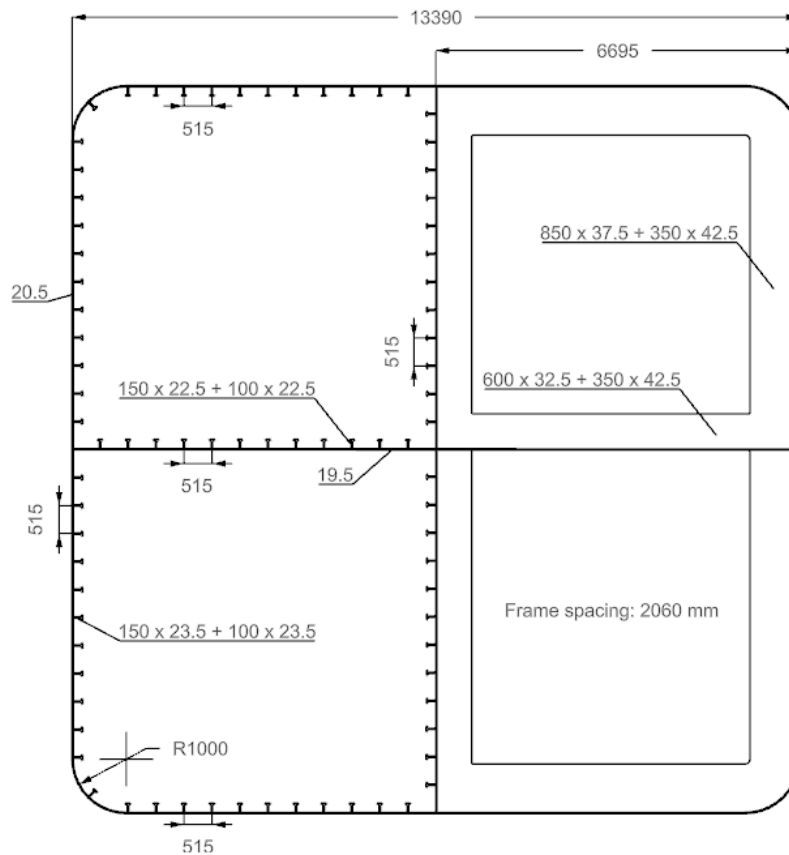


Figure 25. Column cross-section (dimensions in mm).

Tables 16 to 18 provide the cable deck's, bracings' and j-tubes' dimensions.

Table 16. Cable deck scantling.

Member	S_{member} [mm]	t_{web} [mm]	b_{web} [mm]	t_{flange} [mm]	b_{flange} [mm]
Frame	2500	42.5	850	47.5	550
Long. Stiffener	625	12.5	220	N/A	N/A
Trans. Stiffener	125	12.5	110	N/A	N/A

Table 17. Bracings.

Member	Z [mm]	D_{outer} [mm]	t [mm]
Bracing 1	14.58	900	7.25
Bracing 2	20.76	900	7.25
Bracing 3	26.94	900	7.25

Table 18. J-Tubes.

Member	D_{outer} [mm]	t [mm]
J-Tube - EC	813	2.75
J-Tube - IAC	610	2.15

These scantlings are modelled as solids in Rhino so the total mass, centre of gravity, and radius of gyration can be obtained for further analysis, such as stability and seakeeping. Figures 26 to 36 illustrate the 3D model.

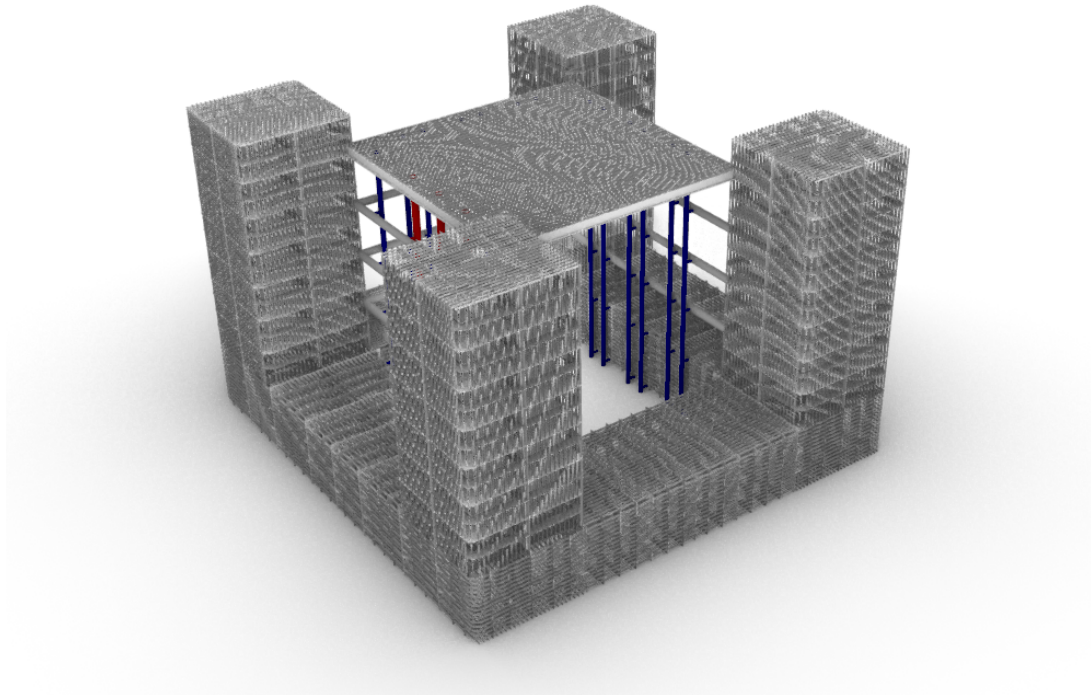


Figure 26. Scantling overview.

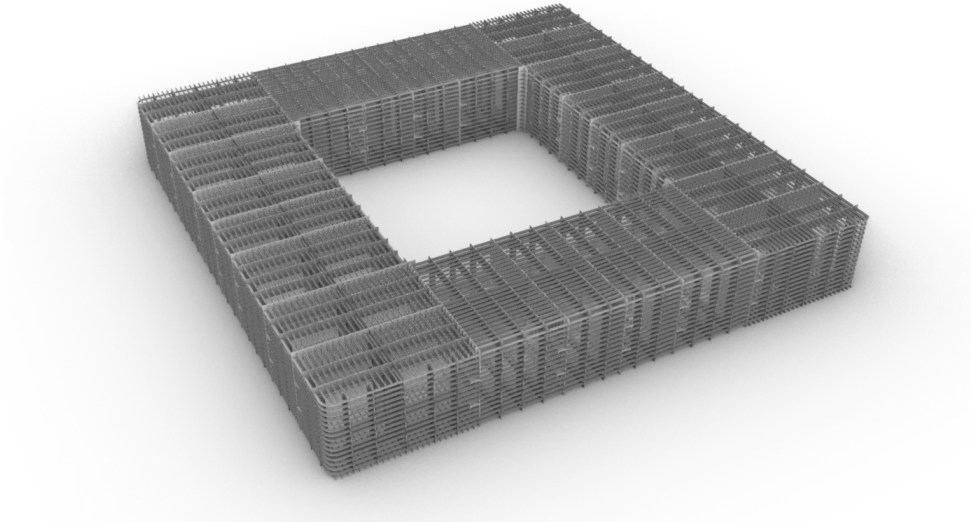


Figure 27. Pontoon and node scantling.

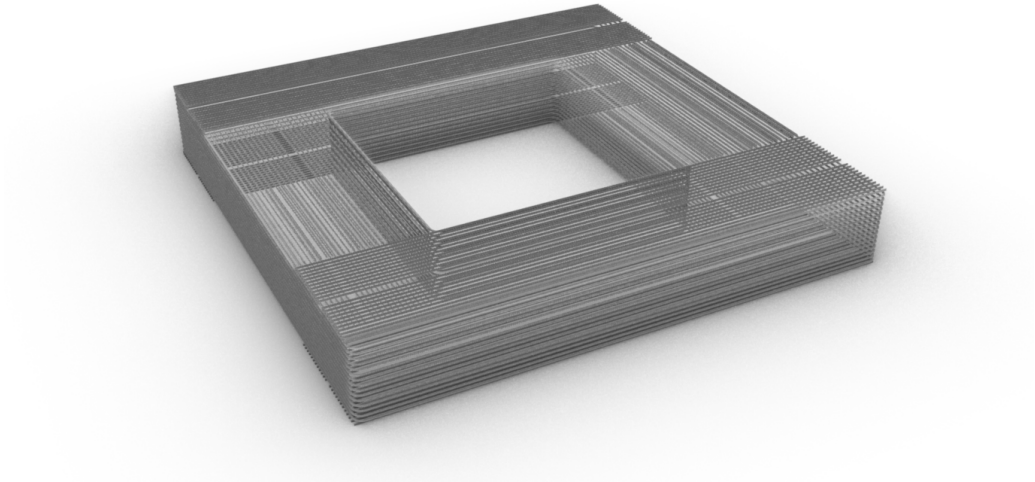


Figure 28. Pontoon and node stiffeners.

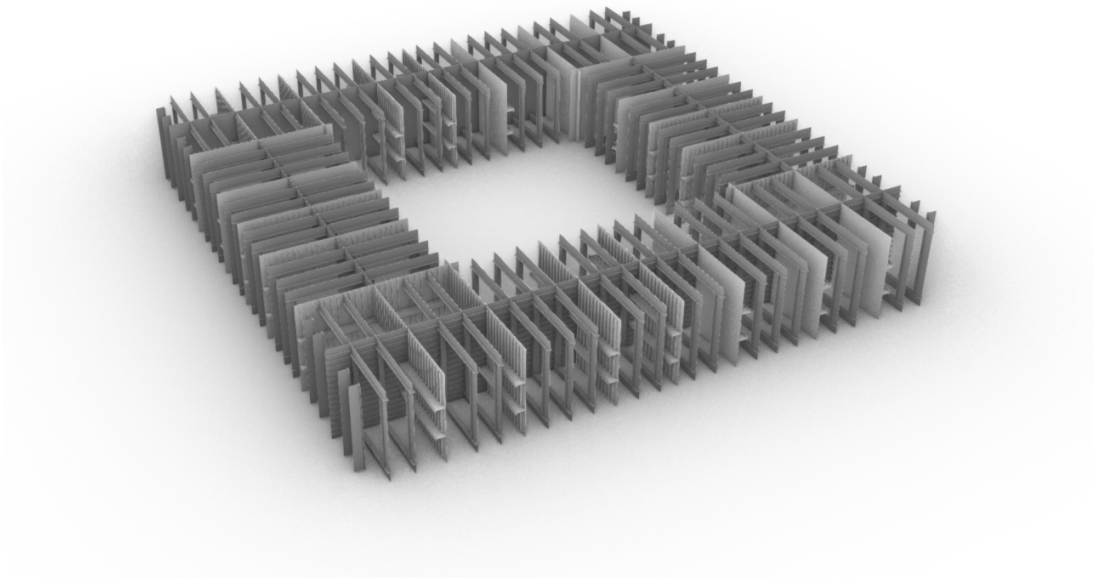


Figure 29. Pontoon and node bulkheads and frames.

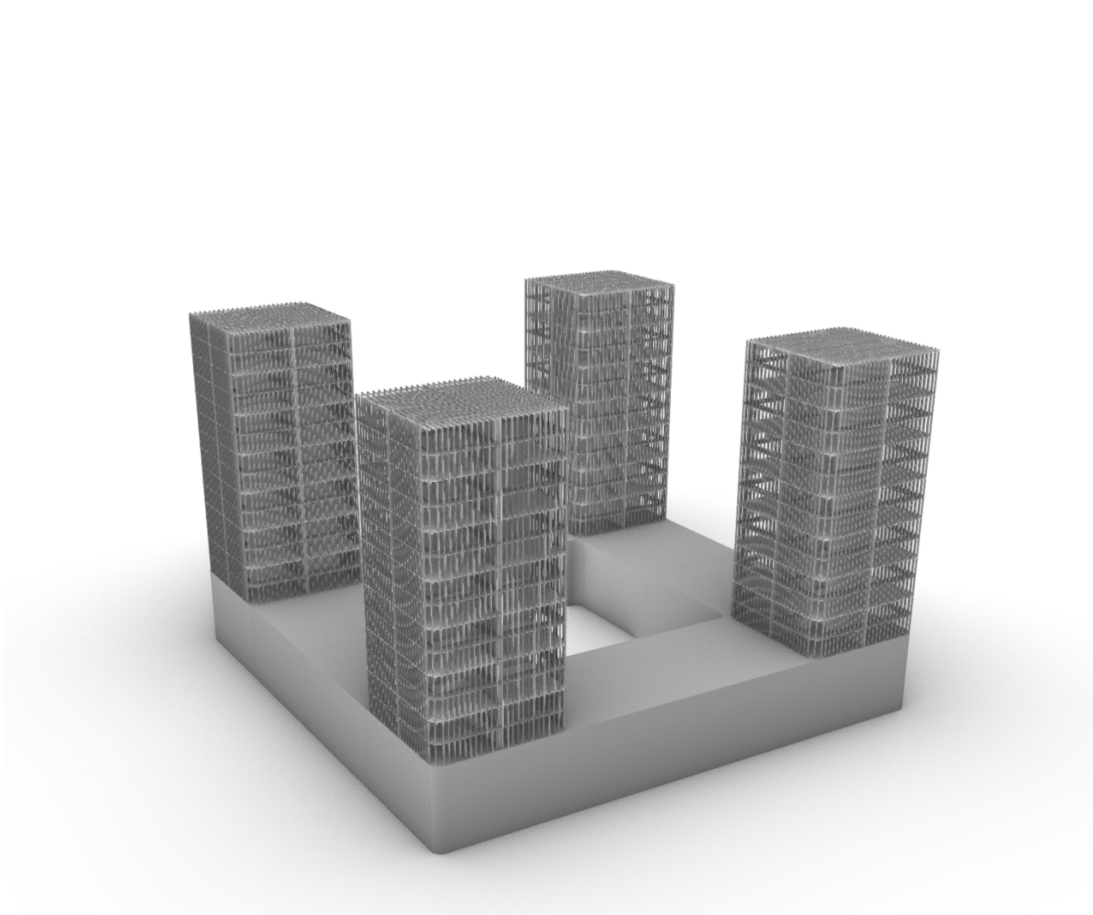


Figure 30. Column scantling.

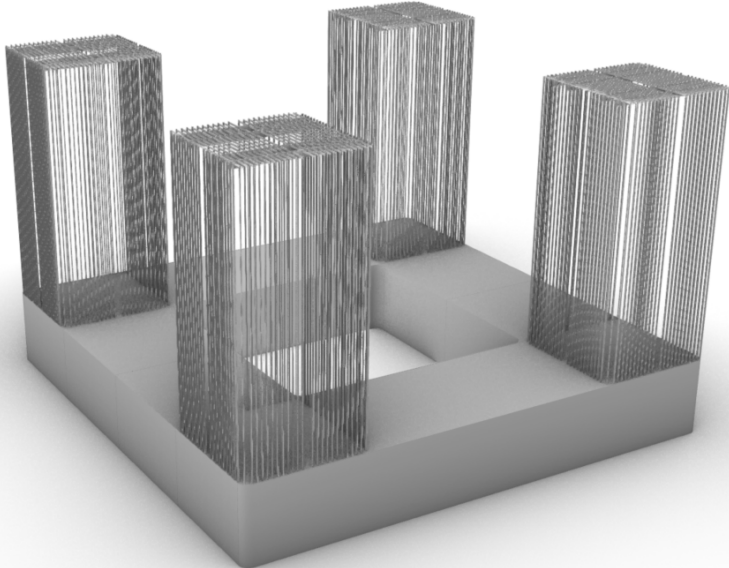


Figure 31. Column stiffeners.

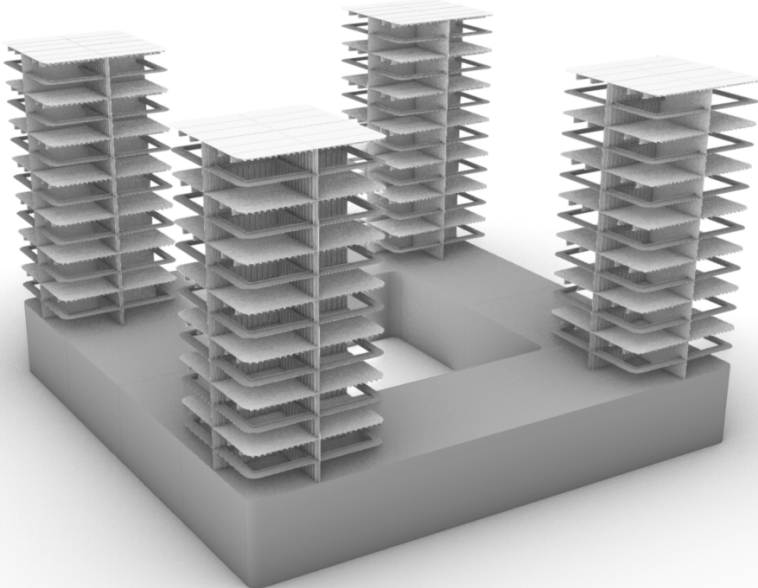


Figure 32. Column bulkheads and frames.

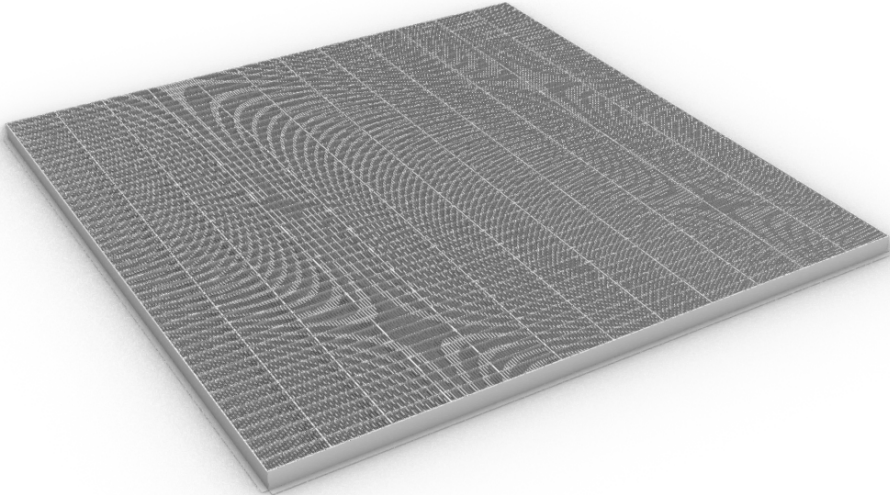


Figure 33. Deck scantling.

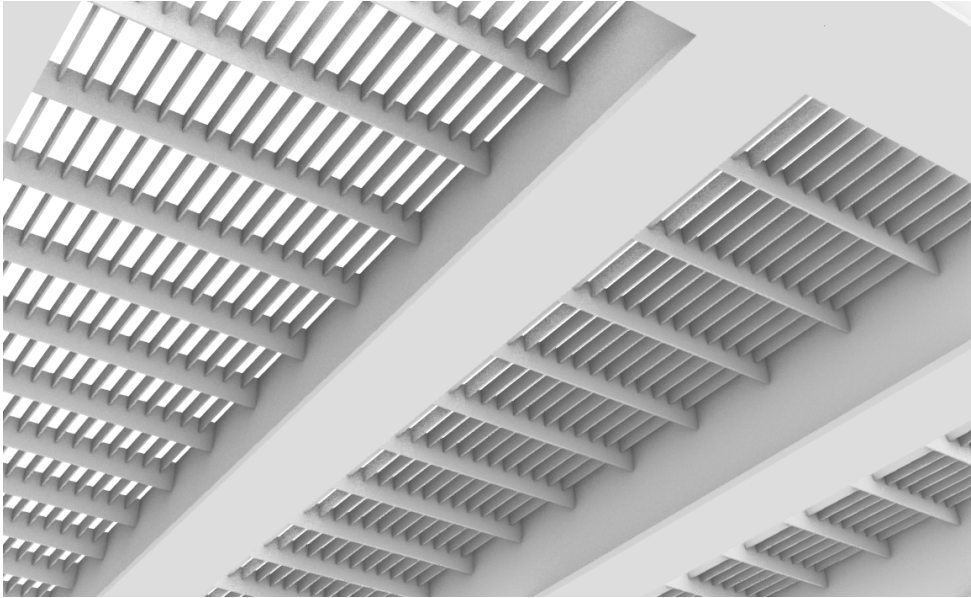


Figure 34. Deck scantling (detail).

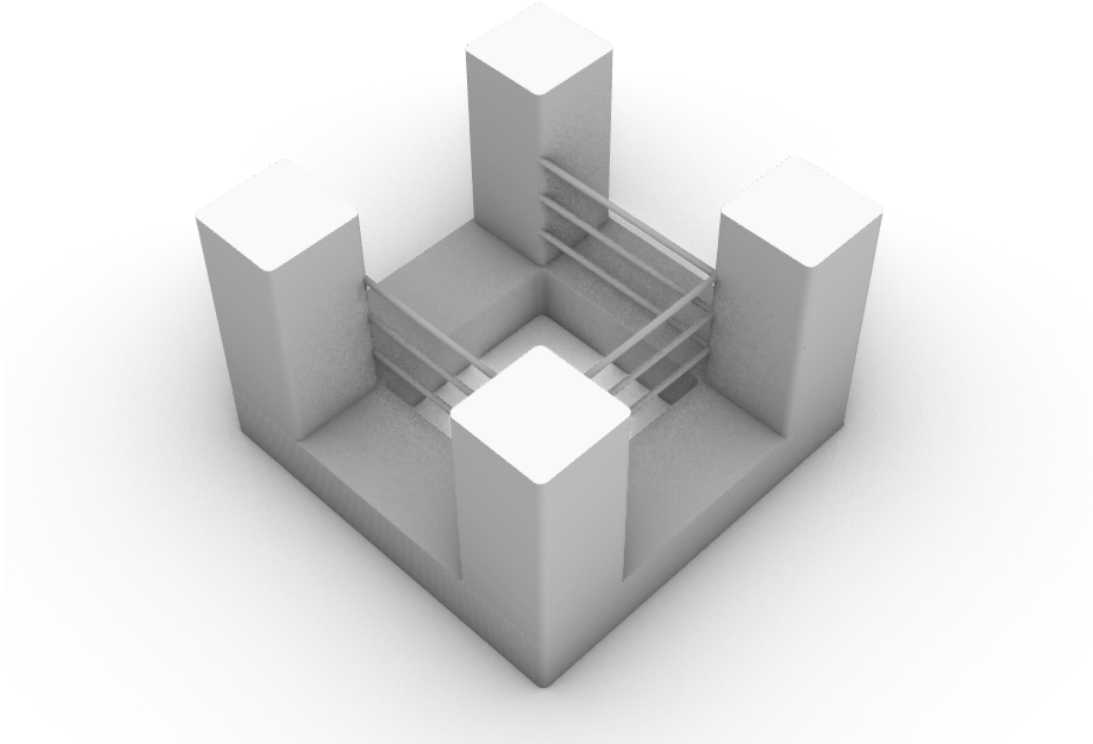


Figure 35. Transversal Bracings.

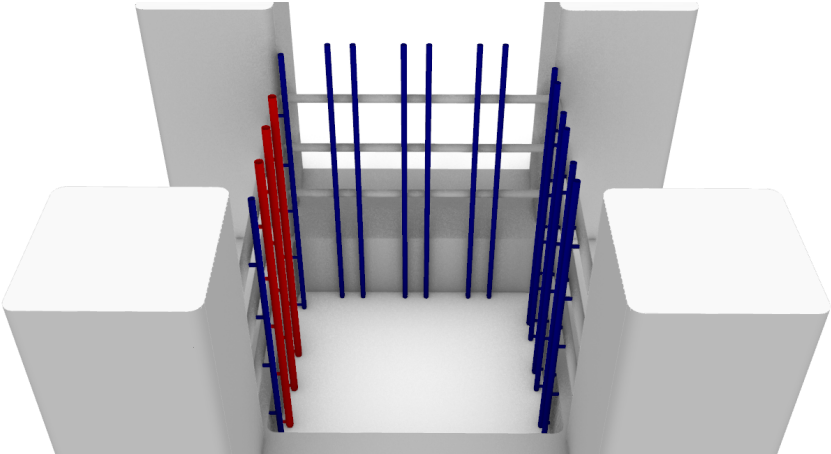


Figure 36. J-tubes.

The floater mass properties obtained from the Rhino model are summarized in Table 19. The LCG, TCG and VCG are referenced at the aft perpendicular, center line and keel of the platform, respectively.

Table 19. Steel mass properties.

Mass [tons]	10011
LCG [m]	27.67
TCG (+port)[m]	0.01
VCG [m]	15.09
I_{xx} [tons.m ²]	5003048
I_{yy} [tons.m ²]	4974715
I_{zz} [tons.m ²]	7242966
r_{xx} [m]	22.35
r_{yy} [m]	22.29
r_{zz} [m]	26.90

4.10.3. *Equilibrium & Stability*

Table 20 presents the mass and center of gravity obtained from the combination of the structural members designed. Also, it provides the required ballast weight, which accounts for 73.0% of the pontoons' and nodes' volume, considering a permeability of 90%.

Table 20. Masses and centers of gravity.

Component	Mass [tons]	LCG [m]	TCG [m]	VCG [m]
Lightweight	9577	27.39	0.00	14.53
Ballast	12547	27.39	0.00	3.09
Topside	6961	27.39	0.00	42.83
Total	29084	27.39	0.00	16.37

Table 21 provides the center of buoyancy, necessary for the initial GM calculation.

Table 21. Volumes and center of buoyancy.

Component	Volume [m ³]	LCB [m]	TCB [m]	VCB [m]
Long. pontoons	6299	27.39	0.00	4.20
Trans. pontoons	6299	27.39	0.00	4.20
Columns	9753	27.39	0.00	15.20
Nodes	6024	27.39	0.00	4.20
Total	28375	27.39	0.00	7.98

Tables 22 and 23 provide the waterline properties and the initial GM, respectively.

Table 22. Waterline properties.

WL Area [m ²]	179
WL Inertia [m ⁴]	2679
Distance CL [m]	20.70
WL Inertia CL [m ⁴]	79466
WL Total Inertia [m ⁴]	317866

Table 23. Initial GM calculation.

BM [m]	11.20
KB [m]	7.98
KG [m]	16.37
GM [m]	2.82

From the solid model built in Rhino, a mass difference of 4.3% and a vertical center of gravity increase of 0.2 meters are obtained. With the new steel mass, the ballast is reduced from 73.0% to 70.5% of the capacity. Tables 24 and 25 present the mass and initial GM calculated with the Rhino model.

Table 24. Masses and centers of gravity from Rhino.

Component	Mass [tons]	LCG [m]	TCG [m]	VCG [m]
Lightweight	10011	27.67	0.01	15.09
Ballast	12112	27.39	0.00	2.98
Topside	6961	27.39	0.00	42.83
Total	29084	27.49	0.00	16.69

Table 25. Initial GM calculation with Rhino input.

BM [m]	11.20
KB [m]	7.98
KG [m]	16.69
GM [m]	2.50

4.10.4. Motion In Heave

The heave added mass is calculated for the pontoons and columns separately. Table 26 and 27 provide the added mass and heave natural period, respectively.

Table 26. Added mass in heave.

Component	Pontoons	Columns
a [m]	6.70	6.70
b [m]	4.20	11.00
a/b	1.59	0.61
C_A	1.44	1.67
A_R	140.82	140.82
m_A [ton/m]	208.38	240.53
A [ton]	23339	12883

Table 27. Motion in Heave.

M [tons]	29084
A [tons]	36221
C_{33} [kN/m]	7211
ω_{33} [rad/s]	0.33
T_{33} [s]	18.91

5. STABILITY

In this section, the intact and damaged stability calculations with Maxsurf are detailed. For this, the load cases are defined, the stability criteria are introduced and the results are discussed.

5.1. Load Cases

5.1.1. *Intact Condition*

The transit and operating loading conditions are considered for the assessment of the floater's intact and damaged stability. The first one represents the condition in which the floater has a draft smaller than the operational one, to facilitate the towing operation to the designated operation site. The operating condition refers to the condition in which the substation is installed at the planned site and operating in the design draft. Tables 28 to 31 describe each load case after the lightweight and topside are included in the Maxsurf model and the ballast tanks are filled to reach the desired draft with no heel or trim. A detailed description of the load cases can be found in Appendix A, where all the compartment locations and tank specifications (volume, filling percentage, mass, free surface moment, and centre of gravity) are provided.

Table 28. Operational load case.

Component	Mass [tons]	LCG [m]	TCG (+port) [m]	VCG [m]
Lightweight	10011	27.67	0.01	15.09
Ballast	12051	27.15	0.00	2.95
Topside	6961	27.39	0.00	42.83
Total	29023	27.39	0.00	17.02 (fluid)

Table 29. Hydrostatics | Operational Load Case.

Draft Amidships [m]	22.00
Displacement [t]	29023
Heel [deg]	0.00
Draft at FP [m]	22.00
Draft at AP [m]	22.00
Trim (+ve by stern) [m]	0.00
KB [m]	7.91
KG fluid [m]	17.02
BMt [m]	11.19
GMt corrected [m]	2.14
KMt [m]	19.16

Table 30. Transit load case.

Component	Mass [tons]	LCG [m]	TCG (+port) [m]	VCG [m]
Lightweight	10011	27.67	0.01	15.09
Ballast	11394	27.14	0.00	2.79
Topside	6961	27.39	0.00	42.83
Total	28367	27.39	0.00	17.28 (fluid)

Table 31. Hydrostatics | Transit Load Case.

Draft Amidships [m]	21.11
Displacement [t]	28367
Heel [deg]	0.00
Draft at FP [m]	21.11
Draft at AP [m]	21.11
Trim (+ve by stern) [m]	0.00
KB [m]	7.66
KG fluid [m]	17.28
BMt [m]	11.447
GMt corrected [m]	1.83
KMt [m]	19.11

Figure 37 shows the Maxsurf model with the ballast tanks (green) and watertight compartments (yellow). It should be mentioned that the geometry had to be simplified due to issues encountered when importing it to Maxsurf Modeler. Nevertheless, the model shown

below is still capable of representing the behavior of the structure introduced in Section 4.10.1.

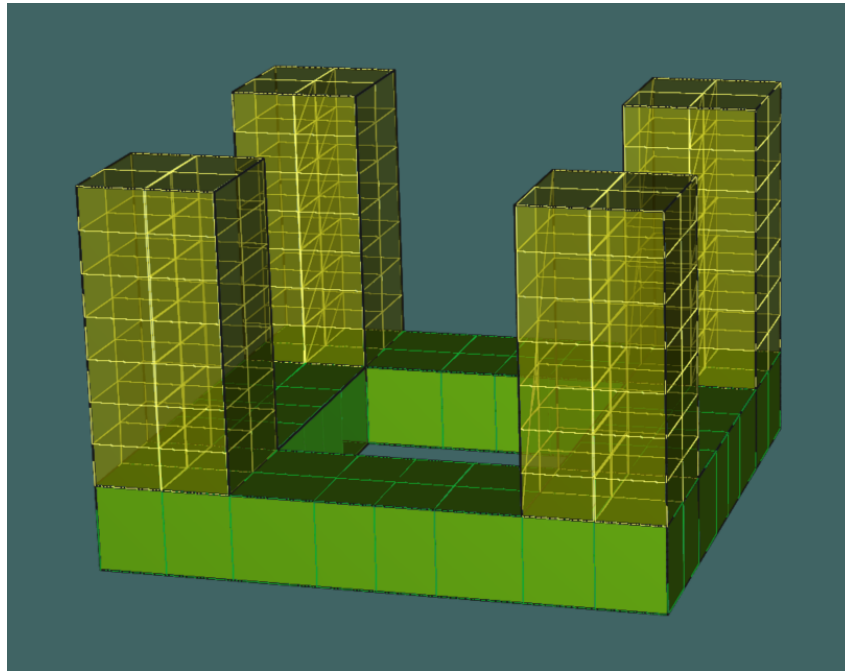


Figure 37. Maxsurf model for stability calculation.

The mooring lines are already installed for the operating condition, but their presence is disregarded for stability purposes. The mooring lines lower the overall center of gravity, which improves the platform's stability. Regarding the overturning wind moment, the mooring lines may increase the wind lever by lowering the resistance point, if the fairleads are located at the baseline. However, these are planned to be installed around 6 meters below the waterline level, to allow the presence of visiting vessels and reduce pitch and roll motions. This position is above the lateral resistance point. Therefore, no detrimental effect related to the presence of mooring lines is expected when it comes to the floater's stability, and disregarding them is a conservative approach.

5.1.2. *Damaged Condition*

The damaged load cases are defined by combining the transit and operating conditions with some of the possible damages the floater might be subjected to. These damages are based on the extent of peripheral damage defined by DNV. These are listed below:

- Horizontal penetration shall be assumed to be 1.5 meters.
- The damage vertical extent shall be 3 meters between 5 meters above and 3 meters below the defined draft. If a watertight flat is within this region, it must be assumed damaged and the adjacent compartments flooded. At least 1.5 meters above and below the water line should be damaged. Figure 38 illustrates the vertical damage extent and horizontal penetration.

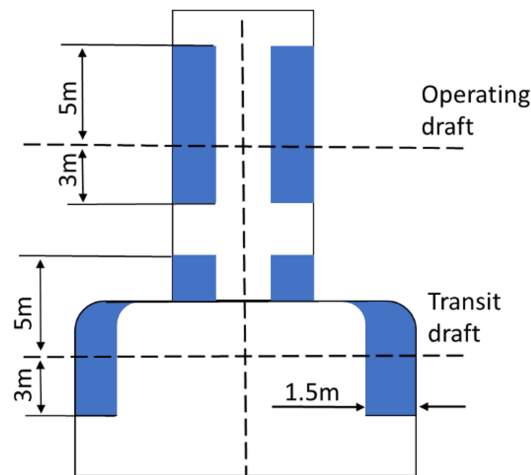


Figure 38. Vertical extent of damage including normal penetration (DNV 2018).

- No column vertical bulkheads shall be assumed damaged unless they are spaced by less than one-eighth of the column perimeter, measured at the periphery. Similarly, pontoon vertical bulkheads shall only be assumed damaged if they are less than 3 meters apart. Figure 39 illustrates the bulkhead spacing described.

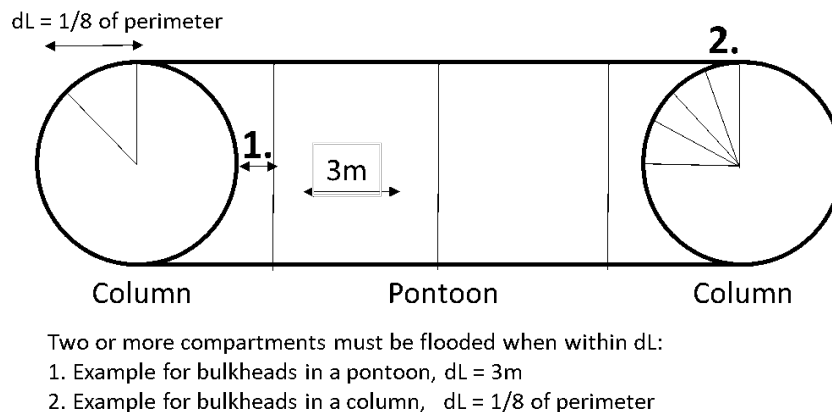


Figure 39. Horizontal extent of damage in the tangential direction to the outer hull (DNV 2018).

Since the waterline in both load cases is more than 5 meters above the pontoons, the damage is assumed to take place only in the columns. Also, no bulkhead damage due to horizontal penetration is assumed since all bulkheads are more than 1.5 meters away from the shell. Regarding the vertical damage, its extent is assumed to be from 1.5 meters below to 1.5 meters above the water line. The waterline position of both load cases results in the damage of a horizontal bulkhead in the columns. Lastly, the vertical bulkheads are 13.39 meters apart measure in the periphery and $1/8$ of the column perimeter is 6.695 meters, so none of them are assumed damaged.

Due to the symmetry of the platform, only one column is damaged. Figure 40 illustrates the damage cases considered. The damaged compartments are BTFC11 and BTFC15 in damage case 1 and BTFC12 and BTFC16 in damage case 2. Details about these compartments can be found in Appendix A.

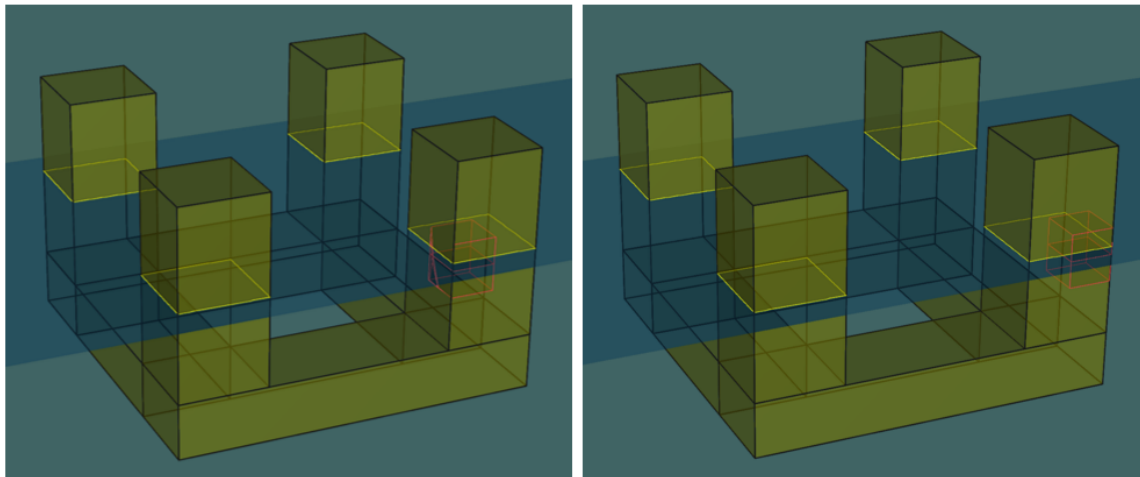


Figure 40. Damage 1 (left) & 2 (right).

5.2. Heeling Moments

According to DNV, the intact floater should be subjected to a wind speed of 70 knots (36 m/s) during the transit and operating conditions and 100 knots (51.5 m/s) during operation conditions under severe storm weather. This increase in the wind speed is to represent an extreme wind gust, long enough to heel the unit.

A wind speed of 50 knots (25.8 m/s) may be assumed for a damaged condition. That is because damage, normally caused by a support vessel, would only take place in mild environmental conditions that allow the vessel's presence. The wind force is given by Equation 25 (DNV 2020).

$$F_{wind} = 0.5 \cdot C_s \cdot C_h \cdot P \cdot V^2 \cdot A \quad [N] \quad (25)$$

Where:

C_s is the shape coefficient.

C_h is the height coefficient

P is the air mass density (1.222 kg/m³).

V is the wind velocity (m/s).

A is the projected area of all exposed surfaces in either upright or heeled (m²).

C_s is set as 1.0, used for large flat surfaces, and C_h is 1.1, recommended for a height above sea level from 15.3 to 30.5 meters. The wind heeling moment is given by Equation 26.

$$M_{wind} = F_{wind} \cdot (Z_{wind} - Z_{resistance}) \quad [N.m] \quad (26)$$

Where:

Z_{wind} is the height where the aerodynamic force acts. It is located in the geometric center of all exposed surfaces.

$Z_{resistance}$ is the height where the resistance force acts. It is located at the geometry center of the submerged hull projected area.

The wind heeling moment of ships can be approximated by the moment in the upright condition multiplied by the heeling angle cosine. However, in the case of a semi-submersible, certain areas are exposed to the wind as the floater heels. Therefore, the windage area, resistance area, and their respective centers are calculated for some heel angles to compose the wind heeling moment curve. Figure 41 shows the heeling moment of the three wind speeds considered.

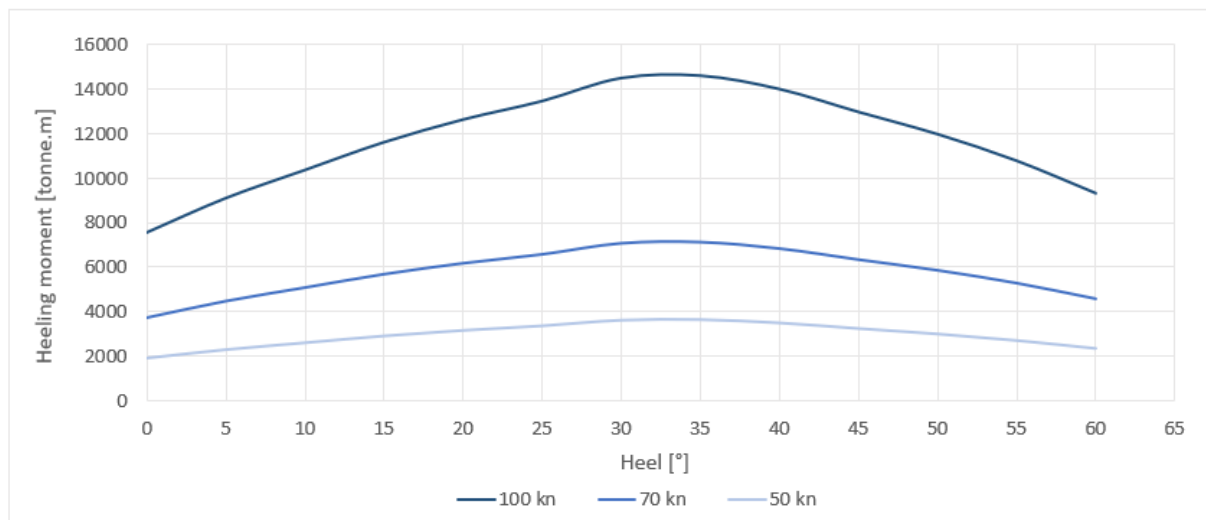


Figure 41. Heeling moment.

As a matter of comparison, the heeling moment calculated for each angle is plotted against the cosine approximation of the vertical heeling moment and a clear discrepancy can be seen. Figure 42 shows these two curves.

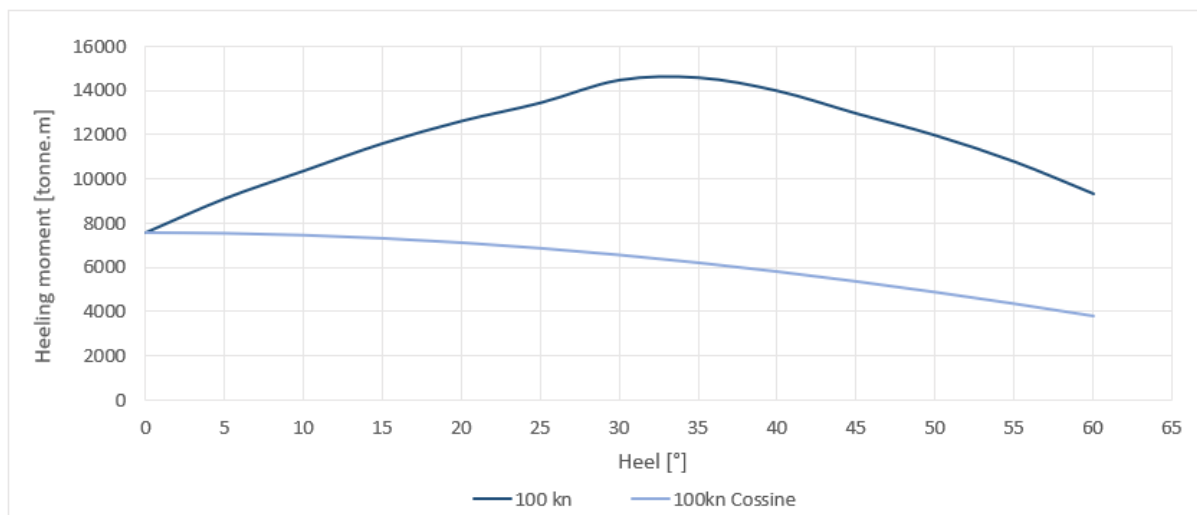


Figure 42. Heeling moment comparison.

5.3. Criteria

5.3.1. *Intact Stability*

The stability is assessed according to a quasi-static methodology, which consists of integrating the moment curves for the heeling angle. The intact stability criteria employed are according to DNV standards (DNV 2020):

- The area under the righting moment curve to the angle of downflooding shall be 30% higher than the area under the heeling moment curve to the same limiting angle.
- DNV does not recommend a maximum static heel angle due to the wind action, θ_1 . However, since the heel angle limit of the electrical equipment under extreme conditions is 13° (Table 6), this is the limiting value for θ_1 under 100-knot wind speed. Also, the maximum heel angle under normal operation is 7° . Therefore, this value must be complied with for a 70-knot wind speed.
- The metacentric height, GM, must be at least 1 meter in operating, transit, and survival conditions and not less than 0.3 meters during temporary conditions.
- The righting moment curve shall be positive over the entire range of angles from upright to the second intercept, θ_2 .

An intact permeability factor of 0.90 is applied to the ballast tanks. The downflooding points are set at the highest point of the external edge of each column. These are summarized in Table 32

Table 32. Downflooding points.

Point	x [m]	y [m]	z [m]
Downflooding Pt. 1	54.78	27.39	37.3
Downflooding Pt. 2	54.78	-27.39	37.3
Downflooding Pt. 3	0.00	-27.39	37.3
Downflooding Pt. 4	0.00	27.39	37.3

5.3.2. Damaged Stability

The stability standards for peripheral damage provided by DNV (DNV 2020) are the following:

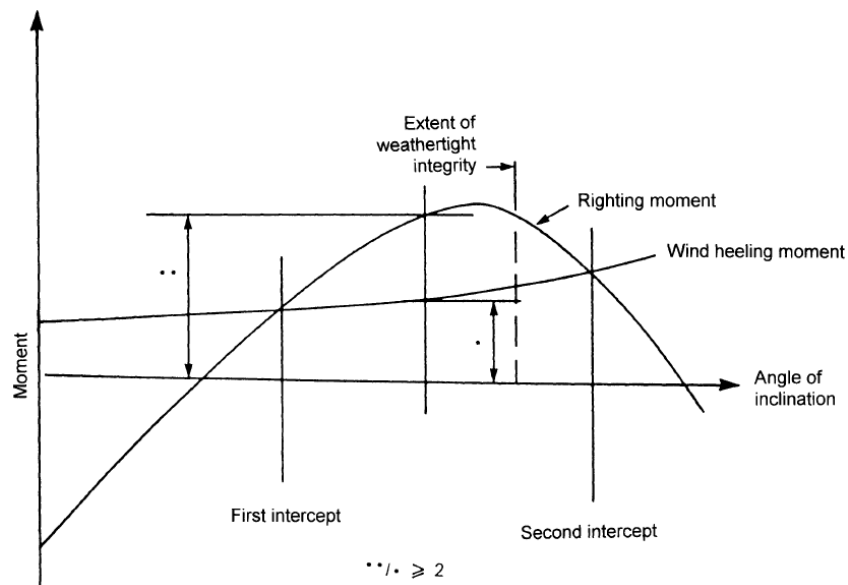


Figure 43. Righting and heeling moment curve (DNV 2020).

- The static angle without wind must be lower than 17° . However, for the same reason established in the previous section, the limiting angle is reduced to 13° .
- The zone of watertight integrity must be higher than 4 meters above any damaged waterplane.
- The damaged righting moment curve shall have, from the first intercept to the extent of weathertight integrity required in the previous item or to the second intercept, whichever is smaller, a range of at least 7° . Within this range, the righting moment should present a value twice higher than the wind heeling moment, measured at the same angle.

A damaged permeability factor of 0.95 (DNV 2020) is applied to the ballast tanks and watertight compartments.

5.4. Results

In the following sections, the intact and damaged equilibrium conditions and stability are described for both conditions analyzed.

5.4.1. Intact Stability

- Operational Load Case

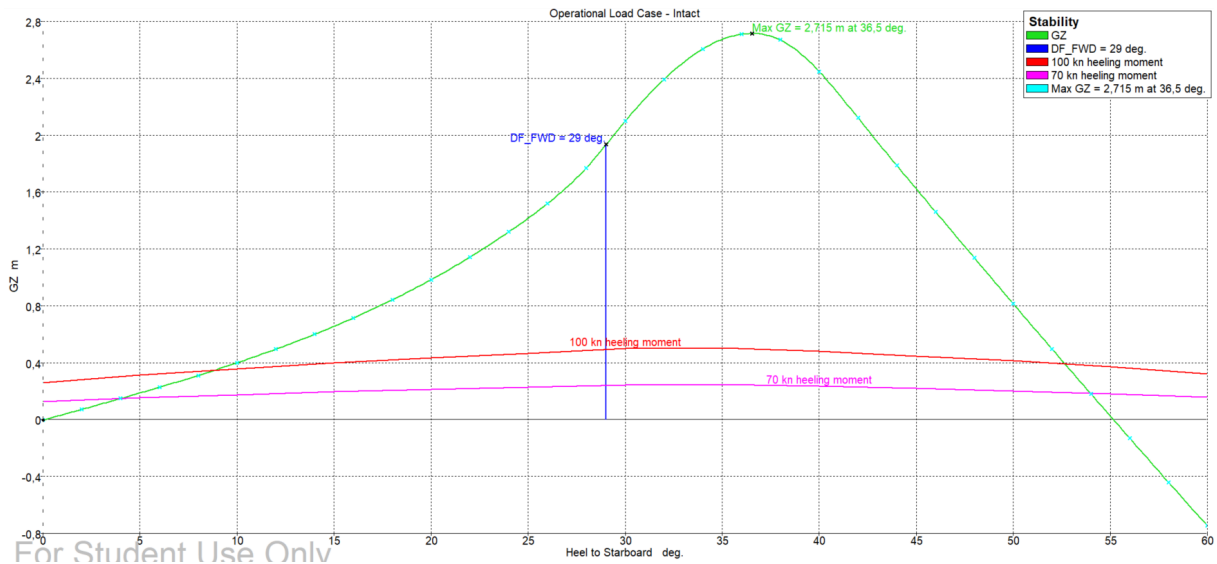


Figure 44. GZ curve | Intact | Operational Load Case.

Table 33. Criteria evaluation | Operational Load Case.

Criterion	Required value	Obtained value
Area ratio	> 130.0%	384.8%
θ_1 (100 knots)	< 13.0°	8.8°
θ_1 (70 knots)	< 7.0°	4.0°
$GM_{initial}$	> 1.00 meter	2.14 meters
Positive GZ	-	OK

- Transit Load Case

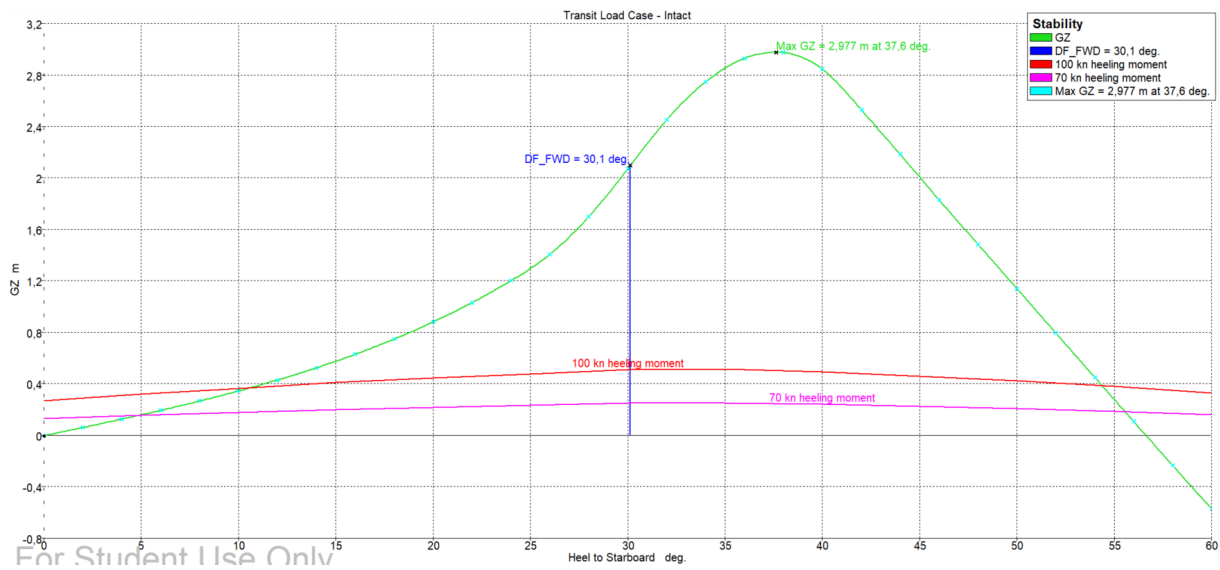


Figure 45. GZ curve | Intact | Transit Load Case.

Table 34. Criteria evaluation | Transit Load Case.

Criterion	Required value	Obtained value
Area ratio	> 130.0%	362.2%
θ_1 (100 knots)	< 13.0°	10.6°
θ_1 (70 knots)	< 7.0°	4.9°
$GM_{initial}$	> 1.00 meter	1.83 meters
Positive GZ	-	OK

5.4.2. Damaged Stability

- Damaged Load Case 1 | Operational

Table 35. Hydrostatics | Damage Case 1 | Operational Load Case.

Draft Amidships [m]	22.47
Displacement [t]	29023
Heel [deg]	7.1
Draft at FP [m]	24.84
Draft at AP [m]	20.09
Trim (+ve by stern) [m]	-4.75
KB [m]	8.12
KG fluid [m]	17.02
BMt [m]	11.50
GMt corrected [m]	2.50
KMt [m]	19.49

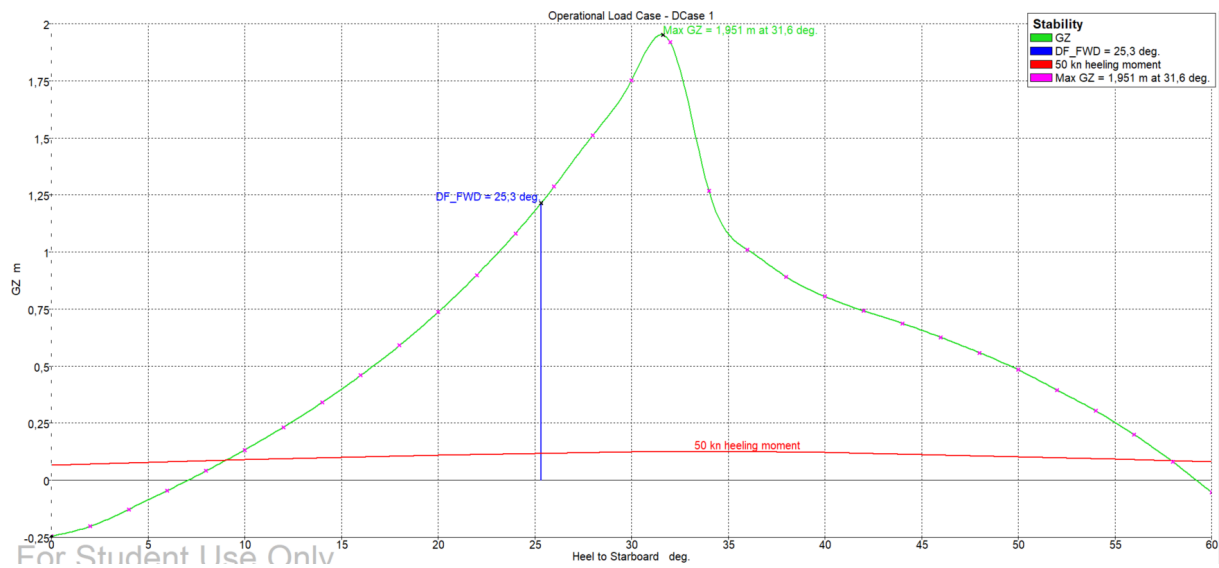


Figure 46. GZ curve | Damage Case 1 | Operational Load Case.

Table 36. Criteria evaluation | Damage Case 1 | Operational Load Case.

Criterion	Required value	Obtained value
θ_{eq}	< 13.0°	7.1°
Watertight integrity zone	> 4.00 meters	9.02 meters
GZ range	> 7.0°	8.8°
GZ/HA	> 2.00	5.47

- Damaged Load Case 2 | Operational

Table 37. Hydrostatics | Damage Case 2 | Operational Load Case.

Draft Amidships [m]	22.46
Displacement [t]	29023
Heel [deg]	7.0
Draft at FP [m]	25.72
Draft at AP [m]	19.21
Trim (+ve by stern) [m]	-6.51
KB [m]	8.15
KG fluid [m]	17.02
BMt [m]	11.53
GMt corrected [m]	2.54
KMt [m]	19.52

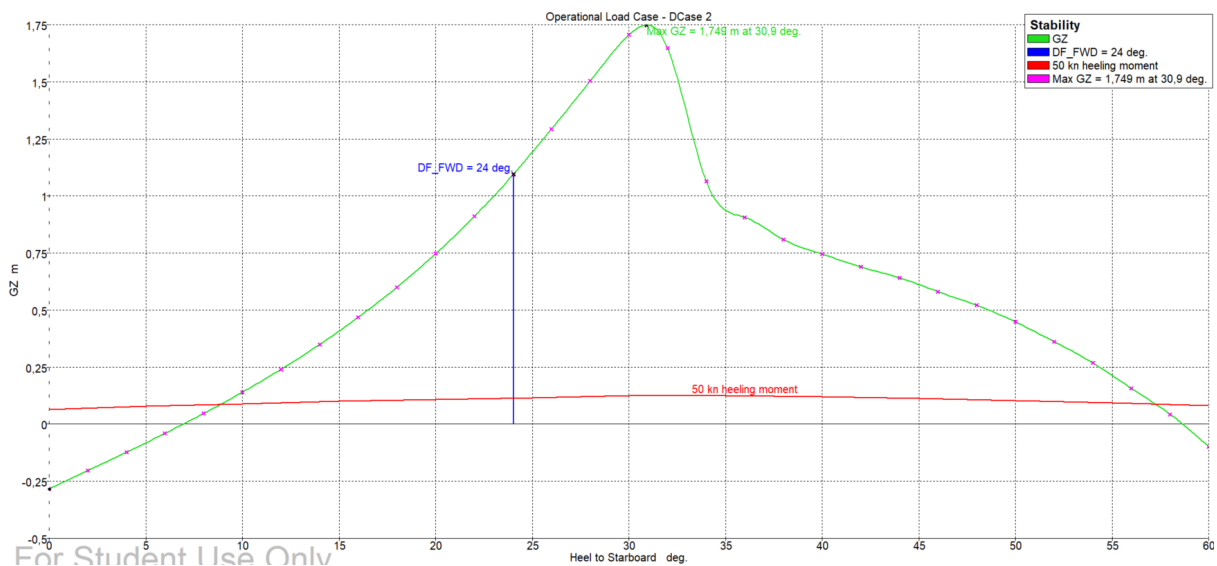


Figure 47. GZ curve | Damage Case 2 | Operational Load Case.

Table 38. Criteria evaluation | Damage Case 2 | Operational Load Case.

Criterion	Required value	Obtained value
θ_{eq}	< 13.0°	7.0°
Watertight integrity zone	> 4.00 meters	8.24 meters
GZ range	> 7.0°	7.3°
GZ/HA	> 2.00	4.70

- Damaged Load Case 1 | Transit

Table 39. Hydrostatics | Damage Case 1 | Transit Load Case.

Draft Amidships [m]	21.57
Displacement [t]	28367
Heel [deg]	8.3
Draft at FP [m]	24.33
Draft at AP [m]	21.57
Trim (+ve by stern) [m]	-5.53
KB [m]	7.84
KG fluid [m]	17.28
BMt [m]	11.89
GMt corrected [m]	2.30
KMt [m]	19.55

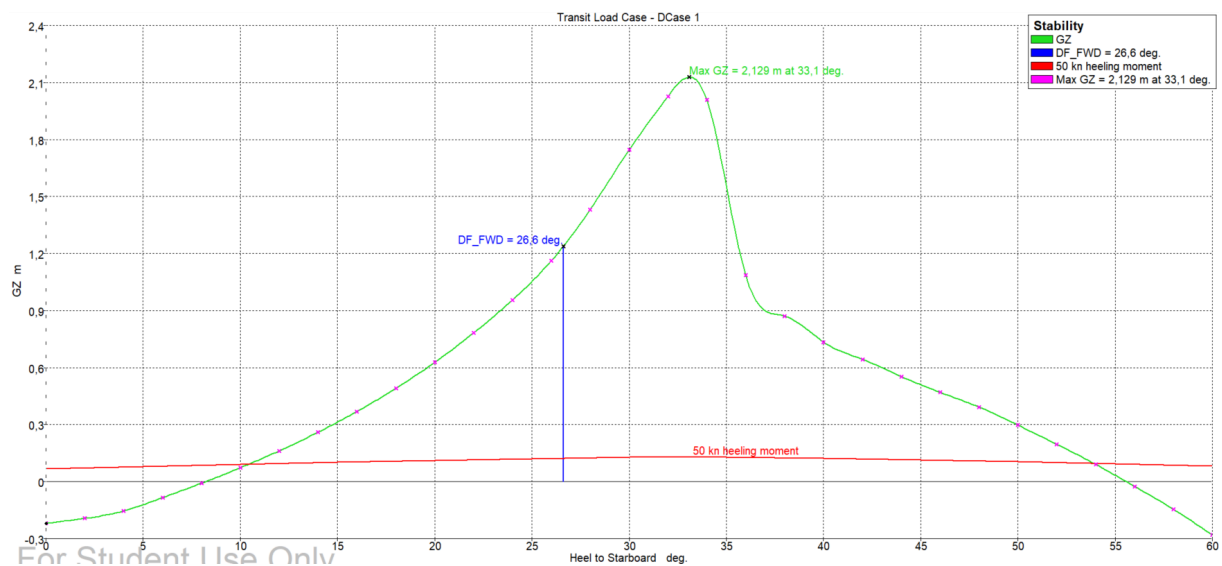


Figure 48. GZ curve | Damage Case 1 | Transit Load Case.

Table 40. Criteria evaluation | Damage Case 1 | Transit Load Case.

Criterion	Required value	Obtained value
θ_{eq}	< 13.0°	8.3°
Watertight integrity zone	> 4.00 meters	8.96 meters
GZ range	> 7.0°	8.6°
GZ/HA	> 2.00	5.08

- Damaged Load Case 2 | Transit

Table 41. Hydrostatics | Damage Case 2 | Transit Load Case.

Draft Amidships [m]	21.57
Displacement [t]	28367
Heel [deg]	8.0
Draft at FP [m]	25.31
Draft at AP [m]	21.57
Trim (+ve by stern) [m]	-7.49
KB [m]	7.89
KG fluid [m]	17.28
BMt [m]	11.91
GMt corrected [m]	2.34
KMt [m]	19.58

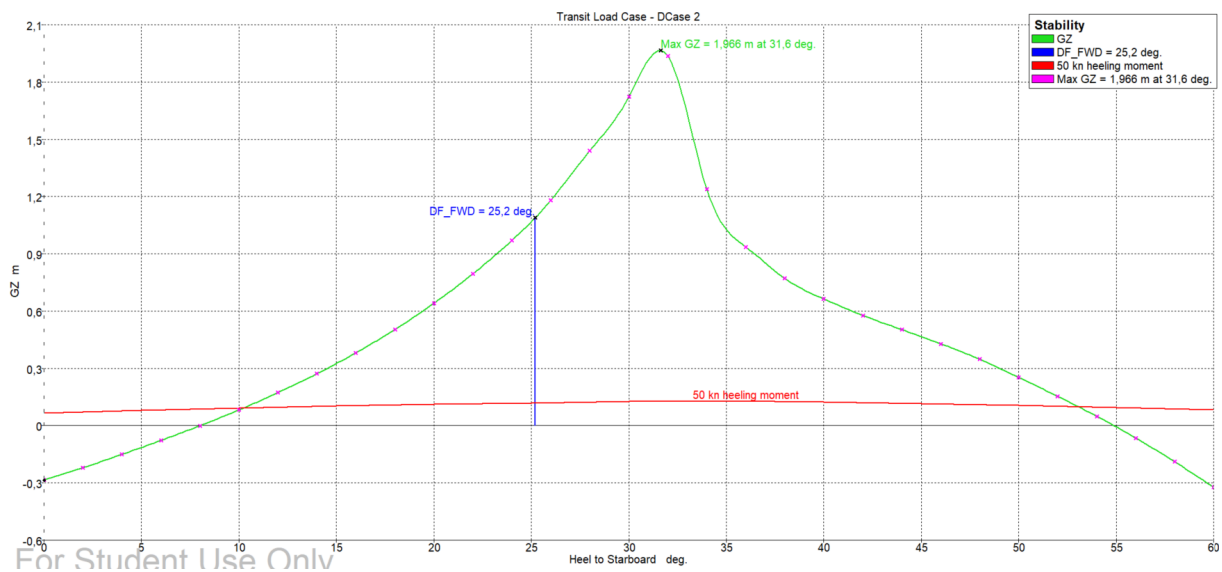


Figure 49. GZ curve | Damage Case 2 | Transit Load Case.

Table 42. Criteria evaluation | Damage Case 2 | Transit Load Case.

Criterion	Required value	Obtained value
θ_{eq}	$< 13.0^\circ$	8.0°
Watertight integrity zone	> 4.00 meters	8.13 meters
GZ range	$> 7.0^\circ$	7.0°
GZ/HA	> 2.00	4.27

6. PLATFORM MOTIONS

In this section, the motion and load Response Amplitude Operators (RAOs) calculated with OrcaWave are presented. They are generated after a mesh that is created and imported from Ansys Aqwa since OrcaWave does not generate the hydrodynamic mesh. The mesh size is defined according to the software recommendation based on the range of frequencies that the RAOs are generated for. The mesh is composed of 1-meter elements. Figure 50 shows the hydrodynamic mesh.

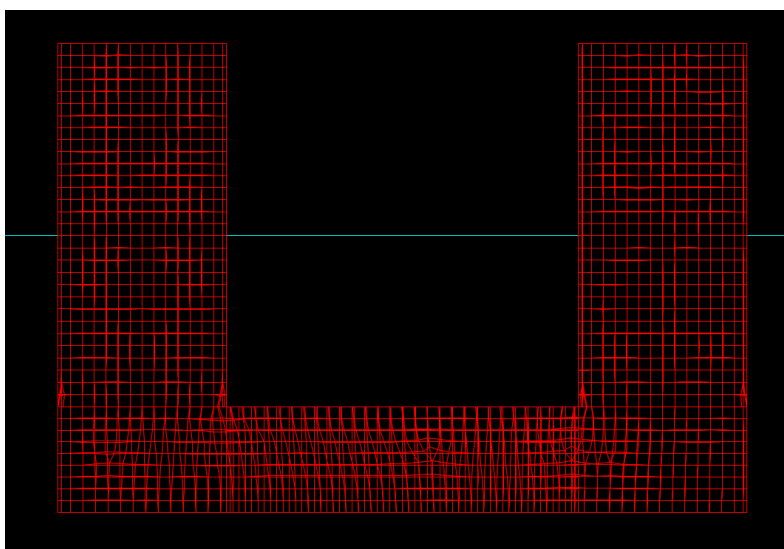


Figure 50. Hydrodynamic mesh.

The total radius of gyration included in OrcaWave is the combination of the structure, ballast water and topside inertia about the overall centre of gravity. Tables 43 and 44 show the platform mass inertia and radius of gyration, respectively.

Table 43. Platform inertia.

Component	I_{xx} [tons.m ²]	I_{yy} [tons.m ²]	I_{zz} [tons.m ²]
Structure	5028542	5000548	7243307
Ballast water	6078140	6113297	7570701
Topside	6486805	6486870	3137111
Total	17593487	17600715	17951119

Table 44. Platform radius of gyration.

r_{xx} [m]	r_{yy} [m]	r_{zz} [m]
24.59	24.60	24.84

OrcaWave performs the calculations using the potential flow theory, which means that no viscous effect is taken into account, such as viscous damping. Even though this effect is relevant for the assessment of offshore structures motions (MALTA 2010), only potential damping is included in the analysis performed in this work. This is approach assumed because, in a preliminary design stage, this effect can be disregarded. Also, a smaller damping results in more severe motions than expected, so this assumption provides a conservative estimation of the platform's dynamic behaviour. Lastly, additional damping would increase the platform's natural periods, moving them further away from the wave excitation periods. Figures 51 to 62 show the RAOs.

Since there is no restoring force in surge, the RAO in this motion shown in Figure 51 only increases with the wave period. The sway motion is not excited by a 0° wave incidence, so its RAO can be disregarded. However, it would be the same as that of surge in case the waves had a 90° incidence.

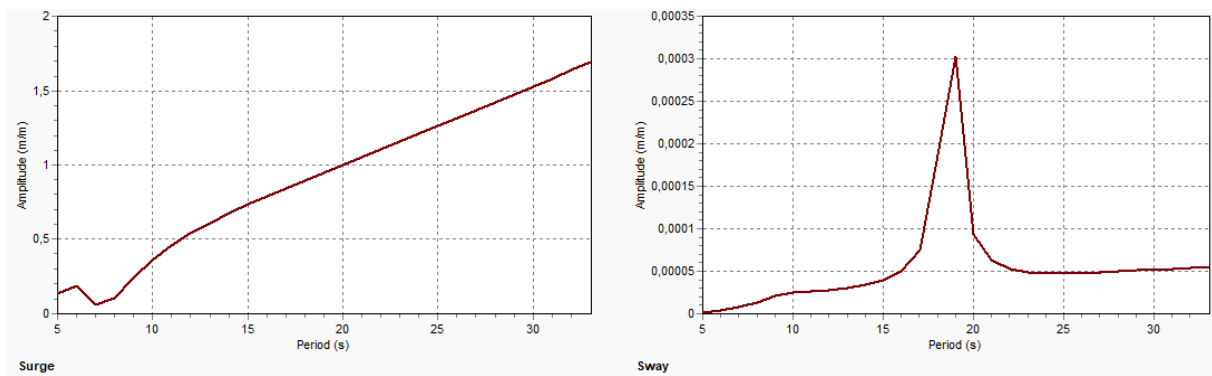


Figure 51. Displacement RAO | Surge & Sway | 0 Degrees.

In Figure 52, the roll RAO can be disregarded, since a wave incidence 0° does not excite this motion. However, its natural period is the same as that of pitch, which is 10 seconds.

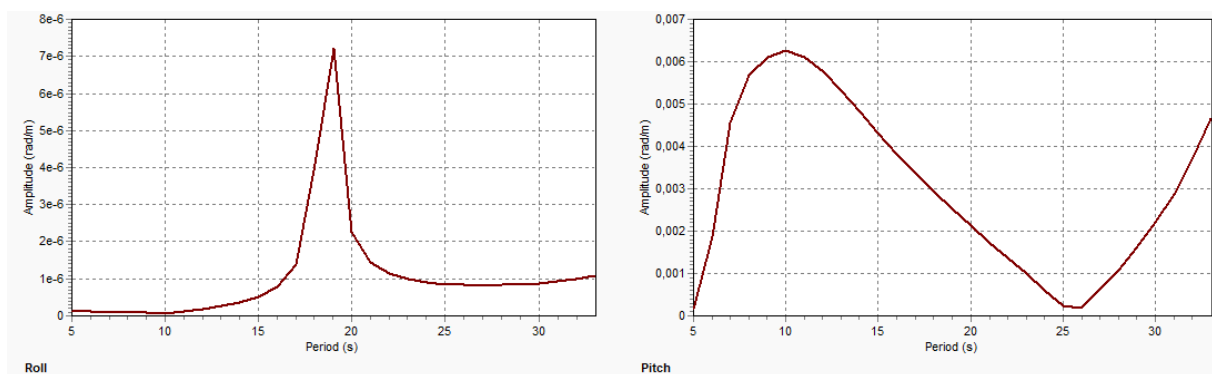


Figure 52. Displacement RAO | Roll & Pitch | 0 Degrees.

In Figure 53, it is clear that the heave natural period is 19 seconds, which agrees with the geometry optimization restrictions. It should be mentioned that the heave natural

period was estimated accurately using the formulations provided by DNV (DNV 2014) because they are also based on potential flow. In case viscosity was included in OrcaWave, a higher heave natural period would have been found for heave, roll and pitch.

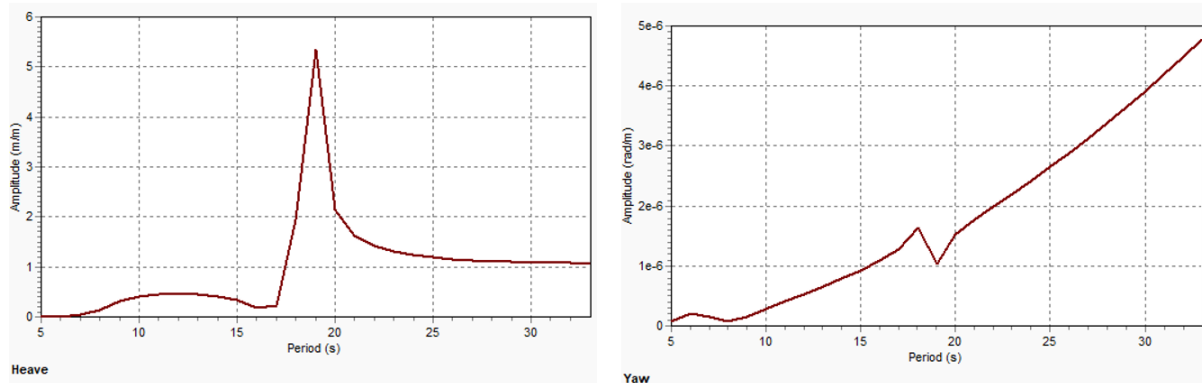


Figure 53. Displacement RAO | Heave & Yaw | 0 Degrees.

In Figures 54 and 55, the RAOs have the same shape and amplitude due to the platform symmetry.

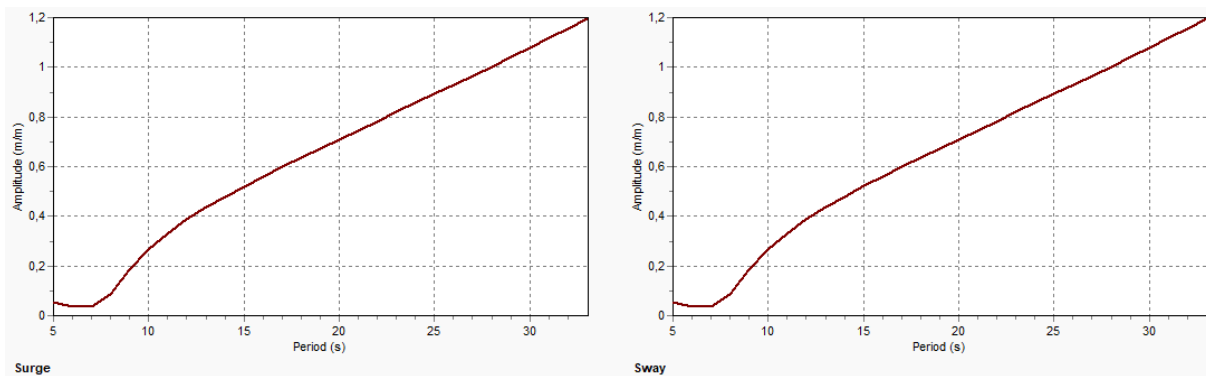


Figure 54. Displacement RAO | Surge & Sway | 45 Degrees.

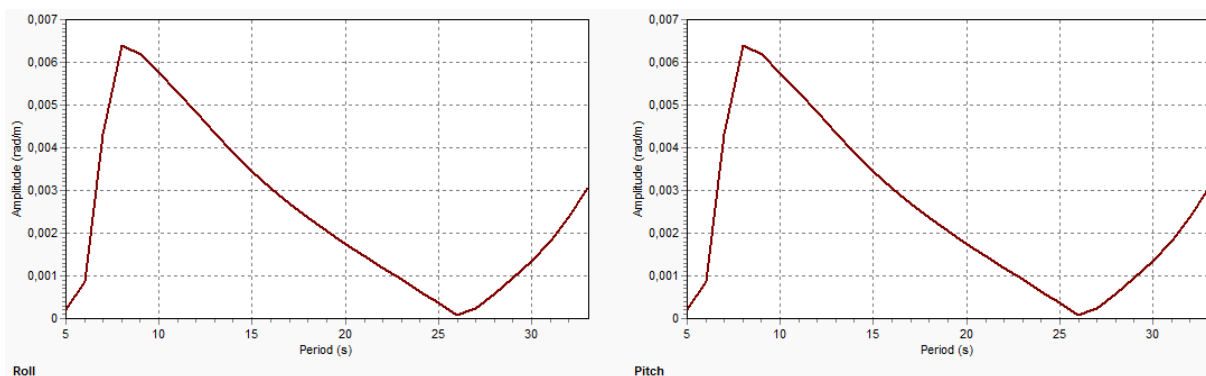


Figure 55. Displacement RAO | Roll & Pitch | 45 Degrees.

The heave RAO shown in Figure 56 is the same as the one obtained for a 0° wave incidence and the yaw movement is not excited due to the platform symmetry in the angle at which the waves approach it.

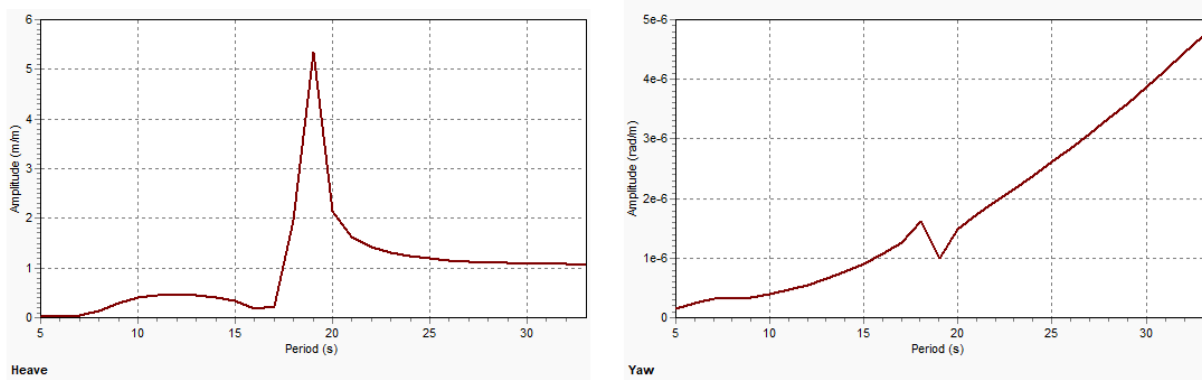


Figure 56. Displacement RAO | Heave & Yaw | 45 Degrees.

The load RAOs provide the force and moments to which the platform is subjected for a certain wave height and period. It can be noticed that, for all load RAOs, there is a trend of convergence to a constant value as the wave period increases, which is an expected behaviour.

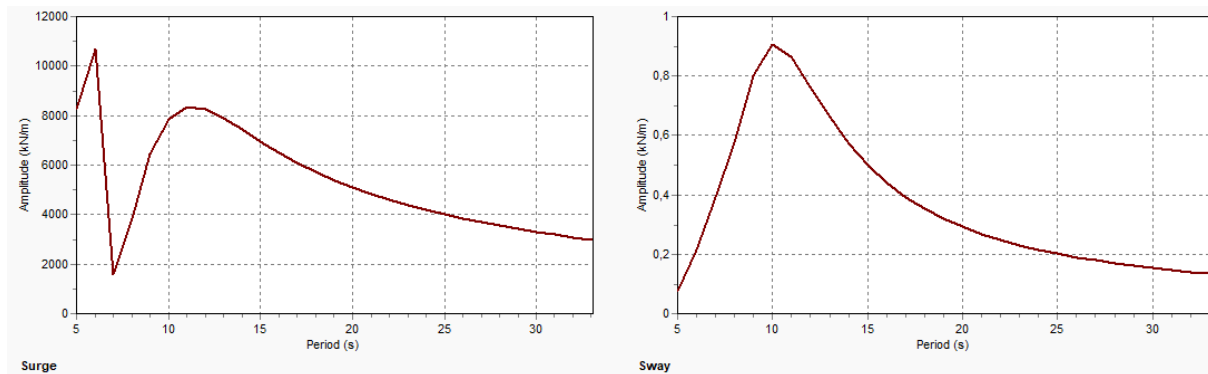


Figure 57. Load RAO | Surge & Sway | 0 Degrees.

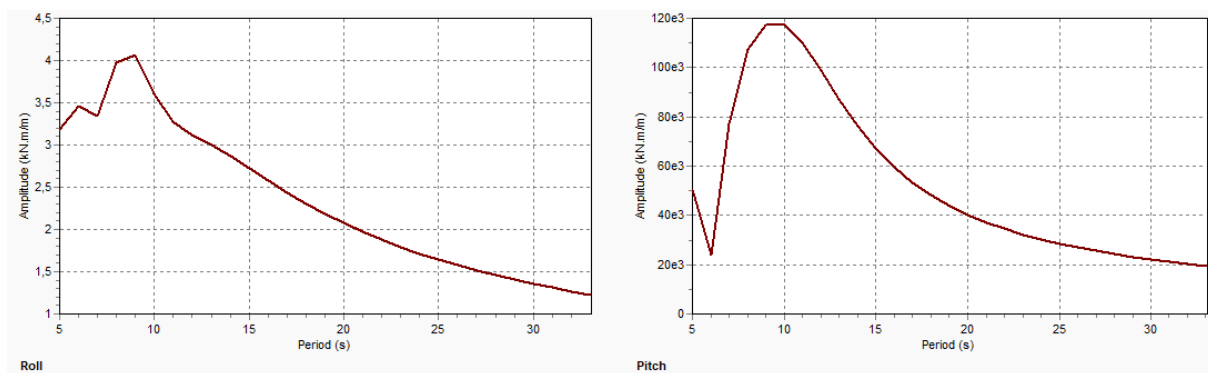


Figure 58. Load RAO | Roll & Pitch | 0 Degrees.

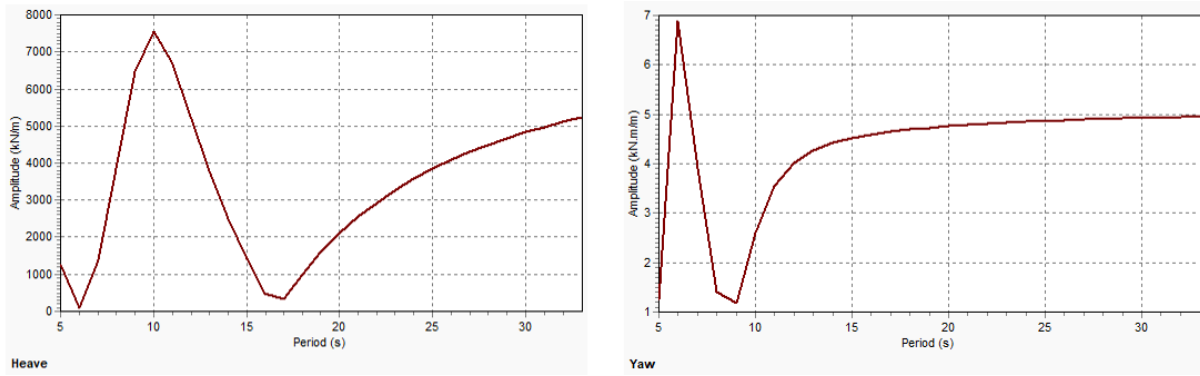


Figure 59. Load RAO | Heave & Yaw | 0 Degrees.

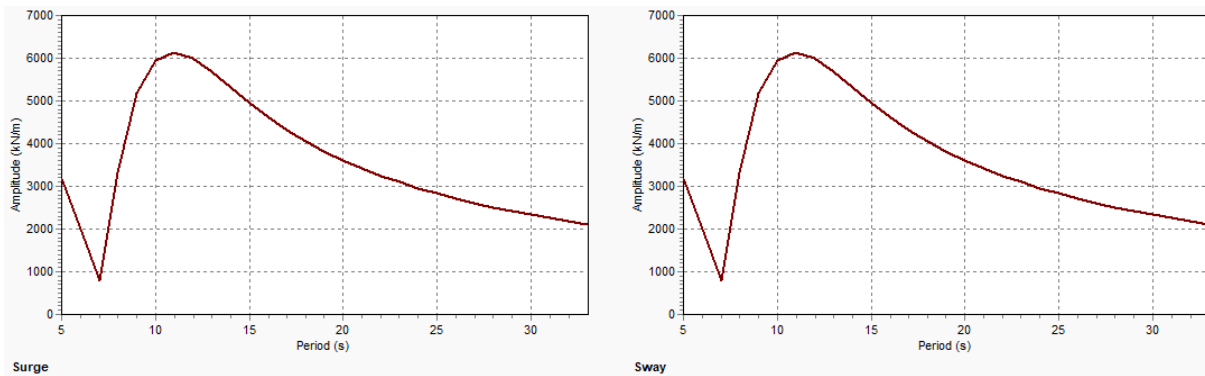


Figure 60. Load RAO | Surge & Sway | 45 Degrees.

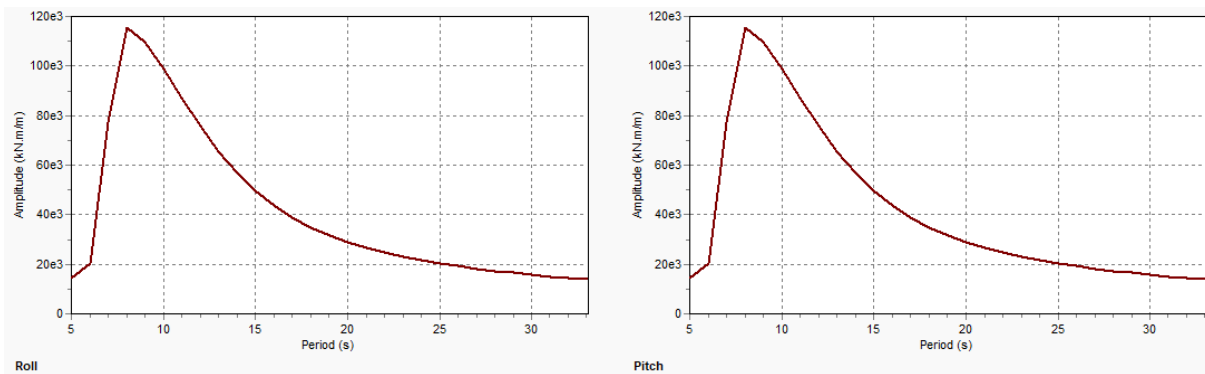


Figure 61. Load RAO | Roll & Pitch | 45 Degrees.

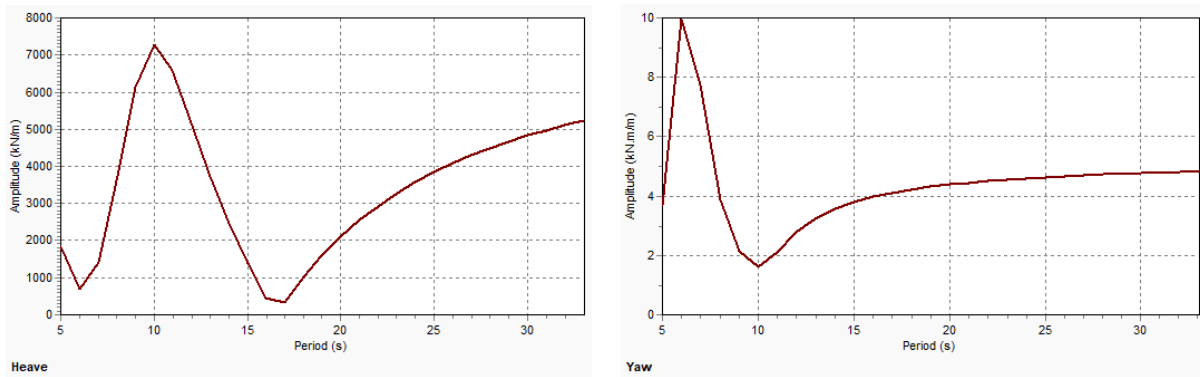


Figure 62. Load RAO | Heave & Yaw | 45 Degrees.

The platform response is also of great relevance since it provides the displacements and accelerations that must comply with established limits. However, differently from a floating wind turbine, which is connected to one or two power cables and usually three mooring lines, a floating substation is connected to several cables and mooring lines. For this reason, it is expected that these structures influence the behaviour of the floater. Therefore, its motions are assessed once the mooring system and cable configuration are defined. The response analysis is detailed in Section 9.

7. MOORNING SYSTEM

In this section, the mooring pattern and line configuration are discussed. Also, a preliminary design of the mooring system is performed. Following this, the chosen configuration is verified with a static and time domain motions analysis in OrcaFlex for a better estimation of the platform excursion and assessment of snap loads in the mooring lines. From the platform excursion and tension time series, necessary adjustments are made. According to DNV, the following environmental effects shall be considered when designing a mooring system (DNV 2021b):

- Waves
- Wind
- Current
- Marine growth
- Tide and storm surge
- Earthquake
- Temperature
- Snow and ice

The first four effects (waves, wind, current and marine growth) are included in the design of the mooring system. The design is based on the ultimate (ULS), fatigue (FLS), and accident (ALS) limit states and the following results are evaluated:

- Platform excursion
- Cable & chain Tension
- Anchor vertical force

The mooring system design follows the steps shown in Figure 63.

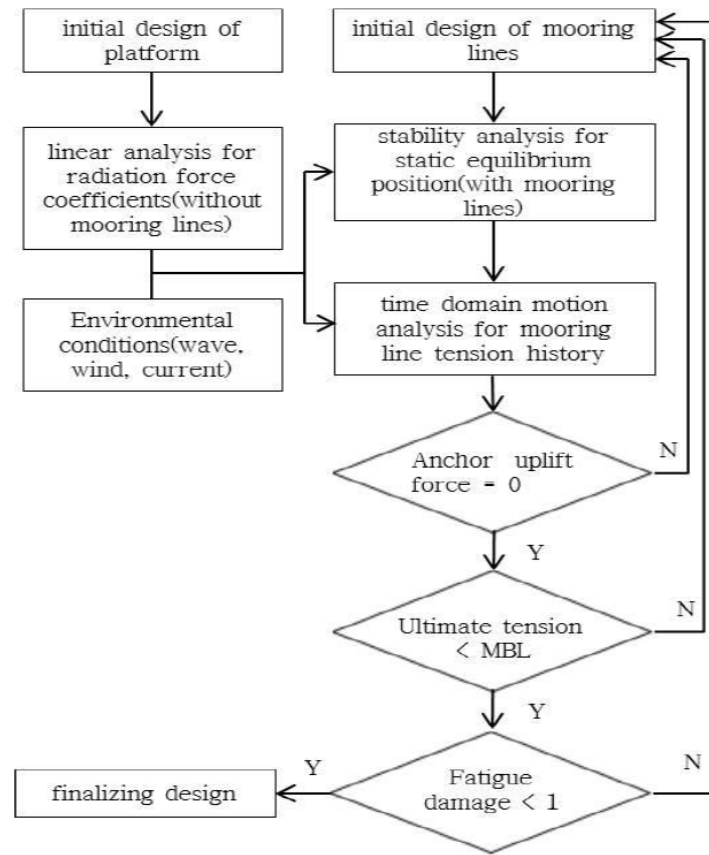


Figure 63. Design procedure for mooring lines (KIM 2013).

7.1. Load Cases

7.1.1. *Ultimate Limit State*

According to DNV (DNV 2021b), in UK sectors a combination of 100-year wind and wave with 10-year current is acceptable for ULS analysis. Since the wind farm considered in this report is located off the coast of Scotland, this assumption is adopted. Also, these environmental agents are assumed to act in the same direction, so the most severe condition is simulated. The wind, wave, and current parameters are shown in Table 1, and the extreme sea state is modelled through a Jonswap wave spectrum with a peak enhanced factor of 1.8. Due to the symmetry of the platform and mooring lines arrangement, only two directions are analyzed, 0° and 45° . The motions analysis performed with OrcaFlex is detailed in Section 7.5.

For the mooring lines' preliminary design, the wave loads are disregarded. The wind and current loads are calculated according to DNV (DNV 2014) for 0° and 45° incidence. Tables 45 and 46 show the parameters used for the wind and current load calculation and their value. For the current force, it is considered that all columns and pontoons

experience the same inflow speed (no wake effect).

Table 45. Wind load.

Component	0 degrees		45 degrees	
	Substation	Columns	Substation	Columns
$U_{T,z}$ [m/s]	35.70	35.70	35.70	35.70
q [kg/ms ²]	781	781	781	781
C_D	2.20	1.64	2.40	1.50
S [m ²]	787	819	1112	1159
α [°]	0	0	45	45
F_{Wind} [kN]	1352	1053	2086	1358
$F_{Total\ wind}$ [kN]	2405		3444	

Table 46. Current load for column-based structures.

Component	0 degrees		45 degrees	
	Pontoons	Columns	Pontoons	Columns
U_{cN} [m/s]	0.76	0.76	0.76	0.76
C_D	1.90	1.64	1.9	1.50
S [m ²]	695	728	983	1030
$F_{Current}$ [kN]	391	355	553	457
$F_{Total\ current}$ [kN]	746		1010	

According to DNV (DNV 2021b), partial safety factors must be included in the pretension and environment tension when designing a mooring system. These depend if the consequences of the mooring system failure are acceptable (Class 1) or unacceptable (Class 2). If the mooring system of an offshore substation fails, a few likely consequences are collision with near wind turbines, capsizing, or sinking. Furthermore, depending on how large the platform excursion is after mooring line failure, the export cables can be damaged, which would result in the disconnection of the whole wind farm from the onshore grid. Therefore, the consequence Class 2 is assumed.

The partial safety factors also depend if the analysis is performed in the time domain or frequency domain. Larger values are assumed for the frequency domain analysis since non-linear effects are not taken into account. Since there is no recommendation on the safety factors for static analysis, those referring to a frequency domain analysis are used for the preliminary calculation of the mooring lines. For the calculations using OrcaFlex, the time domain analysis safety factors are used. Table 47 summarises these safety factors.

Table 47. ULS Safety factors.

Consequence Class	Type of unit	Time domain analysis		Static analysis	
		Pretension factor γ_{pret}	Env. tension factor γ_{env}	Pretension factor γ_{pret}	Env. tension factor γ_{env}
2	Permanent	1.2	1.9	1.2	2.3

These safety factors are applied to Equation 27 where the utilization factor u must be smaller than 1 to assure the integrity of the mooring lines.

$$u = \frac{T_{pret} \cdot \gamma_{pret} + T_{C-env} \cdot \gamma_{env}}{S_C} < 1 \quad (27)$$

Where:

T_{pret} is the pretension.

T_{env} is the environment tension.

S_C is the line characteristic strength.

7.1.2. Fatigue Limit State

The characteristic fatigue damage is calculated through the sum of the damage generated by each loading condition (Equation 28). These are defined by the wind, wave, and current parameters, heading angles, and probability of occurrence (DNV 2021b).

$$d_c = \sum_{i=1}^{i=n} d_i \quad (28)$$

Where:

d_c is the characteristic damage.

n is the number of load cases.

d_i is the damage per load case.

The damage per load case is obtained according to Equation 29, where the number of stress cycles is obtained by Rainflow counting of the line tension time series calculated with OrcaFlex for a 10-minute simulation. The total damage over the platform life span is found by applying the obtained damage to the total duration of a certain load case.

$$d = \sum_{j=1}^{j=m} \frac{n_j}{N_j} \quad (29)$$

Where:

m is the number of stress ranges.

n_j is the number of cycles for a certain stress range.

N_j is the maximum allowable number of cycles for a certain stress range.

The maximum number of cycles the chains can sustain for a certain stress range before failure is given by Equation 30 (DNV 2021b).

$$N = a_D \cdot S^{-m} \quad (30)$$

Where:

a_D is the intercept parameter of the S-N curve. The a_D is $1.2 \cdot 10^{11}$ for a stud chain (DNV 2021b).

S is the stress range.

m is the S-N curve slope. The m is 3 for a stud chain (DNV 2021b).

In the wave scatter diagram shown in Figure 64 192 sea states occur in the chosen site. Therefore, combining these with various wave directions, wind, and current parameters would result in an excessively large number of load cases. To solve this issue, a strategy is followed to reduce the number of sea states while still fairly representing the site conditions.

Hs\Tp	1-2	2-3	3-4	4-5	5-6	6-7	7-8	8-9	9-10	10-11	11-12	12-13	13-14	14-15	15-16	16-17	17-18	18-19	19-20	20-21	21-22	22-23	Total	
0.00-0.50		0.01	0.29	0.61	0.25	0.12	0.07	0.07	0.06	0.02	0.01	0.01	0.01	0.01	0.00	0.00	0.00	0.00	0.00					1.55
0.50-1.00		0.00	0.54	3.74	3.93	3.08	1.57	1.28	0.83	0.40	0.13	0.09	0.09	0.13	0.10	0.05	0.02	0.00	0.00					15.98
1.00-1.50			0.00	1.34	5.79	4.54	3.62	2.60	2.02	1.13	0.51	0.16	0.09	0.09	0.07	0.06	0.06	0.01	0.01	0.00	0.00			22.10
1.50-2.00				0.01	2.53	5.41	3.31	2.80	1.80	1.62	0.97	0.30	0.12	0.06	0.03	0.03	0.02	0.01	0.00	0.00	0.00			19.02
2.00-2.50					0.12	4.05	3.33	2.26	1.58	1.24	1.05	0.46	0.12	0.05	0.02	0.01	0.01	0.00	0.00	0.01				14.30
2.50-3.00					0.00	0.62	3.68	1.87	1.46	0.77	0.61	0.41	0.16	0.04	0.01	0.01	0.00	0.01	0.00					9.64
3.00-3.50						0.01	1.67	2.01	1.26	0.68	0.35	0.26	0.17	0.04	0.01	0.00		0.00						6.46
3.50-4.00							0.19	1.71	1.15	0.61	0.29	0.13	0.08	0.03	0.01		0.00							4.19
4.00-4.50							0.01	0.64	1.04	0.56	0.18	0.08	0.05	0.03	0.01		0.00							2.60
4.50-5.00								0.06	0.80	0.52	0.16	0.05	0.04	0.01	0.00	0.00								1.66
5.00-5.50								0.00	0.32	0.41	0.19	0.04	0.02	0.00										1.00
5.50-6.00									0.09	0.28	0.16	0.05	0.02	0.00										0.60
6.00-6.50									0.01	0.14	0.14	0.06	0.01	0.01										0.37
6.50-7.00										0.05	0.10	0.05	0.01	0.00										0.22
7.00-7.50											0.02	0.06	0.03	0.01	0.00									0.12
7.50-8.00												0.00	0.02	0.04	0.01	0.01								0.08
8.00-8.50													0.01	0.02	0.01	0.00								0.05
8.50-9.00														0.01	0.01	0.01	0.00							0.02
9.00-9.50															0.00	0.00	0.01	0.00						0.01
9.50-10.00																0.00	0.00	0.00						0.00
10.00-10.50																								0.00
10.50-11.00																								0.00
Total		0.01	0.83	5.71	12.61	17.83	17.44	15.30	12.41	8.46	4.95	2.26	1.07	0.51	0.26	0.17	0.12	0.04	0.02	0.00	0.00			100.00

Figure 64. Wave scatter diagram.

If only the sea states with a probability of occurrence of more than 0.5% are taken into account, the number of sea states is reduced to 47 and they account for 90.71% of the time. Therefore, the wave scatter diagram is manipulated so the remaining 9.29% of the time is proportionally distributed to the sea states considered. Figure 65 shows the new wave scatter diagram. These sea states are modelled through a Jonswap wave spectrum with a peak enhanced factor of 1.5.

Hs\Tp	2-3	3-4	4-5	5-6	6-7	7-8	8-9	9-10	10-11	11-12	12-13	Total
0.00- 0.50			0.67									0.67
0.50- 1.00		0.60	4.12	4.33	3.39	1.73	1.41	0.92				16.50
1.00- 1.50			1.48	6.38	5.00	4.00	2.86	2.23	1.24	0.57		23.76
1.50- 2.00				2.78	5.96	3.65	3.09	1.98	1.78	1.07		20.31
2.00- 2.50					4.47	3.67	2.49	1.74	1.36	1.15		14.88
2.50- 3.00					0.68	4.06	2.06	1.61	0.85	0.67		9.93
3.00- 3.50						1.84	2.21	1.39	0.74			6.19
3.50- 4.00							1.89	1.27	0.67			3.83
4.00- 4.50							0.71	1.14	0.62			2.47
4.50- 5.00								0.88	0.58			1.46
5.00- 5.50												
Total		0.60	6.28	13.50	19.51	18.94	16.71	13.16	7.86	3.46		100.00

Figure 65. Wave scatter diagram modified.

Figure 66 shows the wave heading probability during a year. The most likely one is north with around 12% probability. Also, the waves coming from NNW and NNE sum roughly 18%, which results in 30% of the waves being between these three directions. The waves coming from the south represent over 10% of the incoming waves with a total of around 26% between SSE and SSW. Lastly, the ESE is also a relevant heading with 7% probability, which results in 17% when combined with the waves coming from the east and southeast directions. The other wave headings have a low probability of occurring and are disregarded. Therefore, the characteristic wave directions are assumed to be as shown in Table 48.

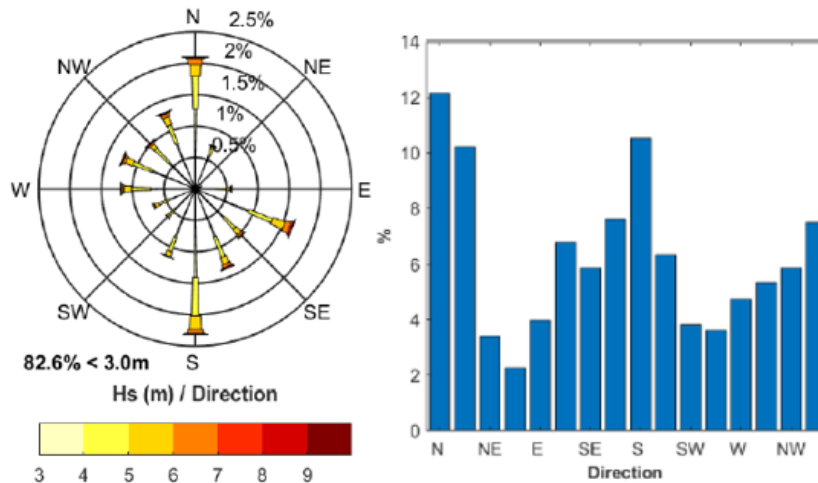


Figure 66. Wave directions.

Table 48. Wave directions.

Direction	Angle	Probability	Final probability
N	0°	30%	40.7%
S	180°	26%	35.9%
ESE	112.5°	17%	23.4%

The wind speed distribution and heading are shown in Figure 67. The wind speed of 10.67 m/s is assumed for all the load cases since it is the one with the highest probability of occurring. Also, even though there is a certain discrepancy regarding the wind and wave heading probability, the wind is assumed to act in the same direction as the waves, for a conservative approach.

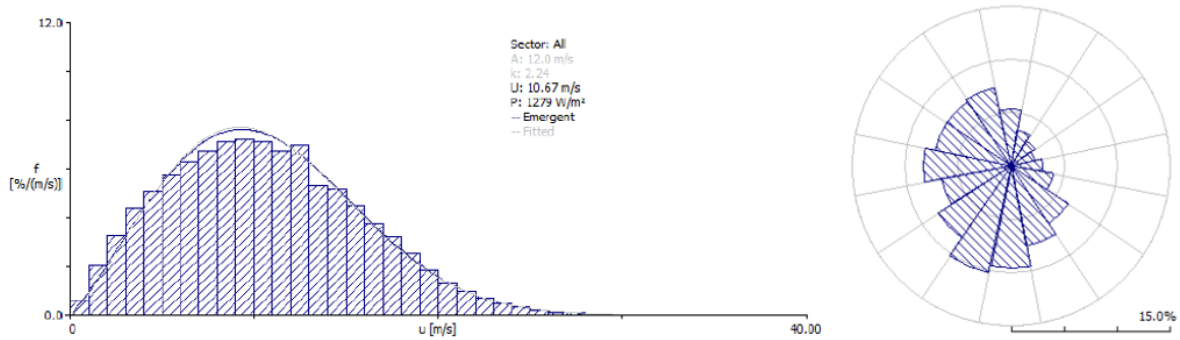


Figure 67. Wind directions and speed.

According to Figure 68, the predominant current directions are north and south. Therefore, the currents are assumed to come from these two directions with a 50% probability each. Also, from Figure 69, the current speed with the highest probability of occurring in these directions is 0.25 m/s. That is the current speed assumed.

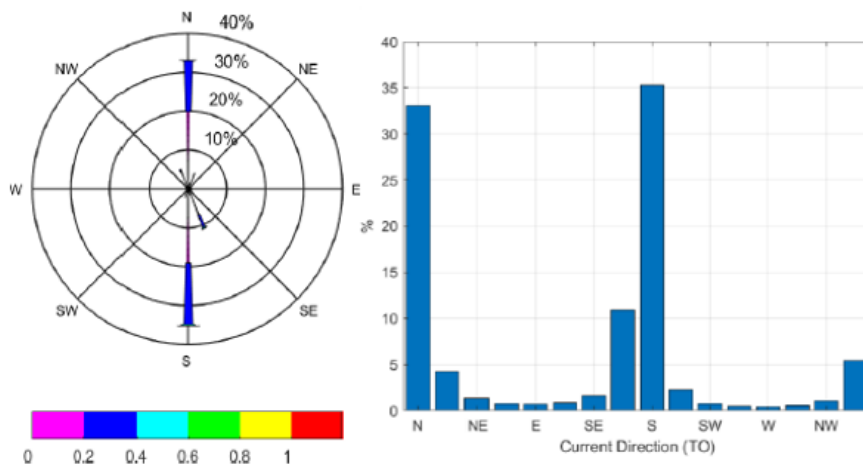


Figure 68. Current directions.

Uc \ Dir	0.0	22.5	45.0	67.5	90.0	112.5	135.0	157.5	180.0	202.5	225.0	247.5	270.0	292.5	315.0	337.5	Total
0.0 - 0.1	3.64	2.04	1.05	0.71	0.63	0.72	1.14	2.46	3.78	1.68	0.70	0.47	0.43	0.53	0.91	2.36	23.25
0.1 - 0.2	9.50	1.60	0.24	0.10	0.08	0.11	0.35	3.26	9.12	0.52	0.06	0.02	0.02	0.03	0.12	2.03	27.17
0.2 - 0.3	11.90	0.55	0.03	0.01	0.01	0.02	0.11	3.01	12.11	0.09	0.00	0.00	0.00	0.00	0.03	0.83	28.70
0.3 - 0.4	6.29	0.05	0.00	0.00	0.00	0.00	0.02	1.43	7.55	0.01	0.00				0.00	0.17	15.52
0.4 - 0.5	1.69	0.00	0.00				0.00	0.63	2.51	0.00						0.03	4.87
0.5 - 0.6	0.07						0.00	0.15	0.21	0.00						0.00	0.43
0.6 - 0.7	0.00							0.02	0.01								0.04
0.7 - 0.8								0.00	0.00								0.01
0.8 - 0.9								0.00	0.00								0.00
0.9 - 1.0																	
1.0 - 1.1																	
1.1 - 1.2																	
Total	33.10	4.24	1.32	0.82	0.72	0.85	1.63	10.96	35.29	2.30	0.77	0.50	0.45	0.57	1.06	5.42	100.00

Figure 69. Current directions and speed.

Combining the wave, wind, and current parameters, a total of 282 load cases are defined and their OrcaFlex files are generated with a code written in MATLAB. The detailed load cases and occurrence probability are found in Appendix B and the MATLAB code is shown in Appendix C.

7.1.3. Accidental Limit State

According to DNV (DNV 2021b), the mooring system must be able to withstand the failure of one mooring line for unknown reasons. Therefore, the mooring system behaviour is analyzed for 0° and 45° heading when one of the lines located in the platform portion that receives the wind, wave, and current action collapses. Figures 70 and 71 illustrate the single failure, where the red line is the one assumed collapsed and the blue arrow indicates the direction of the environmental agents.

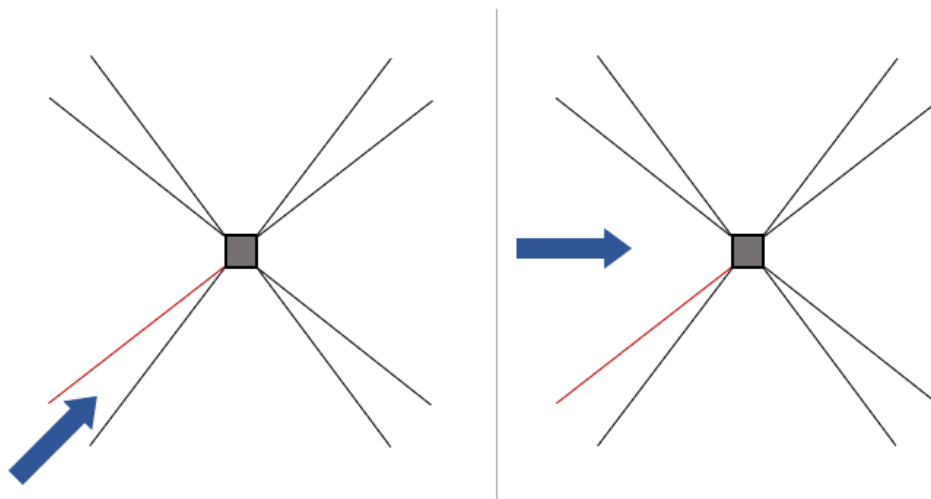


Figure 70. Single failure illustration | 8-line configuration.

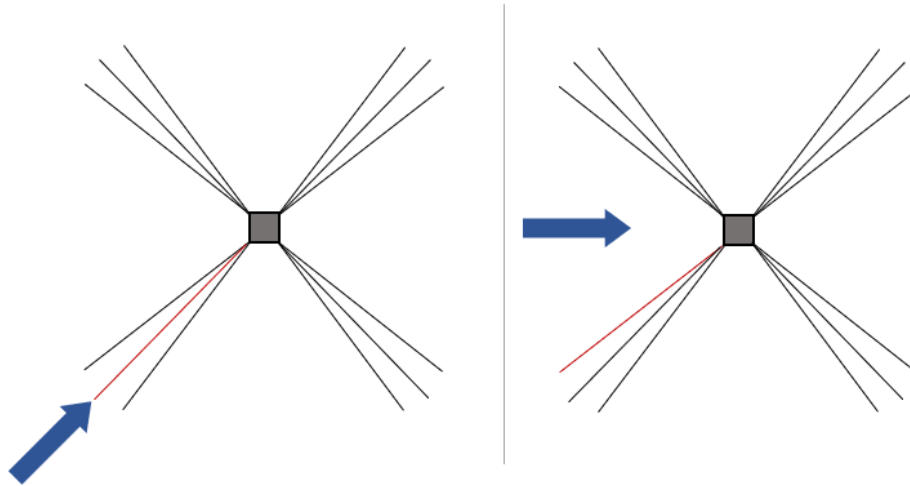


Figure 71. Single failure illustration | 12-line configuration.

The environmental conditions are the same as applied to the ULS analysis. However, since this is a conservative approach (DNV 2021b), smaller safety factors may be applied. Table 49 presents the safety factors used in the time series results. Due to the complex behaviour of the platform after one mooring line collapses, the accidental condition is only analyzed after time series simulations.

Table 49. ALS Safety factors.

Consequence Class	Type of unit	Time domain analysis	
		Pretension factor γ_{pret}	Env. tension factor γ_{env}
2	Permanent	1.0	1.45

7.2. Mooring Pattern

The mooring patterns suitable for a semi-submersible floater are spread mooring or single-point mooring. The former consists of a group of lines arranged symmetrically around the floater to ensure enough horizontal restoration forces to counter the environmental ones. It maintains the floater in a fixed heading, which can be disadvantageous for a ship-shaped structure, but not for a fully symmetric floater. The single-point mooring pattern consists of mooring the floater to a buoy that is moored with a catenary of a taut line system. This way, the floater can move around the buoy and align to the wind, current and wave action to reduce the loads on the mooring lines.

Due to the high number of power cables connected to the substation, the floater excursion must be kept as small as practically possible, to avoid undesired loads in these cables. Therefore, the spread mooring pattern is chosen for the design of the mooring system because of its capacity to restrain horizontal motions and maintain the platform's heading.

7.3. Line Configuration

The spread mooring arrangement may be implemented with catenary or taut lines. The first consists of a line attached to the floater (fairlead) and seabed (drag of deadweight anchor) where the restoration force comes from the weight of the line when it is lifted from the seabed. Catenary lines result in a large footprint due to their operating mechanism and the anchors should experience only horizontal forces under normal operating conditions. Taut lines consist of a stretched line between the floater and an anchor, which must be able to carry vertical and horizontal loads. This configuration results in fewer excursions than catenary lines and the vertical motions are reduced. The restoration force comes from the elasticity of the line. Figure 72 illustrates these two line configurations.

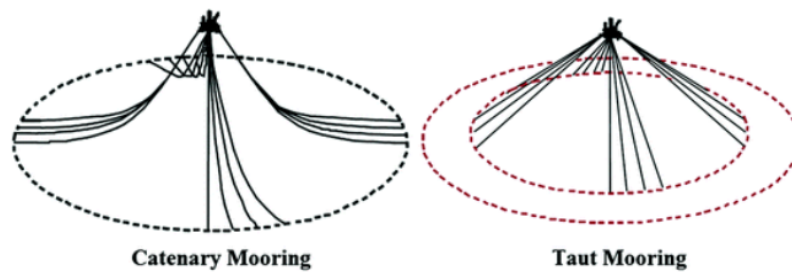


Figure 72. Catenary anchor leg and taut-leg fiber rope mooring systems (INNOSEA et al.).

From the excursion point of view, employing taut lines would be the best strategy to follow. Furthermore, as shown in Figure 72, taut mooring results in a smaller footprint and shorter lines, which reflects in cost reduction. However, it also requires expensive anchoring solutions, such as driven or suction piles. Therefore, taut lines are more suitable for deep waters, where the lines' length reduction by switching from catenary to taut mooring is significant. It is suggested that taut line mooring should be used in water depths from 250 meters and catenary up to 500 meters (RWE n.d.). In shallow waters, catenary mooring has been widely used in offshore wind farm projects, as shown in Table 50. Semi-taut mooring is also an option, being composed of taut and catenary lines, but it is advantageous for deep waters (INNOSEA et al.).

Project	Floater type	Water depth (m)	Mooring configuration
Kincardine	Semi-sub	70	Catenary
Fukushima Mirai	Semi-sub	120	Catenary
Fukushima Shimpuu	Semi-sub	120	Catenary
Wind2Power [56]	Semi-sub	40	Single Point Mooring
Hywind Scotland	Spar	100-120	Catenary
Sea Twirl S1	Spar	35	Catenary
Goto	Spar	97	Catenary
Fukushima Kizuna	Spar	100-120	Catenary
Fukushima Hamakaze	Spar	120	Catenary
Hywind Norway	Spar	186-204	Catenary
Floatgen	Barge	33	Taut / Tensioned Catenary
Hibiki	Barge	55	Catenary

Table 50. Mooring configuration in current projects (INNOSEA et al.).

It can be seen that there is a clear trend towards the utilization of catenary lines for semi-submersible foundations in water depths near 100 meters. Therefore, catenary lines are chosen for the design of the mooring system.

Regarding the line composition, as water depth increases, the "all-chain" design becomes unfeasible due to the excessive line weight. Therefore, chains are combined with steel cables or fibre ropes. However, the "all-chain" design has been a common solution in the oil & gas industry for water depths between 60 and 100 meters (INNOSEA et al.). Because of this, the mooring lines designed in this report are composed only of chains. Stud chains are used due to their higher fatigue resistance when compared to the studless chain.

7.4. Mooring System Design | Preliminary

A preliminary mooring system is designed to define the number, orientation, and length of mooring lines. The line length is defined according to the catenary equations provided by Faltinsen (Faltinsen 1993). The minimum line length (l_s), the portion of the line that is not in contact with the seabed, depends on the water depth, line distributed mass, and line pretension. The length of the line portion that lays on the seabed ($l - l_s$) dictates how much force is required to move the anchor or, as a simplification, the force necessary to lift the whole line. Figure 73 illustrates how the mooring line is idealised according to

Faltinsen.

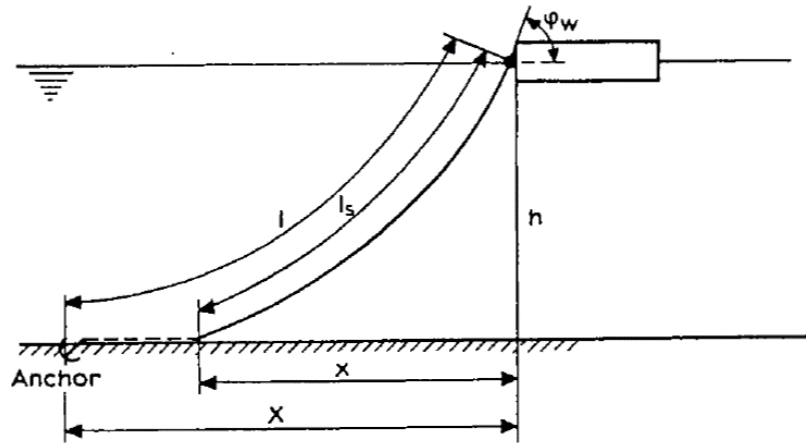


Figure 73. Mooring system idealisation (Faltinsen 1993).

Due to uncertainties regarding the environmental loads, the line pretension is chosen in a way that the calculated wind + current force is 95% of the force necessary to cause the average excursion. The line portion laying on the seabed is defined after the assumption that the force necessary to lift the anchors is 1.5 times the force necessary to cause the average excursion. The platform is set to drift an average of 10 meters (10% of the water depth) from its initial position.

Four common links are experimented with. Regarding the number of lines, 8-line and 12-line configurations are designed and then compared. The 4-line configuration is not considered because the accidental limit state is very unlikely to be complied with. Both configurations are symmetric and the angle between the lines in each corner is 15° in the 8-line configuration and 8° in the 12-line configuration. The line characteristic strength (S_C) is taken as the R_5 break load. Lastly, the maximum breaking load after corrosion is calculated for 25 years of service life with a 0.4 mm/year corrosion allowance according to Equation 31 (DNV 2021b).

$$S_{mbs-corr} = S_{mbs} \cdot \left(\frac{D_{corr}}{D_{new}} \right)^2 \quad (31)$$

Where:

S_{mbs} is the chain maximum breaking load, which is also the S_C .

D_{corr} is the corroded chain diameter.

D_{new} is the un-corroded chain diameter.

Even though the mooring chain datasheet used provides links with a diameter of up to 210mm, the maximum size experimented is 150mm. This is because chains with larger diameters make the installation process too complicated. Table 51 presents the relevant

data for each link tested.

Table 51. Links tested.

Diameter [mm]	150	140	130	120
w [kg/m]	493	429	370	315
S_C [kN]	23040	20572	18171	15852
$S_{mbs-corr}$ [kN]	20070	17738	15483	13320

As mentioned in Section 5.1.2, if the hull is damaged by a vessel, the damage extension below the water line is expected to be 3 meters. Therefore, the fairleads are located 6 meters below the water line. This way, an eventual ship impact would not damage the mooring system.

7.4.1. Results / 8 Lines Configuration

Table 52 summarizes the 8-line configurations obtained. As expected, as the diameter reduces, the line weight also decreases, even though its length increases. However, the utilization factor of these lines is higher than that of the ones with large diameters. In summary, small diameter lines require a bigger footprint but are lighter, which reflects in cost reduction. For a better comparison of the utilization factor, the results from the time domain analysis are compared, since static analysis considerably underestimates the line tension.

Table 52. Feasible | 8 Lines Configuration.

Configuration	1	2	3	4
Link diameter [mm]	150	140	130	120
Pretension [kN]	1040	985	925	865
L_{total} [m]	419	446	477	514
u	0.45	0.50	0.54	0.65
Line mass [tons]	206	191	176	162

Figures 74 and 75 show the configuration number 1 for illustration purposes.

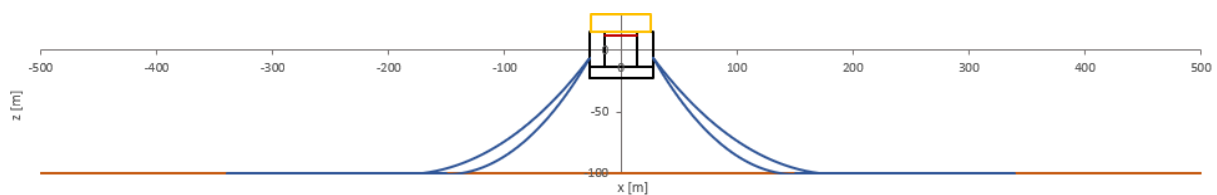


Figure 74. Preliminary 8 mooring lines layout | Side projection view.

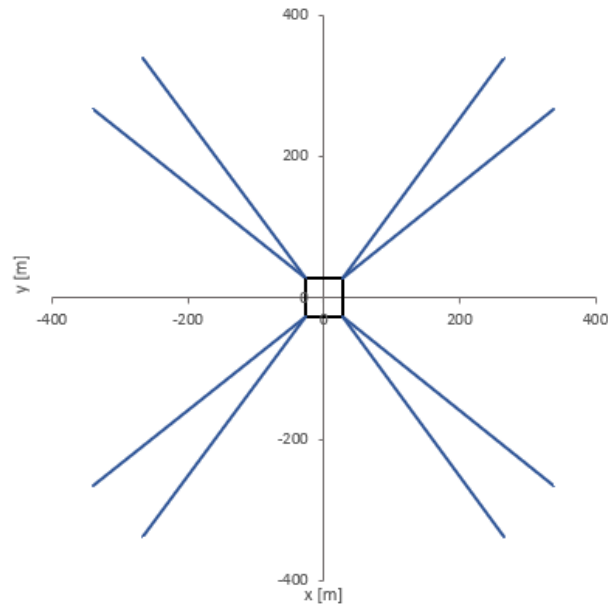


Figure 75. Preliminary 8 mooring lines mooring layout | Top view.

7.4.2. Results / 12 Lines Configuration

Table 53 summarizes the 12-line configurations obtained. The same behaviour seen with the 8-line configuration is found in the 12-line configurations found. For a better comparison of the utilization factor, a time domain analysis is also used to assess the line tension.

Table 53. Feasible 12-line configurations.

Configuration	1	2	3	4
Link diameter [mm]	150	140	130	120
Pretension [kN]	900	855	800	750
L_{total} [m]	381	405	430	462
u	0.37	0.39	0.44	0.50
Line mass [tons]	188	174	159	146

Figures 76 and 76 show the configuration number 1 for illustration purposes.

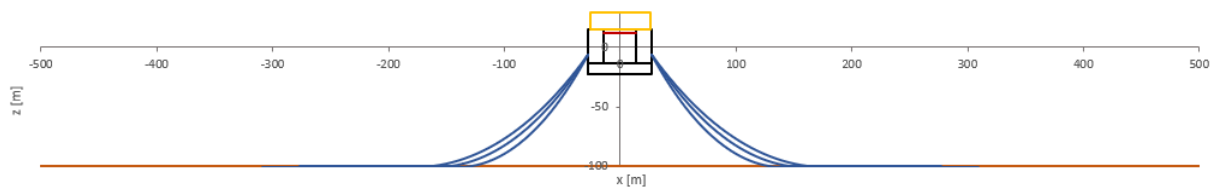


Figure 76. Preliminary 12 mooring lines mooring layout | Side projection view.

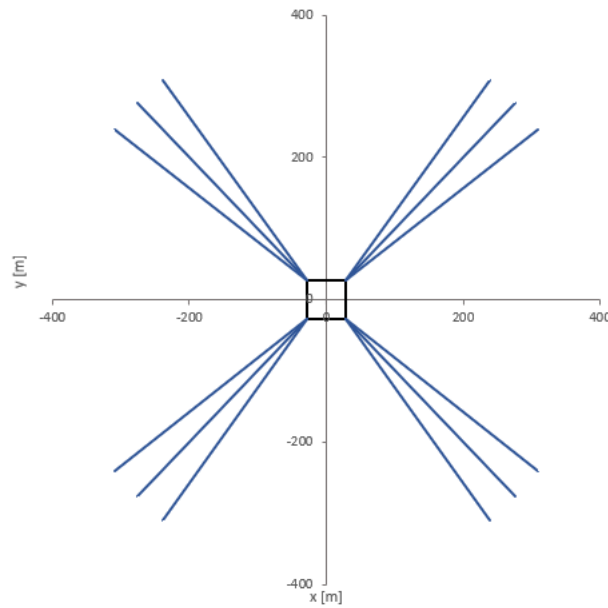


Figure 77. Preliminary 12 mooring lines mooring layout | Top view.

7.4.3. Conclusion

The choice between an 8-line or 12-line configuration is mainly a matter of how redundant the mooring system must be. As discussed in Section 7.1.1, a Class 2 consequence is chosen for an eventual failure of the mooring system. Therefore, an 8-line configuration could be enough due to the high safety factor employed in the choice of the mooring lines. Therefore, the choice between an 8-line or 12-line configuration is done based on the time domain analysis performed in Section 7.5. From these results, the maximum line tensions can be better assessed and the feasible solutions can be compared.

7.5. Mooring System Design | OrcaFlex

In this section, the mooring system arrangements proposed after the static analysis are verified with a model in OrcaFlex. This model is based on the RAOs, damping and added mass coefficients obtained from OrcaWave.

The lines are divided into finite elements for the calculation of their dynamic behaviour. The length of these elements varies along the line so more sensible areas are better detailed. For instance, the area around the touchdown point is more refined than the vertical section of the catenary. This way, computing time is saved while maintaining the quality of results. The line portion close to the waterline, around the touchdown point and resting on the seabed have 6, 3 and 8 meters, respectively.

In the static analysis, the start of life (SOL) condition is considered, when there is no marine growth. This assumption is acceptable for the verification of the average platform

excursion, but the end-of-life (EOL) condition should be considered for the line tension correct assessment. That is because the marine growth increases the drag coefficient and line mass, resulting in higher drag forces, weight and tension. Therefore, the SOL condition is simulated for the verification of the maximum excursion and the EOL condition is investigated for the assessment of the maximum line tensions. Table 54 shows the links tested and their corresponding marine growth weight and drag coefficients for depths up to 40 and 100 meters (DNV 2021b).

Table 54. Links tested | OrcaFlex.

Diameter [mm]	150	140	130	120
W [kg/m]	493	429	370	315
$W_{\text{marine growth (up to 40m)}}$ [kg/m]	204	196	188	180
$W_{\text{marine growth (up to 100m)}}$ [kg/m]	82	78	74	69
Long. C_D	1.4	1.4	1.4	1.4
Trans. C_D	2.6	2.6	2.6	2.6
Trans. C_D marine growth (up to 40m)	6.1	6.3	6.6	6.9
Trans. C_D marine growth (up to 100m)	4.3	4.5	4.6	4.8
S_C [kN]	23040	20572	18171	15852
$S_{mbs-corr}$ [kN]	20070	17738	15483	13320

Figure 78 shows the sea spectrum used for the ULS and ALS analysis.

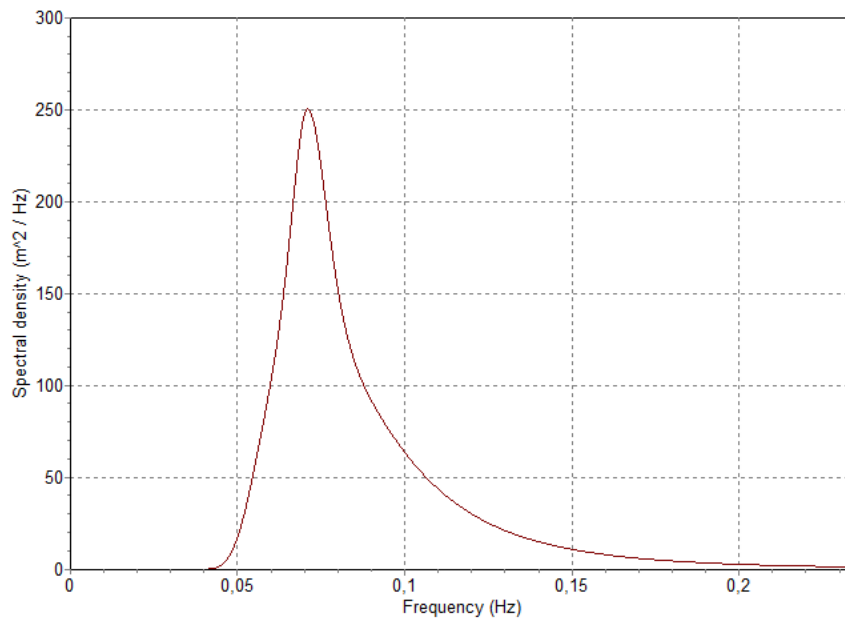


Figure 78. ULS Sea Spectrum.

7.5.1. Results / 8 Lines Configuration

Firstly, the 8-line configuration is tested. Also, the chain diameter chosen is 150mm, so the other 8-line configurations can be discarded in case this one is not suitable. This configuration is illustrated in Figure 79.

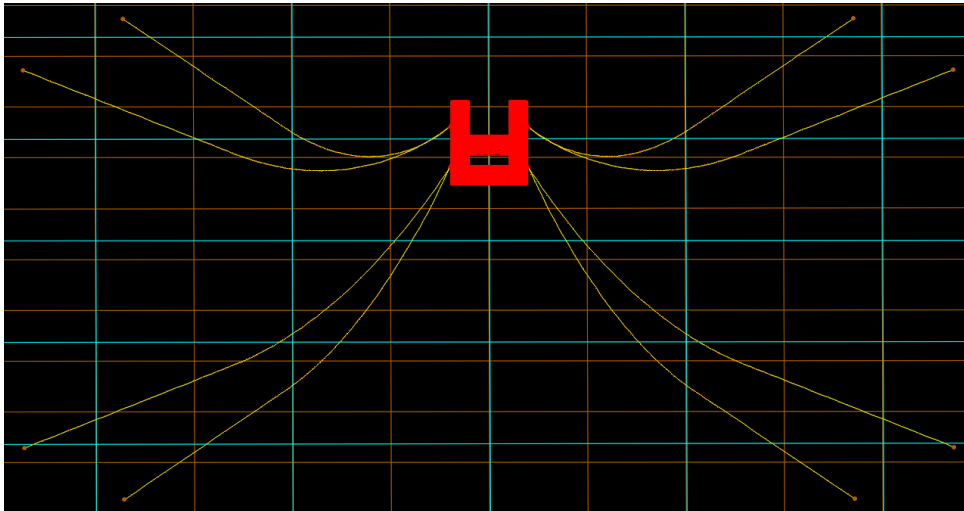


Figure 79. ULS condition | 8 Lines.

The platform excursion for a SOL condition with the environmental factors acting at 0° and 45° are shown in Figures 80 to 83.

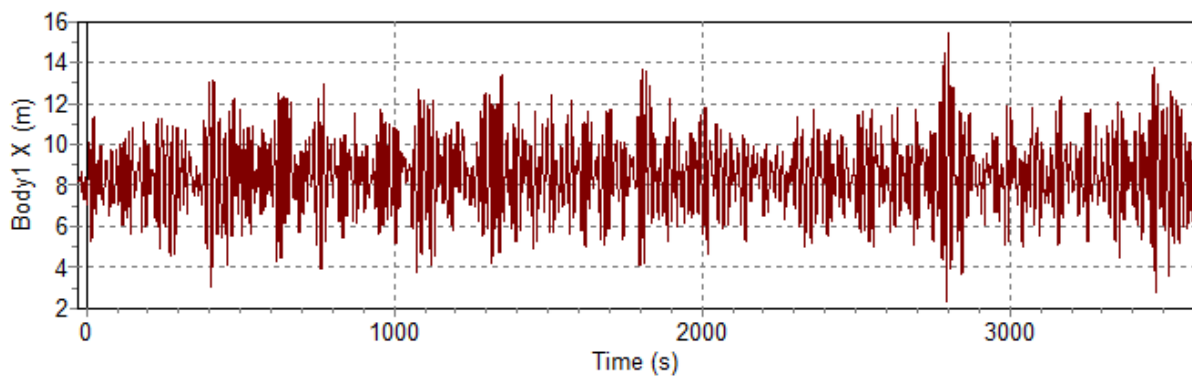


Figure 80. Platform excursion | Global X | 0° incidence.

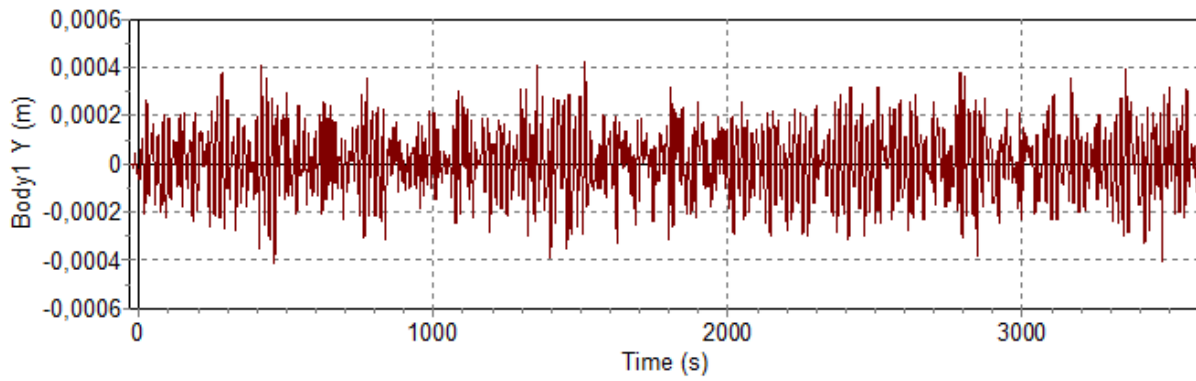


Figure 81. Platform excursion | Global Y | 0° incidence.

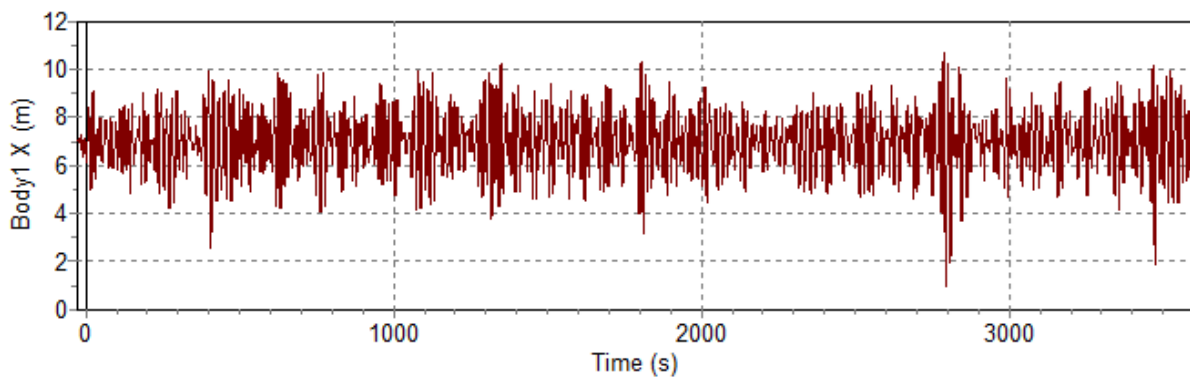


Figure 82. Platform excursion | Global X | 45° incidence.

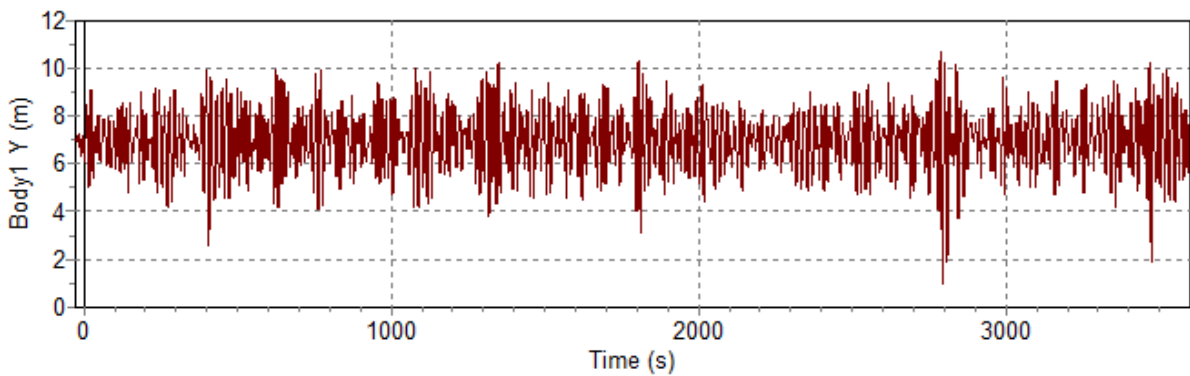


Figure 83. Platform excursion | Global Y | 45° incidence.

The average platform excursion is 8.49 and 9.78 meters for a 0° and 45° incidence, respectively. The maximum excursion obtained is 15.44 meters when a 45° incidence is experienced.

After checking the platform excursion, the lines' utilization factor and anchor vertical force are verified. The former is checked at the EOL, while the latter is checked at the SOL condition. For a 45° incidence, the anchor uplift is too high, so the lines are increased

from 419 to 500 meters by moving the mooring point further away, which reflects in a weight increase of 41 tons (20%) per line.

The maximum anchor uplift force obtained is nearly 60kN, which would require an anchor of at least 6 tons. Since drag anchors can weigh up to 65 tons, this is not considered an issue. Also, both incidences result in a utilization factor lower than 1 in all lines. Table 55 summarizes the highest utilization factor.

Table 55. Utilization factor | ULS | 8 lines | 150mm.

Incidence	0°	45°
Pretension [kN]	1740	1740
Tension [kN]	6878	10479
u	0.590	0.931

Figures 84 to 87 show the effective tension at the fairlead and anchor vertical force of the line with the most severe results for the intact condition. It should be noted that the anchor uplift force is a negative vertical force in the graphs provided.

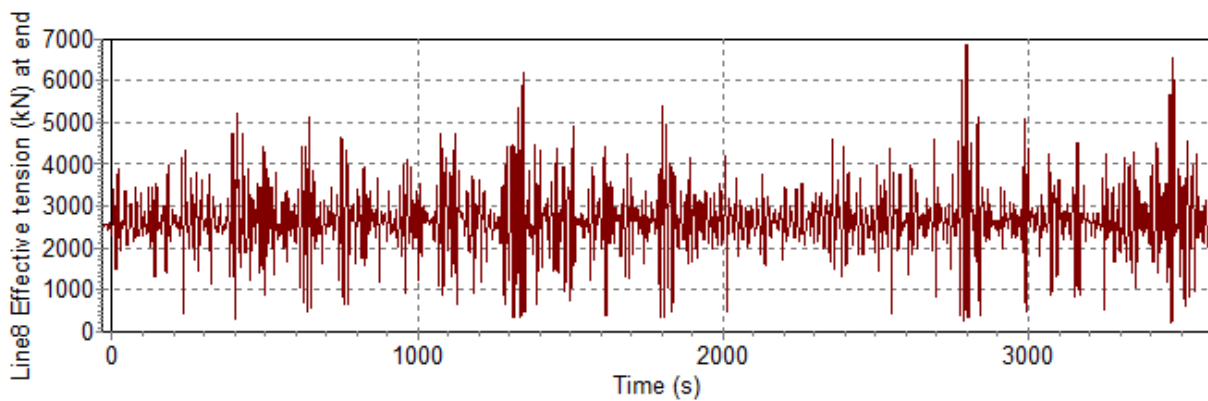


Figure 84. Line effective tension at fairlead | 0° incidence | ULS.

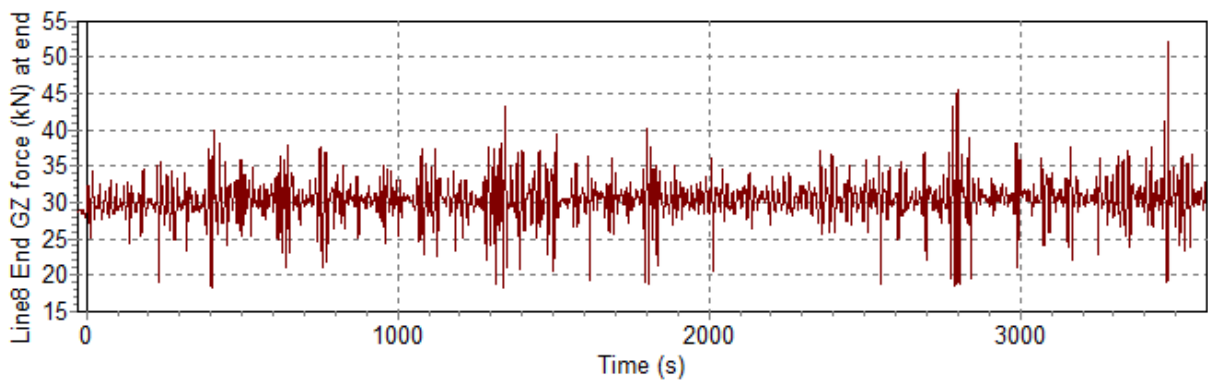


Figure 85. Anchor vertical force | 0° incidence | ULS.

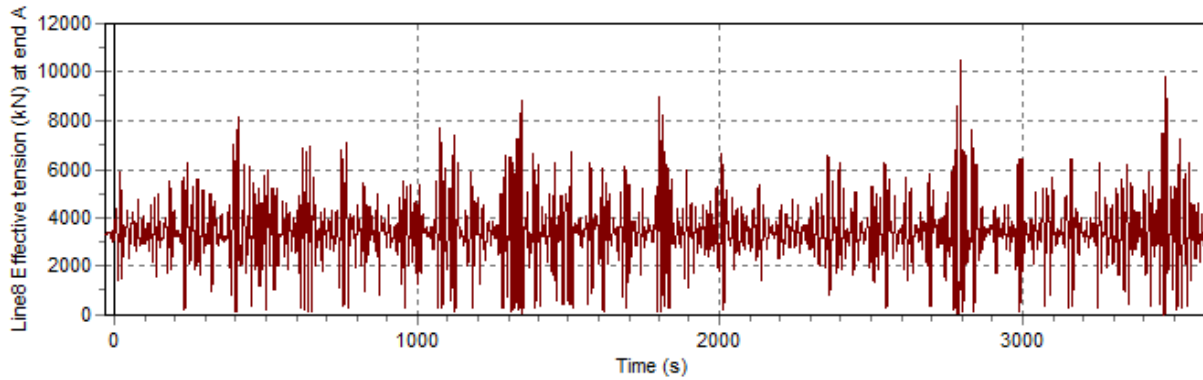


Figure 86. Line effective tension at fairlead | 45° incidence | ULS.

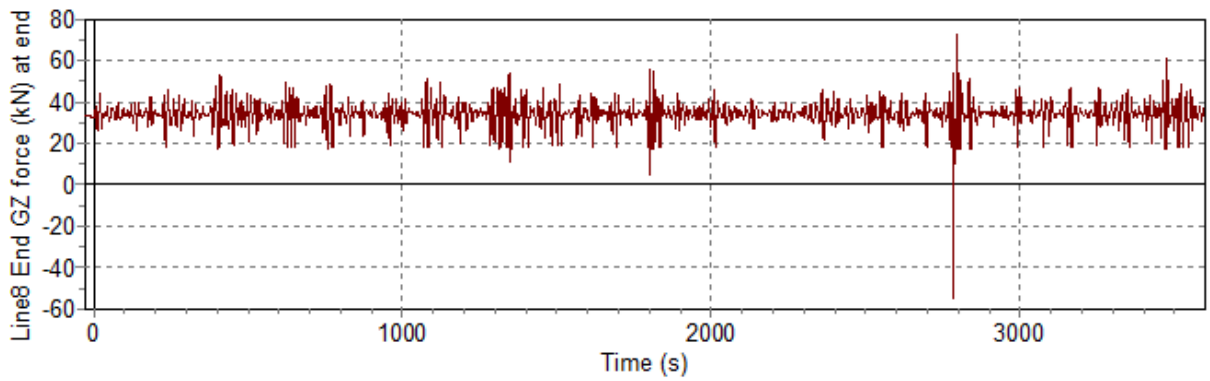


Figure 87. Anchor vertical force | 45° incidence | ULS.

From the results shown above, the 8-line configuration with 150mm chains complies with the requirements of ULS. The next step is to check how this arrangement behaves after a single failure. Since the tensions are the highest for a 45° incidence at the EOL condition, the ALS is analysed first for this scenario. Figure 88 illustrates the mooring system after one line collapses.

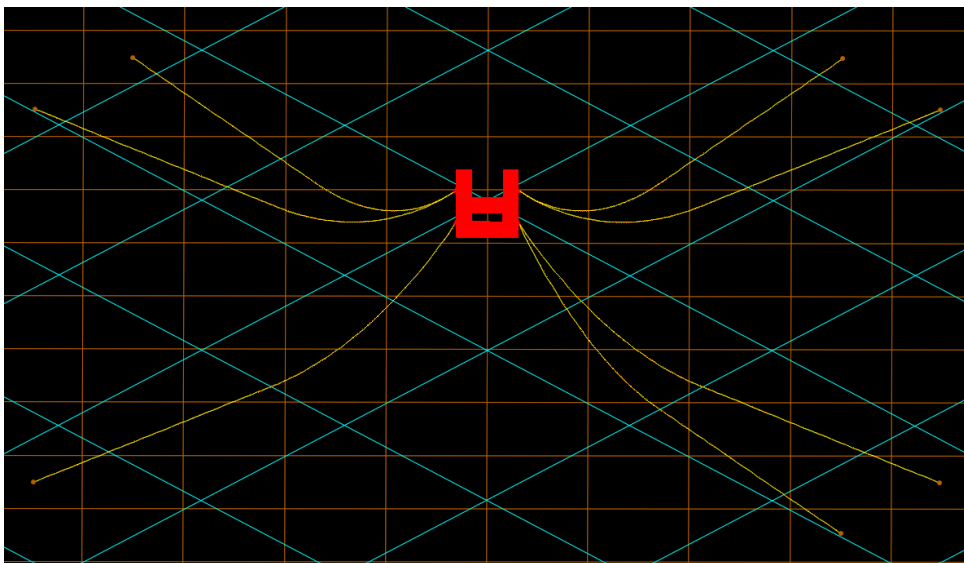


Figure 88. ALS condition | 8 Lines.

As it can be seen in Figures 89 and 90 if the line in one corner fails, the remaining one is not capable of withstanding the environmental loads and will also collapse. The maximum effective tension obtained is 21742 kN, which combined with a pretension of 1740 kN, results in a utilization factor of 1.549. Also, the uplift forces are too high for a drag anchor to hold.

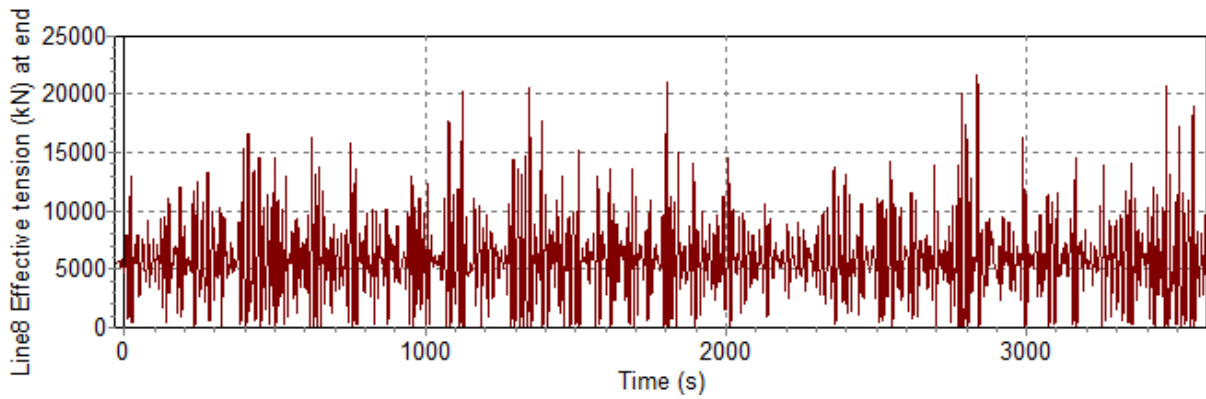


Figure 89. Line effective tension at fairlead | 45° incidence | ALS.

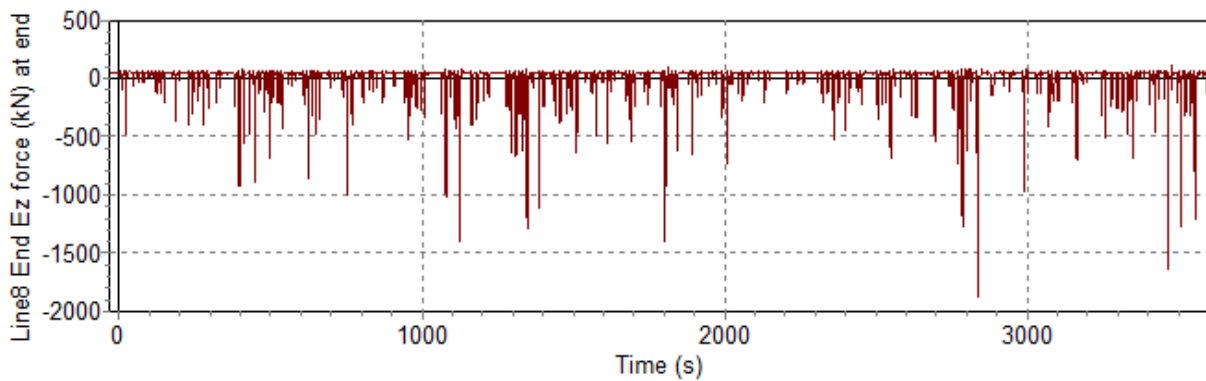


Figure 90. Anchor vertical force | 45° incidence | ALS.

The mooring point is moved further from the platform, increasing the line length to 600 meters to avoid high line tensions due to anchor uplift, but the maximum effective tension found still results in an utilization factor higher than 1 ($u = 1.373$). Therefore, it is decided to include one more mooring line on each corner. Figures 91 and 92 illustrate the results found after the last modification.

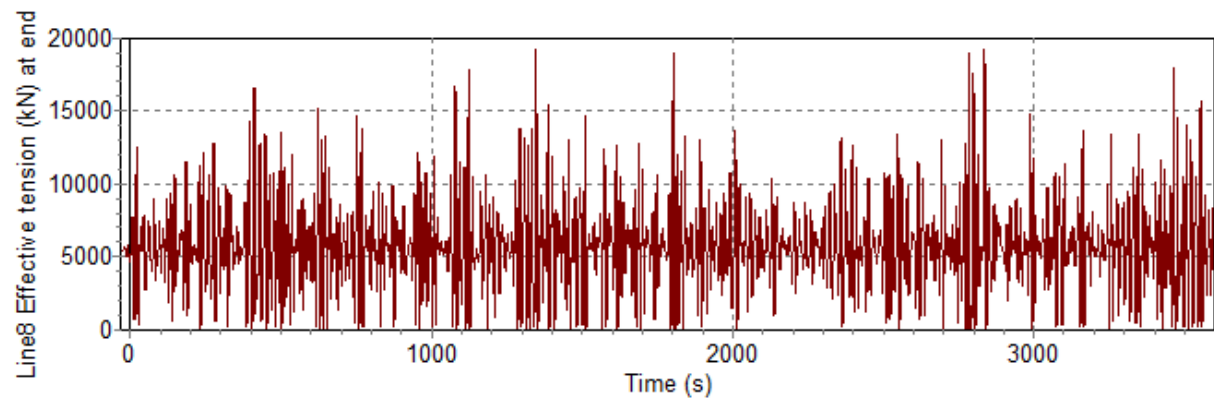


Figure 91. Line effective tension at fairlead | 45° incidence | ALS | 600m lines.

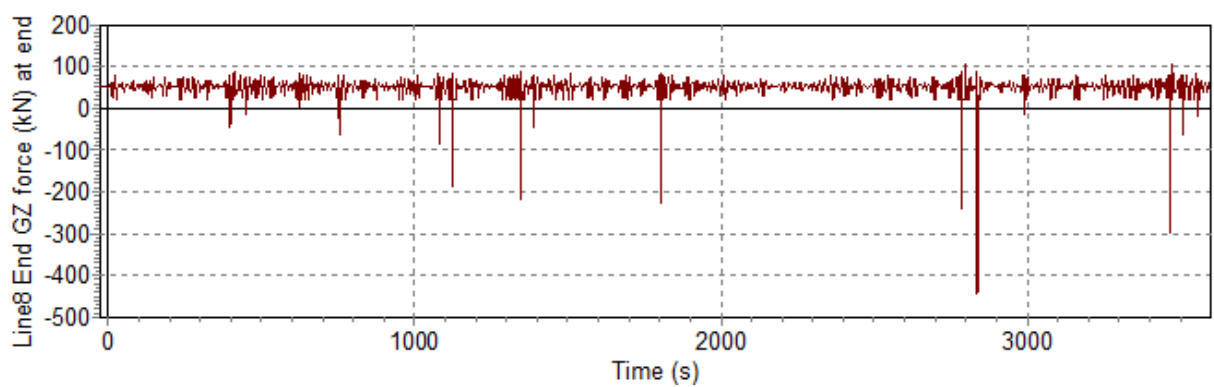


Figure 92. Anchor vertical force | 45° incidence | ALS | 600m lines.

7.5.2. Results / 12 Lines Configuration

Now, the 12-line configuration is tested with 150mm diameter chains. This configuration is illustrated in Figure 93.

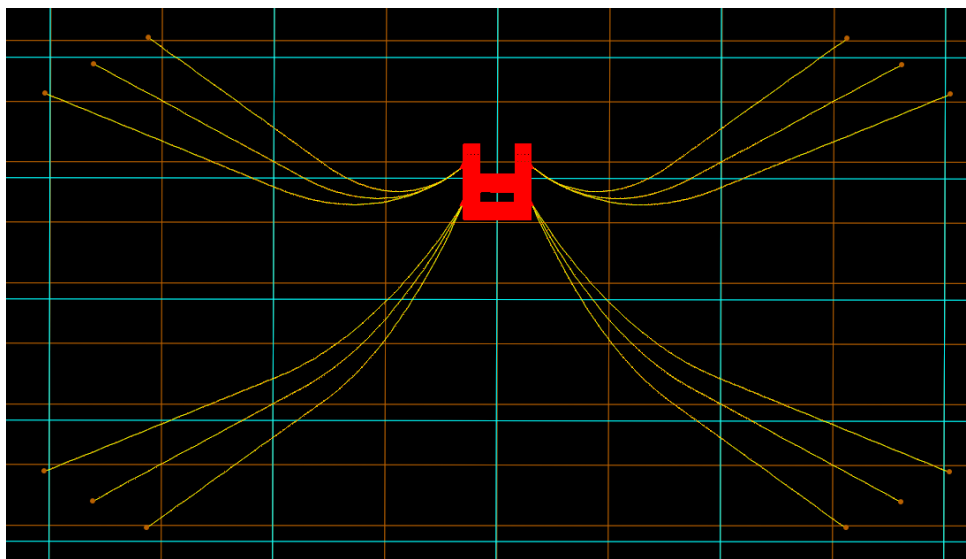


Figure 93. ULS condition | 12 Lines.

The platform excursion for a SOL condition with the environmental factors acting at 0° and 45° are shown in Figures 94 to 97.

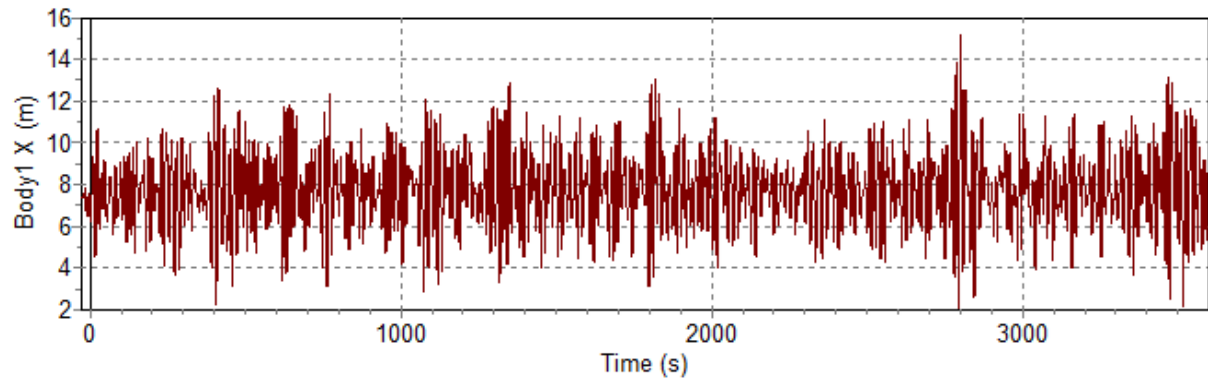


Figure 94. Platform excursion | Global X | 0° incidence.

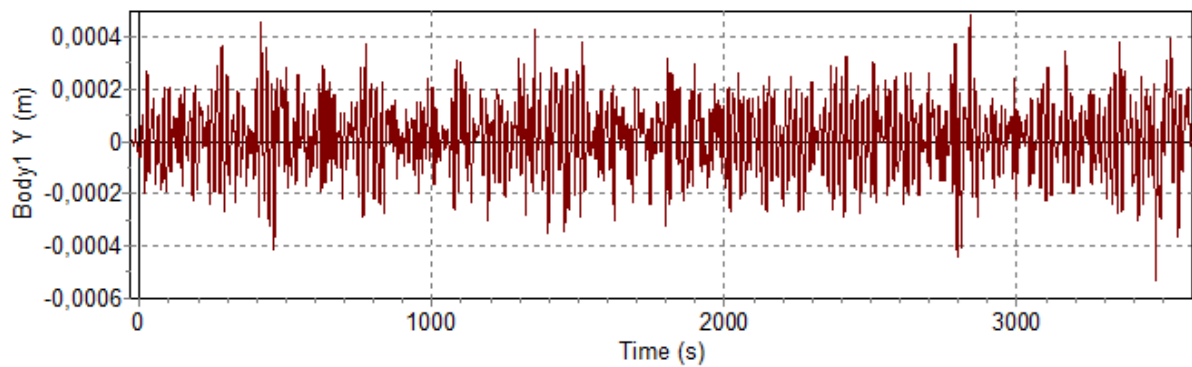


Figure 95. Platform excursion | Global Y | 0° incidence.

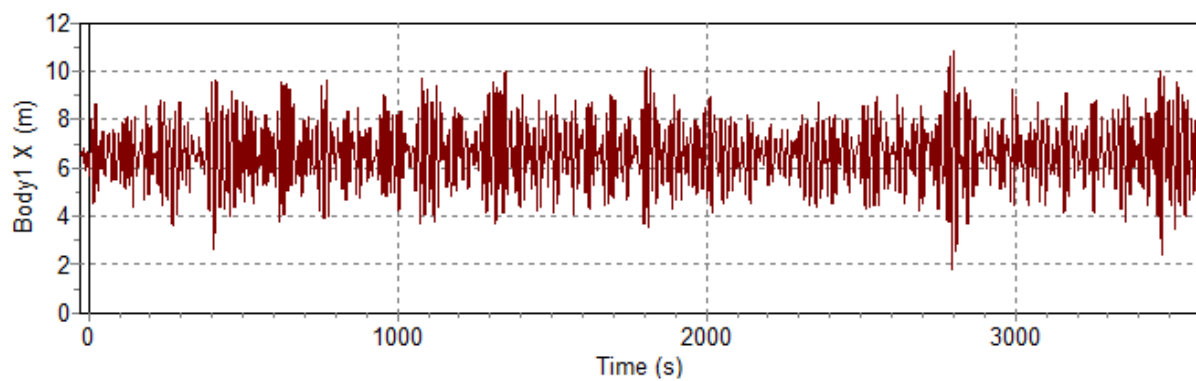


Figure 96. Platform excursion | Global X | 45° incidence.

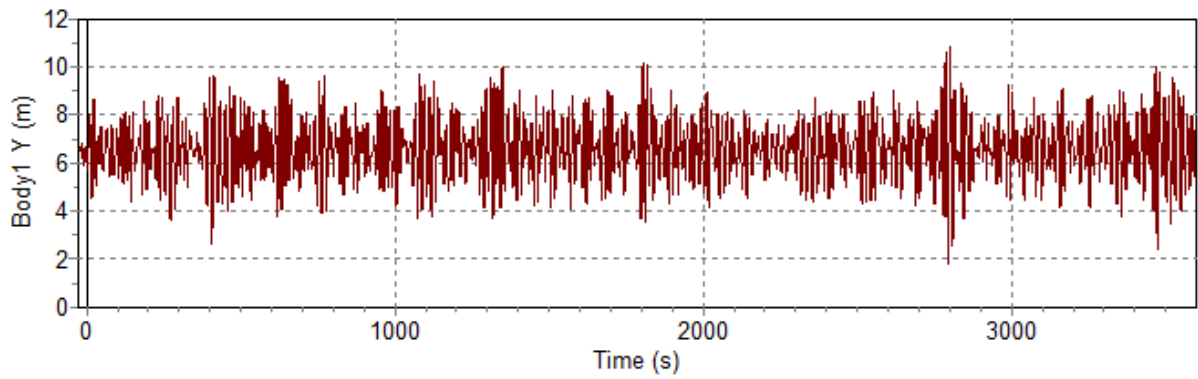


Figure 97. Platform excursion | Global Y | 45° incidence.

The average platform excursion is 7.75 and 9.32 meters for a 0° and 45° incidence, respectively. The maximum excursion obtained is 15.36 meters when a 45° incidence is experienced.

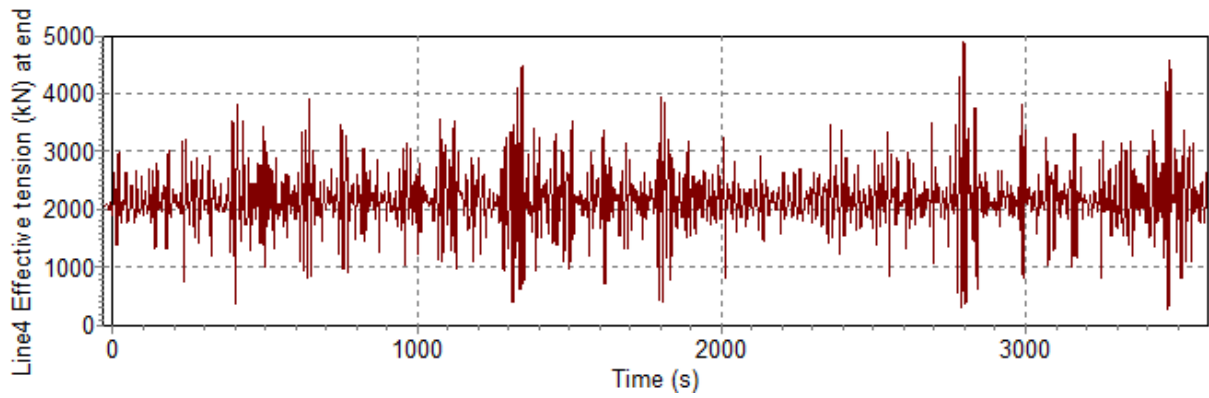
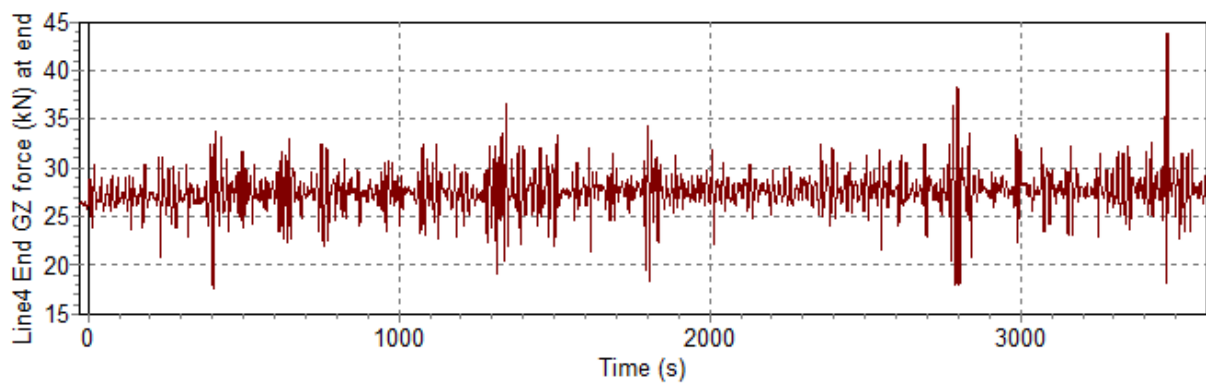
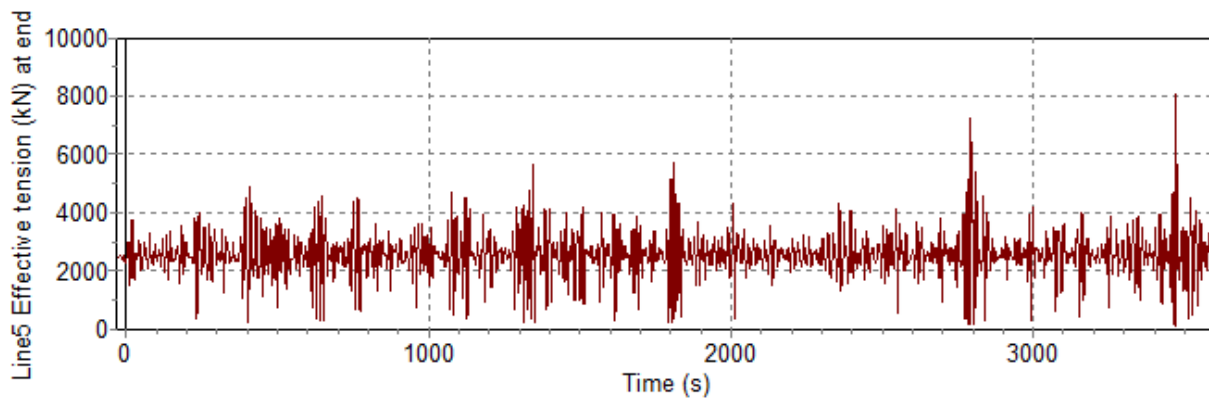
After checking the platform excursion, the lines' utilization factor and anchor vertical force are verified. For this, the line properties are modified according to how they are expected to be at the EOL condition. For a 45° incidence, the anchor uplift is an issue, so the mooring point is moved to increase the lines' length from 381 to 450 meters, resulting in a new line weight of 222 tons.

After this modification, there is no uplift force in the anchors. Also, both incidences result in a utilization factor lower than 1 in all lines. Table 56 summarizes the highest utilization factor.

Table 56. Utilization factor | ULS | 12 lines | 150mm.

Incidence	0°	45°
Pretension [kN]	1513	1513
Tension [kN]	4906	8104
u	0.412	0.714

Figures 98 to 101 show the effective tension at the fairlead and anchor vertical force of the line with the most severe results for the intact condition. It should be noted that the anchor uplift force is a negative vertical force in the graphs provided.

Figure 98. Line effective tension at fairlead | 0° incidence | ULS.Figure 99. Anchor vertical force | 0° incidence | ULS.Figure 100. Line effective tension at fairlead | 45° incidence | ULS.

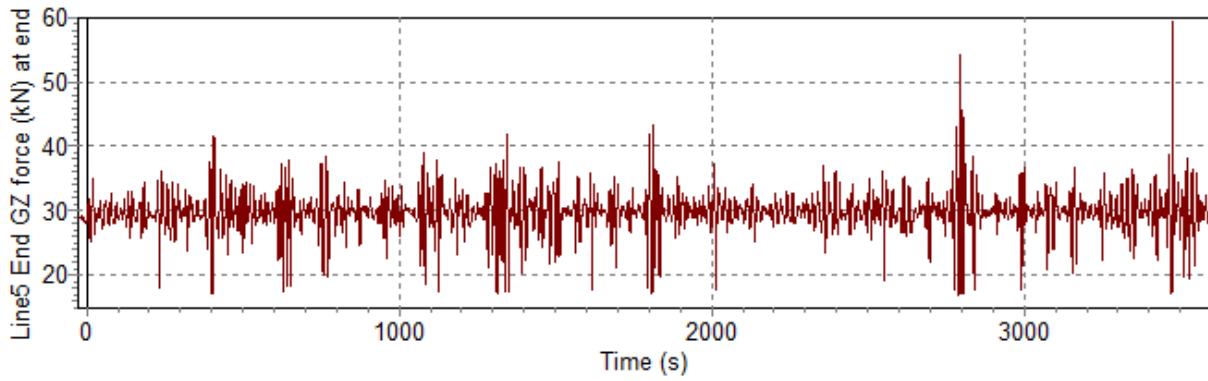


Figure 101. Anchor vertical force | 45° incidence | ULS.

From the results shown above, the 12-line configuration with 150mm chains complies with the requirements of ULS. The next step is to check how this arrangement behaves after a single failure. Since the tensions are the highest for a 45° incidence at the EOL condition, the ALS is analysed first for this scenario. Figure 102 illustrates the mooring system after one line collapses.

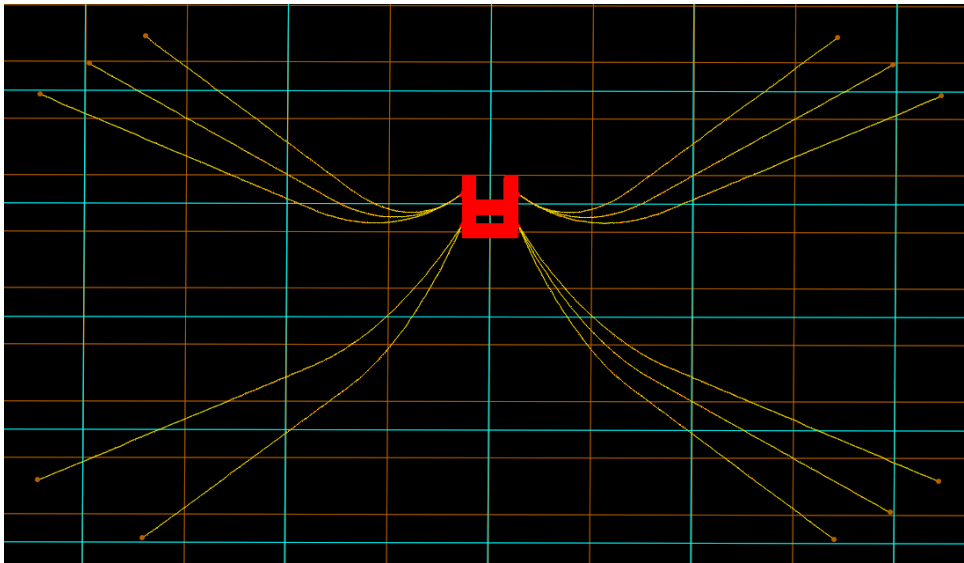


Figure 102. ALS condition | 12 Lines.

Due to high uplift forces at the anchor, the line length is further increased from 450 to 550 meters. After this modification, there is no uplift force and the maximum effective tension of 10450 kN, combined with a pretension of 1513 kN, results in a utilization factor of 0.740. Also, the maximum platform excursion is 17.42 meters. Figures 100 and 104 show the tension and anchor vertical force time history for the ALS.

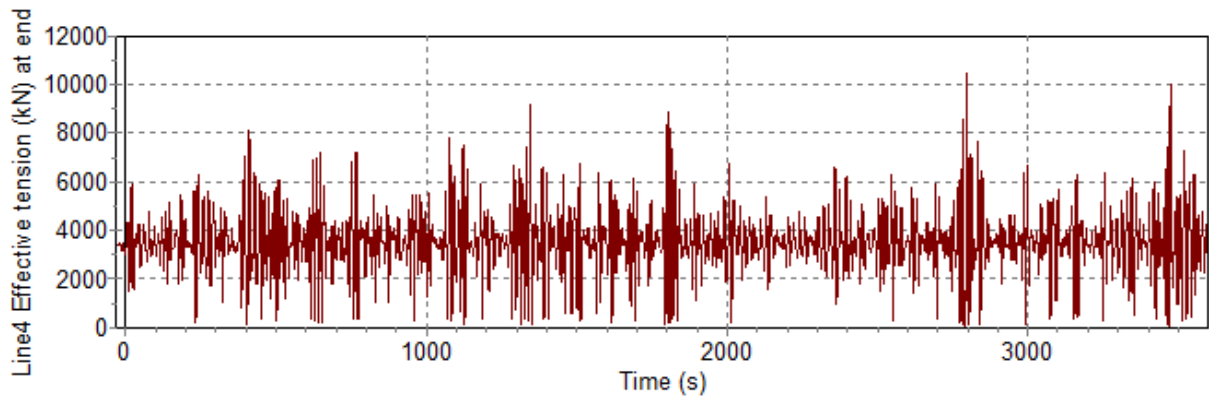


Figure 103. Line effective tension at fairlead | 45° incidence | ALS.

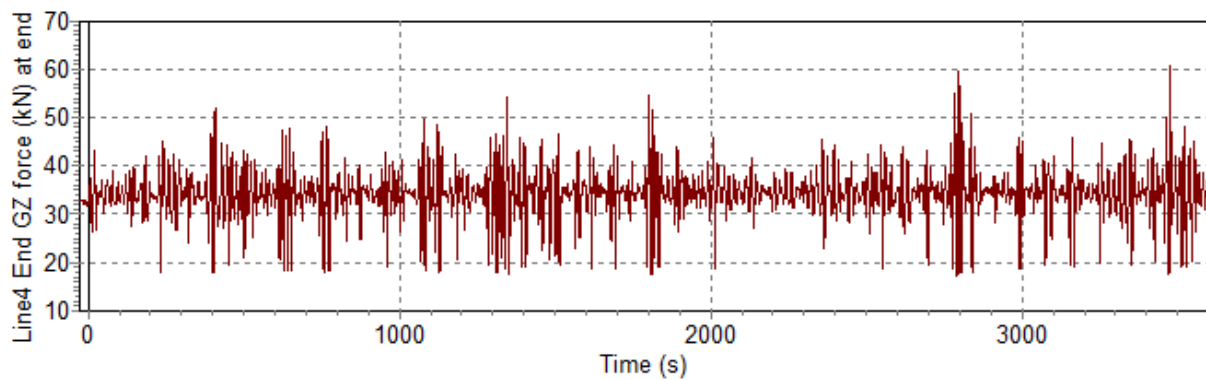


Figure 104. Anchor vertical force | 45° incidence | ALS.

Once the mooring lines' integrity is assured for the ultimate and accidental limit states, the next step is to verify their fatigue life. After performing a Rainflow analysis, it is found that the maximum damage occurs in line 3, reaching 1.85 and resulting in a fatigue life of only 13 years, while the minimum required is 25 years.

Until this point, the line length increase was followed by the displacement of the anchor, so the pretension could be maintained. This way, the excursions remained within the established limits. However, this excursion was proven to be too restrictive due to the short fatigue life obtained. Therefore, to avoid the inclusion of more mooring lines, the line length is further increased by 10 meters while maintaining the anchors at the same position, which allows for more excursion but reduces the line tension.

After this modification, the total line length is 560 meters. Figure 105 shows the highest fatigue damage occurs at the fairlead, while the bump around 150 meters corresponds to the touchdown point, where the line is constantly lifted from the seabed.

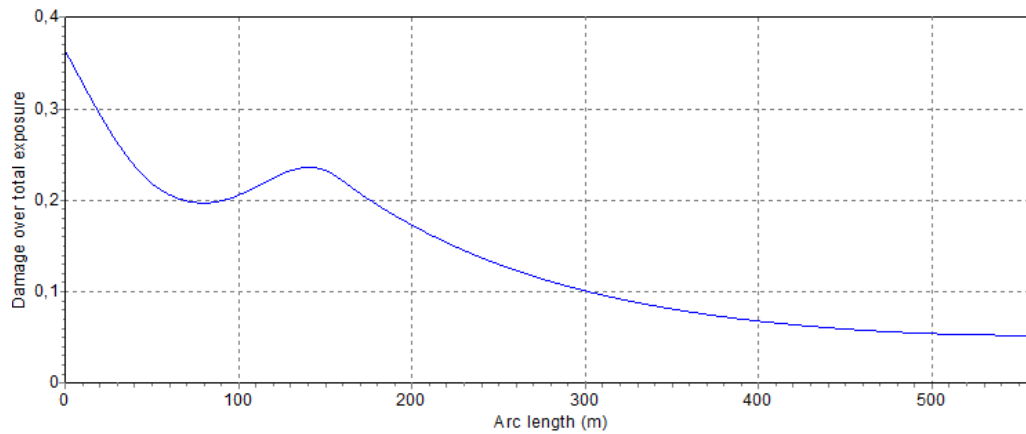


Figure 105. Total fatigue damage over line length.

Therefore, the fatigue life at the fairlead is taken as the limiting factor. As it can be seen in Table 57, the fatigue life of all lines is above the service life of 25 years.

Table 57. Fatigue results

Line	1	2	3	4	5	6	7	8	9	10	11	12
Damage	0.30	0.32	0.36	0.25	0.22	0.19	0.25	0.27	0.31	0.28	0.25	0.23
Life [years]	83	77	69	100	116	129	101	91	80	90	101	110

Finally, the final line configuration results in a maximum platform excursion of 24.1 meters and a utilization factor of 0.616 for the ALS.

7.5.3. Conclusion

The time domain analysis shows that the tension sustained by the mooring lines in an 8-line configuration results in an excessively high utilization factor during an accidental scenario. To solve this issue, the line pretension could have been reduced, but the platform excursion would have been higher than previously established. Furthermore, fatigue issues could arise, requiring the lines' pretension to be further decreased and leading to even larger platform excursions.

Therefore, the chosen solution is to add a mooring line in each corner of the platform. By doing this, the lines' utilization factor becomes lower than 1 and the average excursions are within 10 meters. However, for the mooring system fatigue life to be longer than 25 years, the pretension is reduced. This results in an average platform excursion of 17.6 meters and a maximum of 24.1 meters. To ensure the platform average excursion remains lower than 10% of the water depth, more mooring lines should be included. However, the costs this solution would incur do not compensate for its benefits. Therefore, the platform is allowed to drift slightly more than initially defined.

It should be highlighted how a small variation of the mooring line length, from 550m to 560m, causes a significant reduction in the line pretension and, consequently, in its fatigue life. Even though the mooring line with the shortest fatigue life has more than twice what is required (69 years), it should be borne in mind that more severe conditions, those with less than 5% of occurrence probability, are not taken into account and would increase fatigue damage. Also, the costs involved in adding a few meters of mooring lines are marginal if compared to how much damage their failure can cause.

Tables 58 and 59 compare the results for each mooring configuration. The 12-line configuration results are updated for the 560m line length, which makes it clear that fatigue life is the main design driver.

Table 58. Utilization factor | ULS | 8 lines x 12 lines.

Number of lines	8		12	
Incidence	0°	45°	0°	45°
Pretension [kN]	1740	1740	1008	1008
Tension [kN]	6878	10479	3590	5461
u	0.590	0.931	0.305	0.482

Table 59. Utilization factor | ALS | 8 lines x 12 lines.

Number of lines	8	12
Pretension [kN]	1740	1008
Tension [kN]	19300	8699
u	1.372	0.616

Table 60 provides the details of the final mooring configuration.

Table 60. Mooring details

Number of lines	12
Angle between lines [°]	8
Chain size [mm]	150
Chain length [m]	560
Chain mass [tons]	276
Mooring footprint radius [m]	396
Line pretension [kN]	1008
Average excursion (ULS) [m]	17.6

8. POWER CABLES

The load cases assumed to analyse the behaviour of the power cables are the same as those employed in the mooring system design. The SOL and e EOL conditions are analysed for the NEAR and FAR scenarios. Since the power cables are composed of various components with different mechanical properties, the fatigue verification would require specialised software to account for how much each component contributes to the cable strength and obtain the damage they sustain. Therefore, the analyses in this report are limited to the cable's ultimate strength.

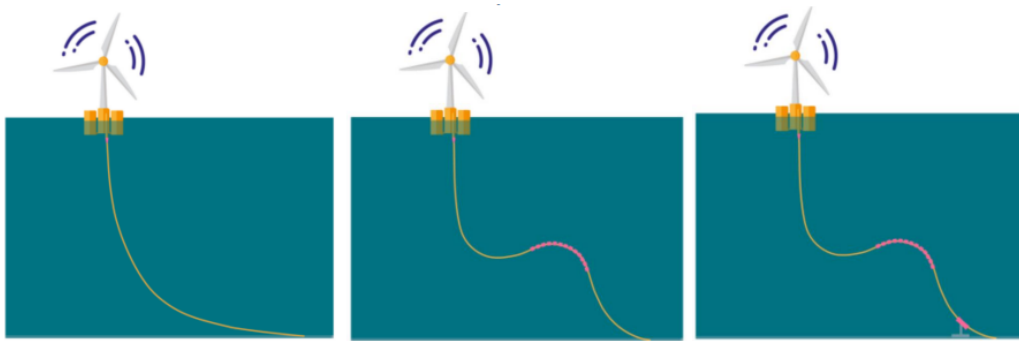


Figure 106. Dynamic cable configurations (free hanging, lazy wave and pliant wave) (COREWIND n.d.).

Figure 106 illustrates three common cable configurations for wind turbines. On the left, the free-hanging configuration is shown. This arrangement is the simplest since there is no need for buoyancy modules, making it also the cheapest solution. However, it does not decouple the floater movement from that of the cable, resulting in high cable excitation. Therefore, it is recommended for confined areas or areas in which no severe environmental action is expected. For these reasons, this configuration is not considered in this project.

In the middle, the lazy wave arrangement is presented. It consists of the free-hanging configuration with the introduction of buoyancy modules that create a slack zone and decouple the cable movement from that of the floater. By doing this, the floater can be exposed to more severe waves and wind due to the smaller effect on the cables' movement. However, this solution behaves poorly when subjected to strong transversal currents. In this case, the touchdown point can migrate to another location, causing damage by abrasion over time. Furthermore, in the case of a floating substation, where many cables are installed relatively close, this lateral movement can lead to a collision between cables and damage.

On the right, the pliant wave configuration is illustrated. This one aims at solving the touchdown point migration by introducing a tether just before this point to keep it within a

small area. This way, the dynamic cable position can be better predicted, avoiding contact between cables under lateral currents. Therefore, this solution is used for the analysis of the power cables in this project. Figure 107 illustrates the pliant wave configuration with more details.

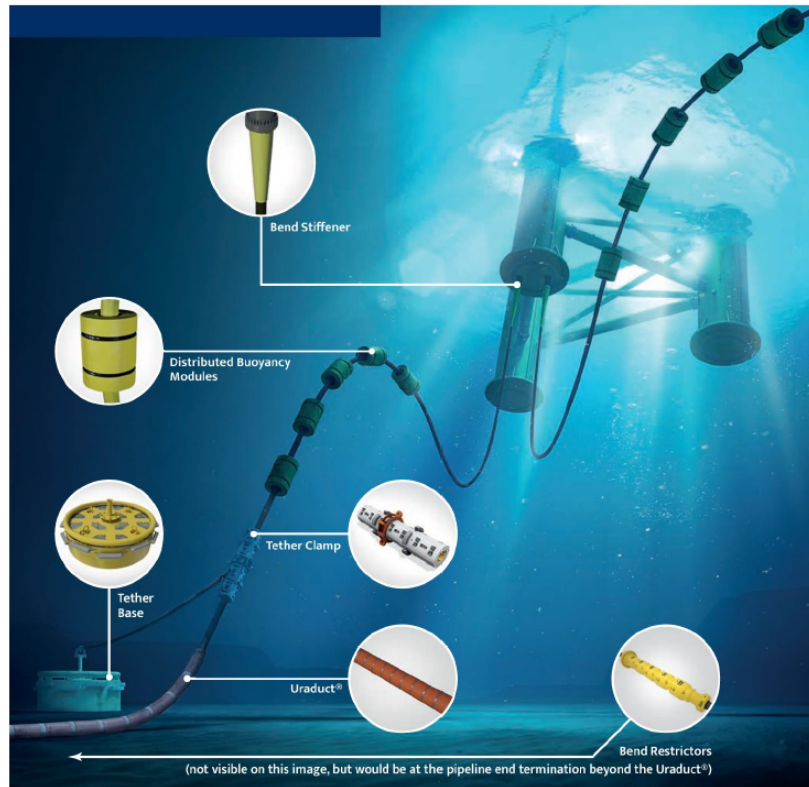


Figure 107. Pliant wave configuration in detail (Subsea n.d.).

The 275 kV and 66 kV dynamic cable properties are assumed to be the ones shown in Table 61.

Table 61. Cable properties.

Cable	275 kV (EC)	66 kV (IAC)
Outer diameter [mm]	278.7	113.3
$W_{\text{flooded cable in air}}$ [kg/m]	146	22
$W_{\text{marine growth (up to 40m)}}$ [kg/m]	155	87
$W_{\text{marine growth (up to 100m)}}$ [kg/m]	67	33
Long. C_D	0.008	0.008
Trans. C_D	1.2	1.2
Trans. C_D marine growth (up to 40m)	1.7	2.8
Trans. C_D marine growth (up to 100m)	1.4	1.9
Axial stiffness [MN]	1384	115
Bending stiffness [kNm^2]	125	19.5
Maximum bending radius [m]	6.85	1.7
Maximum allowable tension [kN]	1758	86.5

Since the capacity curve is not provided, it is estimated by a linear variation from the point of maximum tension, where no curvature is present, and MBR, where the allowable tension is zero. Also, an 80% utilization line is introduced, which is the recommended limit for operational conditions. Figures 108 and 109 show the capacity curve for each cable.

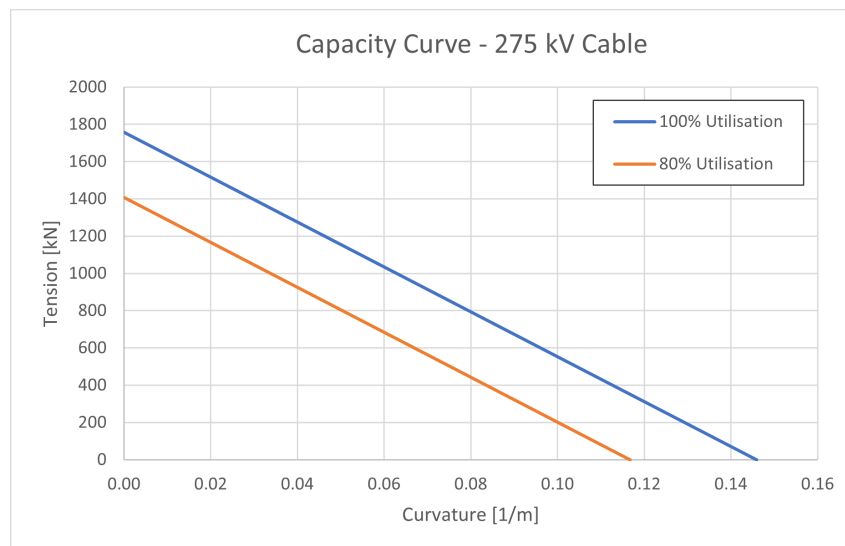


Figure 108. 275 kV cable capacity curve.

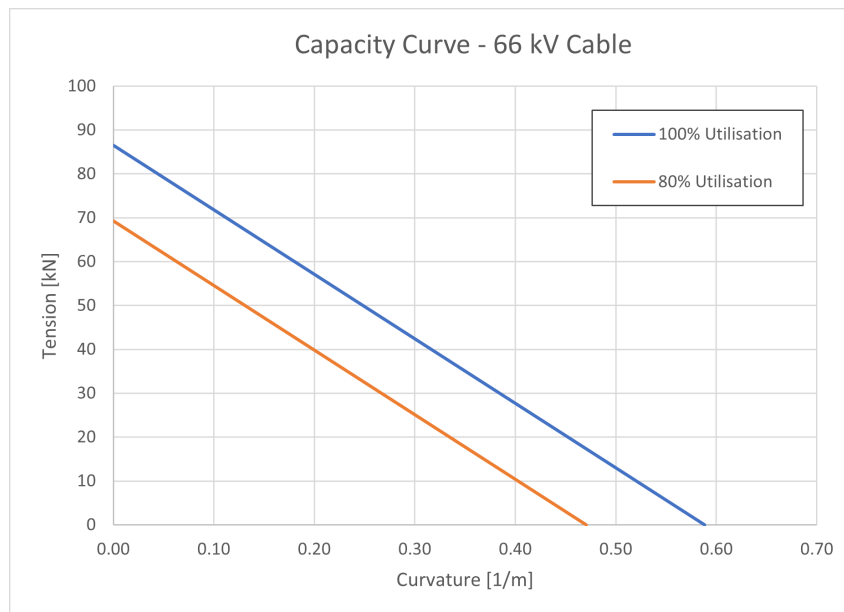


Figure 109. 66 kV cable capacity curve

To avoid cable clashes, a different number of buoyancy modules are introduced in adjacent cables. This way, the slack zone of a cable is always at a different depth from that of the cables next to it. The buoyant section of the cable is modelled by introducing an equivalent cable section, which is the combination of the cable and buoyancy module properties. The buoyancy modules' dimensions and spacing are illustrated in Figure 110 and detailed in Table 62.

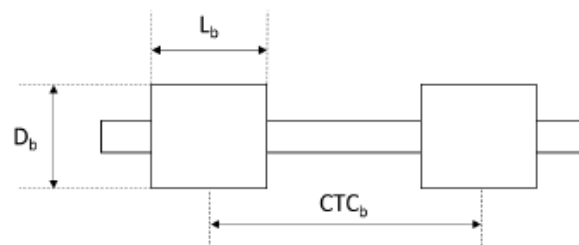


Figure 110. Buoyancy modules.

Table 62. Buoyancy modules' details.

Cable	D_b [m]	L_b [m]	m [kg]	$b(\text{SOL})$ [kg]	$b(\text{EOL})$ [kg]
EC	1.1	1.1	310	700	652
IAC	0.55	0.785	47	88	82

The final static configuration of the cables is defined by checking compliance with the cable bending radius and tension according to the cable capacity curve. Following this, cable clash occurrence is verified.

The most sensitive areas of a cable are between the tether clamp and touchdown point and at the end of the j-tube. In these areas, excessive curvature and/or abrasion can be expected due to the shape the cable assumes or due to the movements of the platform. Therefore, ancillaries must be added to address these issues. It should be noted that abrasion at the touchdown point is not expected to be an issue for a pliant wave configuration due to the limited migration of this point.

Due to the proximity between the tether clamp and the touchdown point, the cable may assume a small bending radius between these two points and exceed the MBR. Therefore, a bend restrictor must be included in this region so the cable reaches the seabed with an acceptable curvature. The design of such a structure is complex and requires local analysis of the cable. Therefore, an eventual excessive curvature in this area is disregarded due to the assumption that it can be handled by a bend restrictor.

There are two main solutions for the issues that may arise just after the cable leaves the J-tube. The first one is the installation of a bell mouth. This is a simple, inexpensive and easy-to-install structure in the form of a cone that makes sure the MBR is always respected, regardless of how the floater moves. However, this device can result in cable damage by abrasion. To solve this issue, a bend stiffener may be used. This is a flexible structure that controls the cable deflection and bending radius, but it is extremely expensive. Figure 111 illustrates a typical bell mouth and bend stiffener.

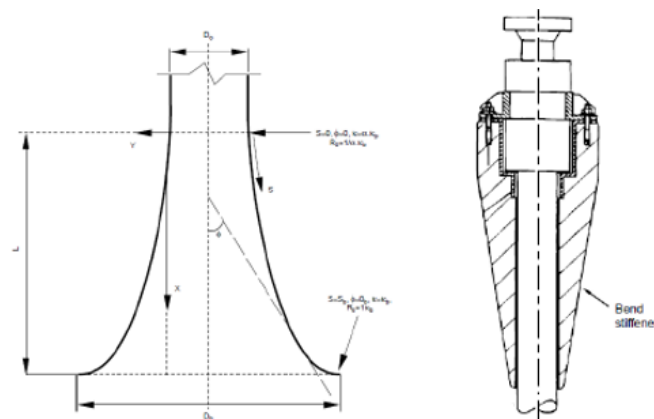


Figure 111. Bell mouth (left) and bend stiffener (right).

The choice between one of these solutions depends mainly on how severely the floater is expected to move, on where the j-tube is located (the further from the floater centre, the more motions are expected) and on the submarine current profile. Since this decision requires a local analysis of the cables, it is not covered by this work and should be tackled in the detailed design phase.

8.1. Cable Configuration

A scheme of the cable configuration is shown in Figure 112 and Table 63 provides the correspondent values for the two configurations assumed for each cable type.

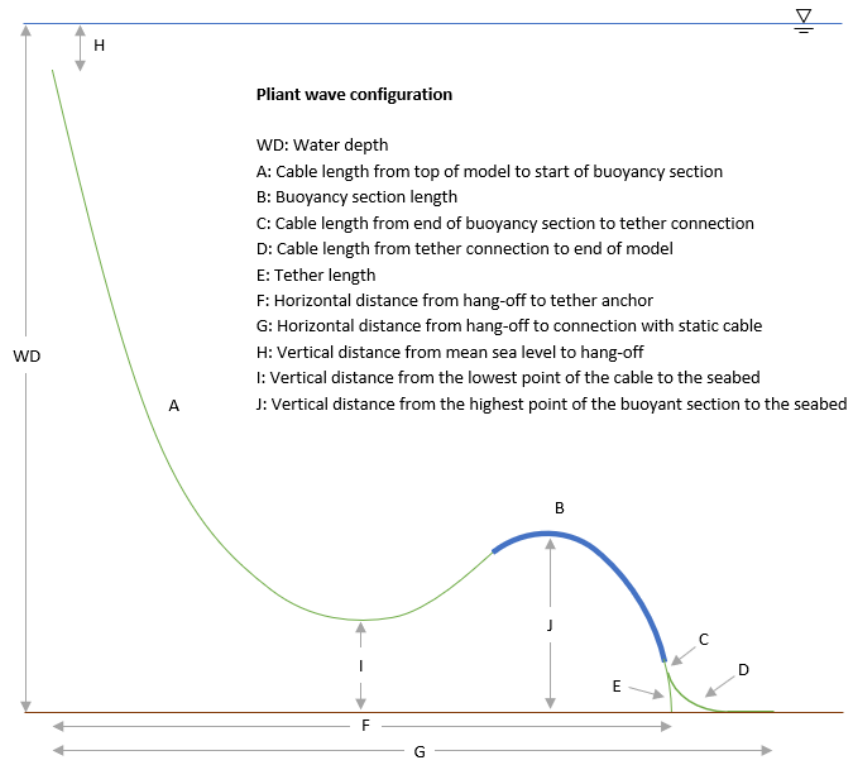


Figure 112. Pliant wave configuration.

Table 63. Cable configuration.

Configuration	WD [m]	H [m]	A [m]	B [m]	C [m]	D [m]	E [m]	F [m]	G [m]	CTC _b [m]
EC_Lower	100	22	65	65	5	45	8	87	127	2.5
EC_Upper	100	22	60	80	5	49	8	105	151	2.5
IAC_Lower	100	22	70	60	5	45	6	85	127	1.3
IAC_Upper	100	22	66	80	9	41	6	113	151	1.3

8.2. Results

To void the wave loading, the cables shouldn't be too close to the surface. However, they must also have some clearance from the seabed to avoid touching it due to the platform's heave motion. Also, the tether must be constantly in traction during the 25 years of operation. Table 64 provides the cable clearances for the SOL and EOL conditions.

Table 64. Cable clearances.

Condition	SOL		EOL	
	I [m]	J [m]	I [m]	J [m]
EC_Lower	37.6	47.5	30.0	38.4
EC_Upper	48.6	56.7	38.9	45.9
IAC_Lower	40.9	50.8	25.6	34.7
IAC_Upper	56.2	65.0	35.4	45.0

The upper IAC SOL configuration might experience some wave excitation for being only 35 meters away from the surface. However, this is the solution found to ensure that the tether remains in traction at the EOL condition. Furthermore, marine growth is fully developed in roughly 2 years, so the EOL condition is considered more relevant for the design. The other configurations present a satisfactory clearance both from the surface and seabed. Figures 113 and 114 illustrate these configurations.

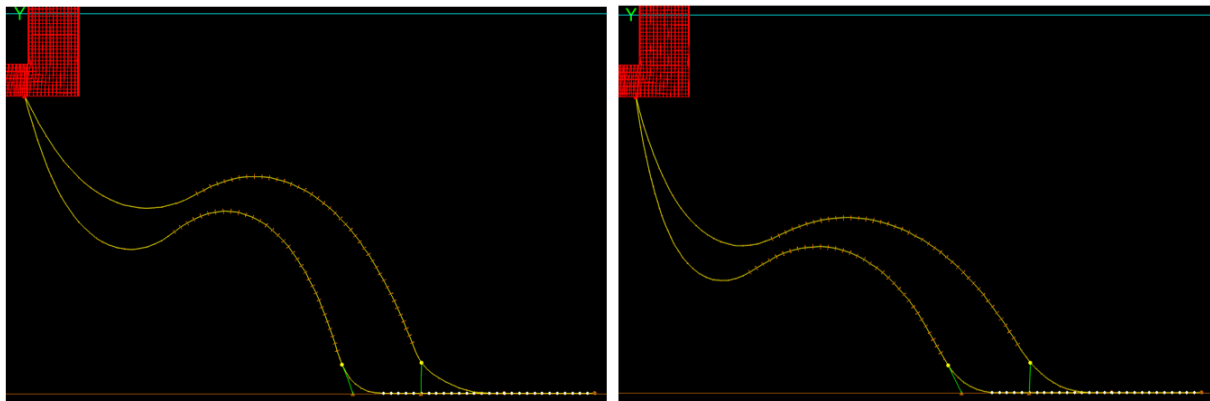


Figure 113. Export cable configurations at SOL and EOL.

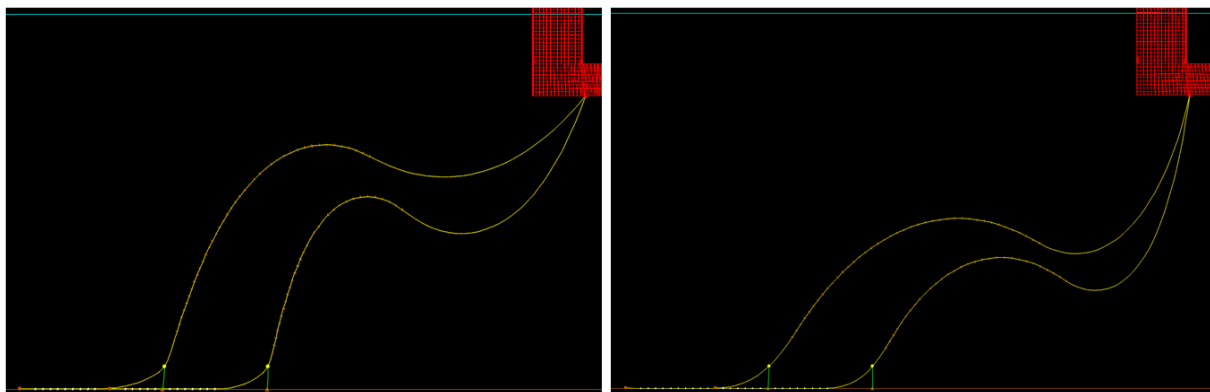


Figure 114. Inter array cable configurations at SOL and EOL.

Figure 115 and 116 compare the capacity curve with the curvature and tension obtained after the static analysis for the FAR and NEAR scenarios at the SOL.

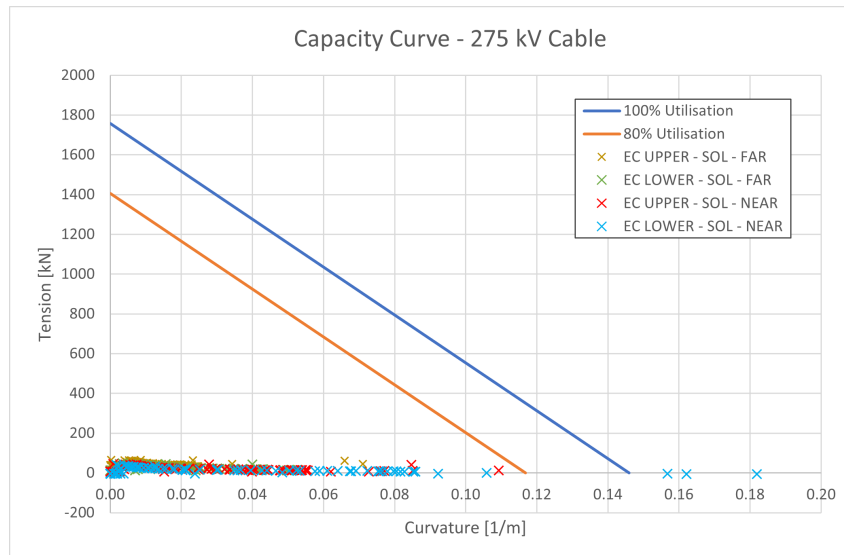


Figure 115. EC static results - SOL

A few points of the lower EC present a curvature higher than the capacity curve allows. These points are located between the tether and touchdown points, naturally where the highest curvatures occur. To solve this issue a bend restrictor should be introduced. Also, axial compression is identified but it is not considered an issue due to its very low values.

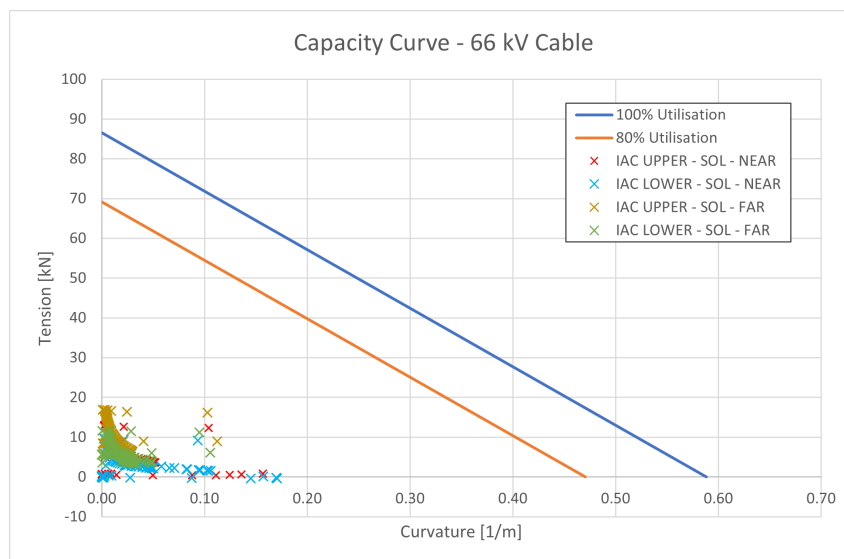


Figure 116. IAC static results - SOL

There is no issue related to the curvature limits for the IACs. Also, axial compression is present, but the value is much lower than the limit of 3kN. Figures 117 and 118 illustrate these configurations.

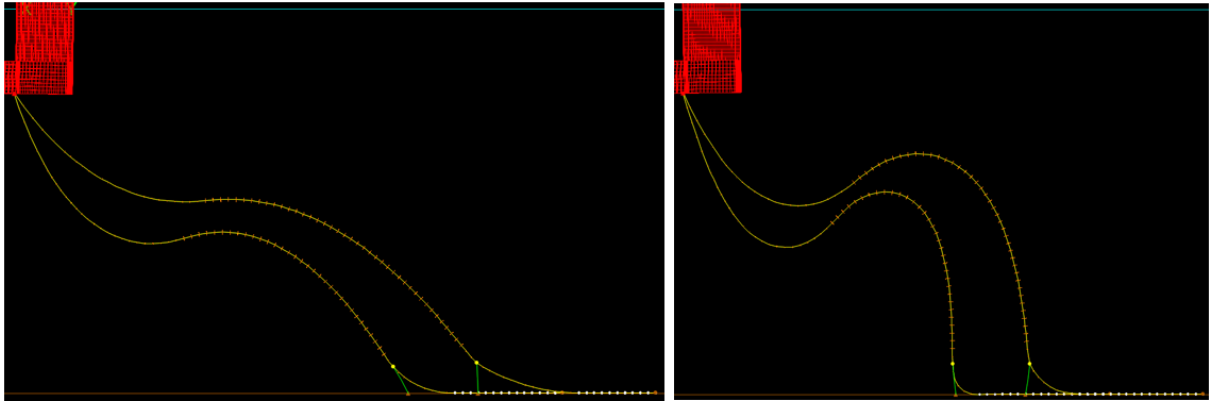


Figure 117. Export cable configurations FAR and NEAR at SOL.

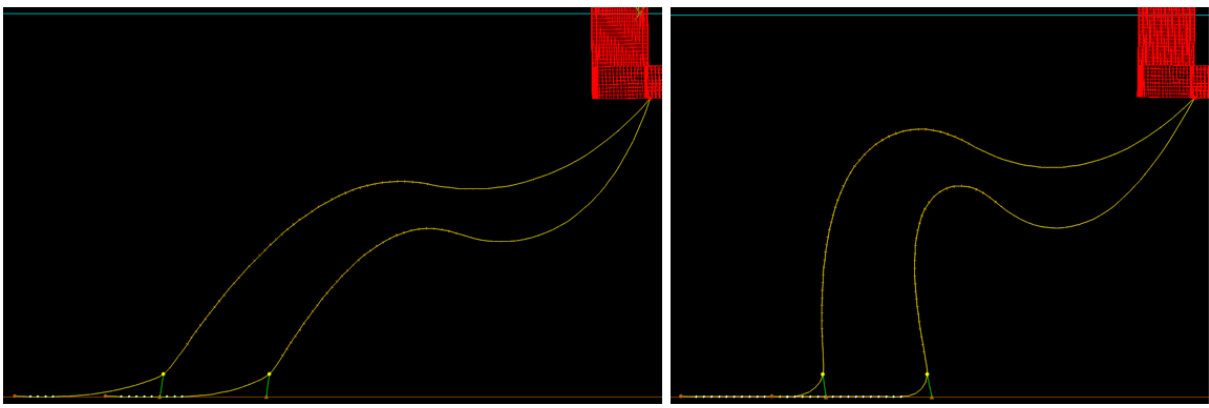


Figure 118. Inter array cable configurations FAR and NEAR at SOL.

Figure 119 and 120 compare the capacity curve with the curvature and tension obtained after the static analysis for the FAR and NEAR scenarios at the EOL. The points in these graphs are very similar to those in an SOL condition, but a higher curvature can be noticed in the ECs and IACs.

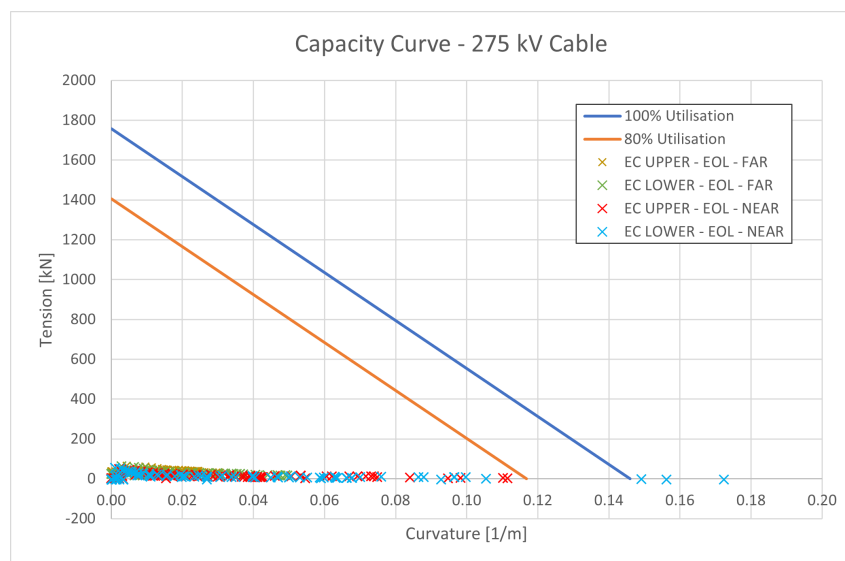


Figure 119. EC static results - EOL

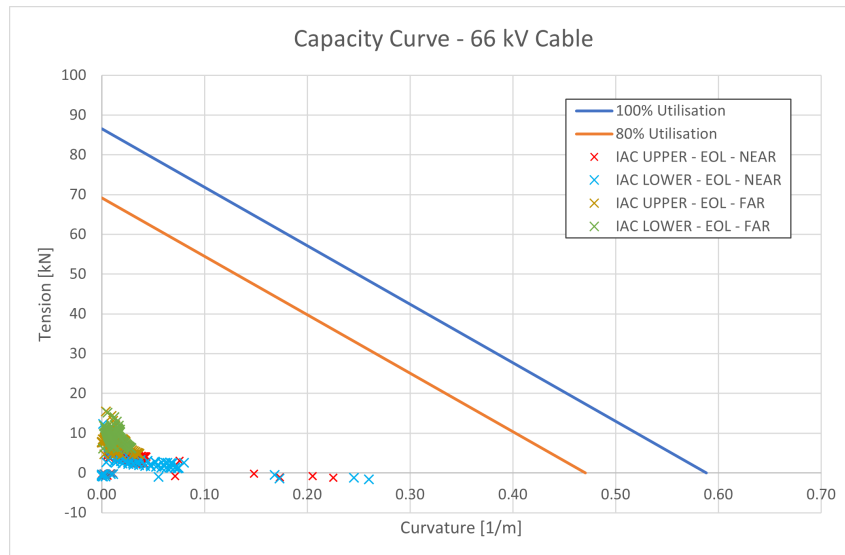


Figure 120. IAC static results - EOL

Figures 121 and 122 illustrate these configurations.

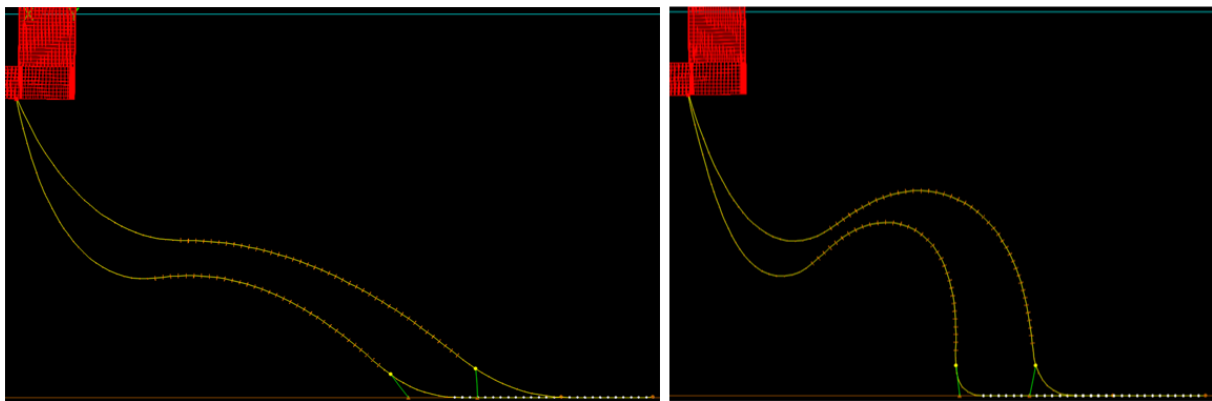


Figure 121. Export cable configurations FAR and NEAR at EOL.

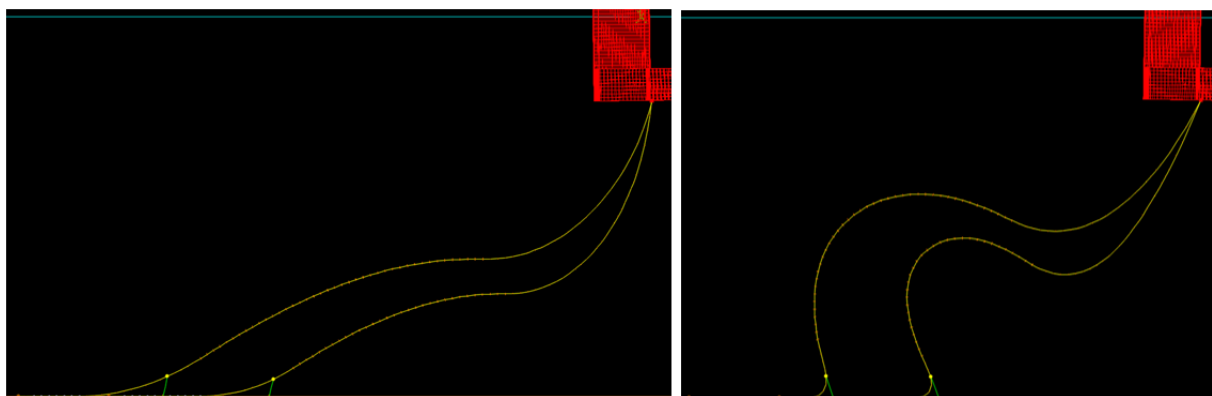


Figure 122. Inter array cable configurations FAR and NEAR at EOL.

Due to the absence of a wind farm layout, the cables are assumed to leave the platform parallel to each other. This is done to simulate the most critical condition. In reality, the

cables could leave the substation with different orientations to further reduce the risks of cable clash. A clash check is run for the cables most susceptible to touching others under perpendicular current and no contact is detected. Figure 123 illustrates the cables' shape when the extreme transversal current acts on them.

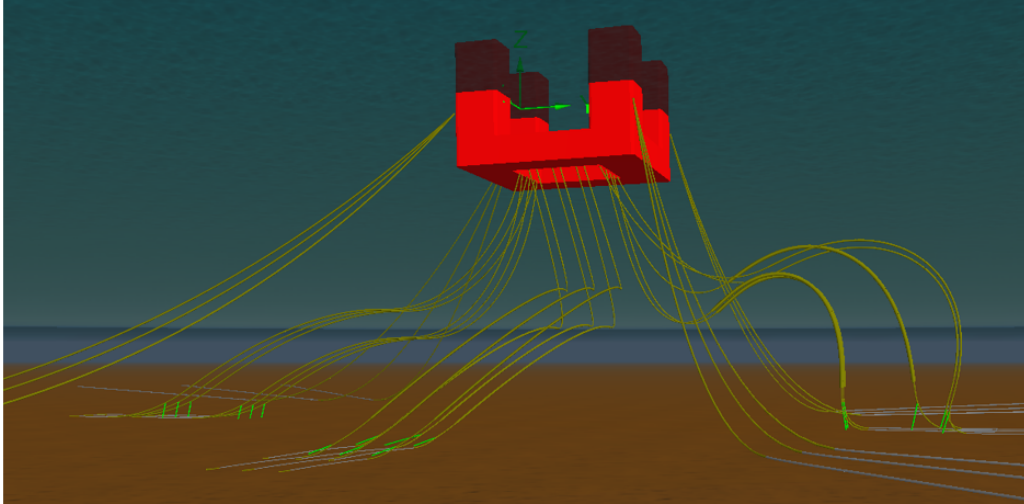


Figure 123. Cables under transverse current.

The final cable configuration is illustrated in Figure 124.

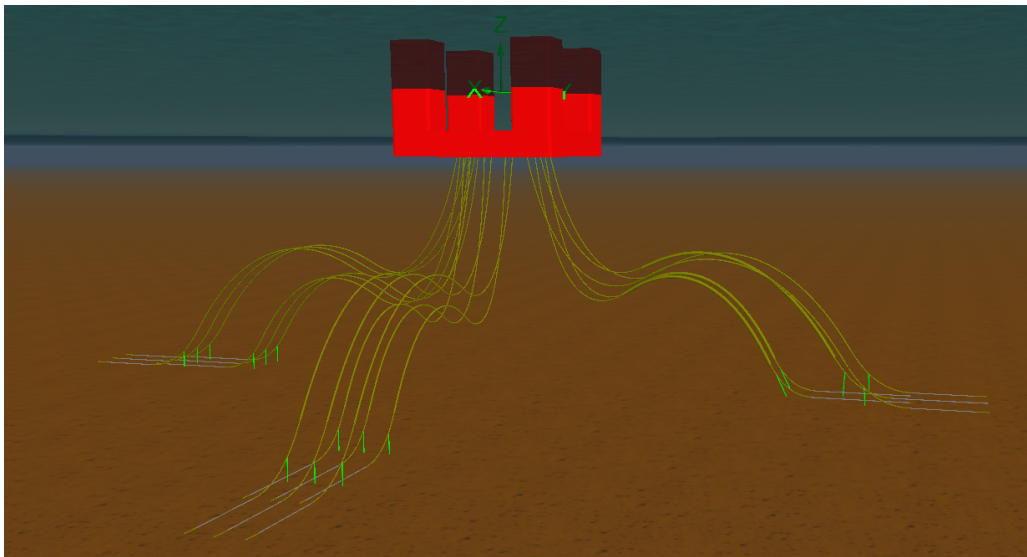


Figure 124. Overview of cable arrangement.

9. PLATFORM RESPONSE

This section investigates the platform's response for the 1-year (operational) and 100-year (extreme) return period storms shown in Table 1. Then, the rotation and accelerations are verified against the limitations imposed by the electrical equipment, shown in Table 6. The waves are represented by a Jonswap wave spectrum with a peak-enhanced factor of 1.8. The current, wave, and wind are assumed to be co-linear. Figure 125 shows the complete OrcaFlex model used to assess the floater motions.

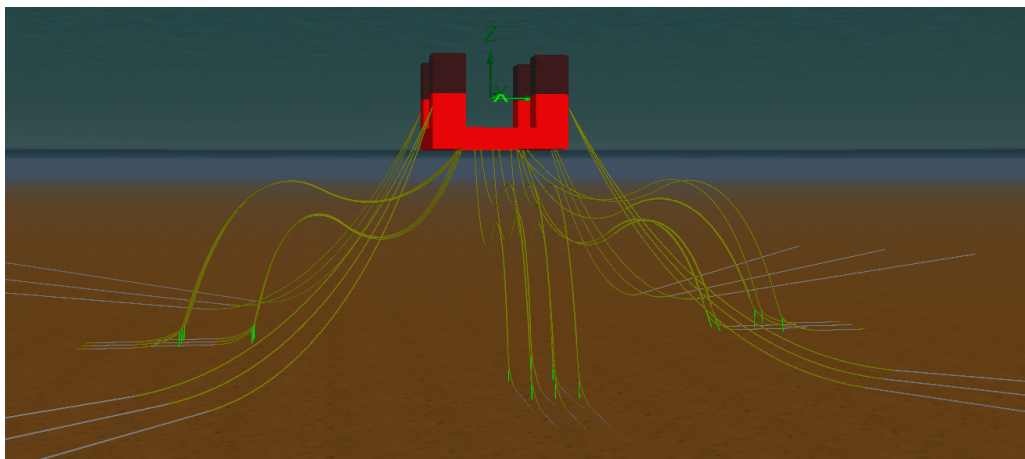


Figure 125. Complete OrcaFlex model.

9.1. Results

The accelerations are measured in two representative locations at the substation. The first point (A) is located at one of the upper corners of the topside. This location experiences the highest vertical acceleration due to the contribution of roll, pitch and heave. The second point (B) is located horizontally at the centre and vertically at the top of the topside. This way, the highest horizontal acceleration is assessed. Table 65 provides the coordinates of these points about the waterline.

Table 65. Points for acceleration measurement.

Location	x [m]	y [m]	z [m]
A	26.00	26.00	28.65
B	0.00	0.00	28.65

Table 66 provides the maximum accelerations and rotation experienced by the platform.

Table 66. Platform response.

Condition	Extreme			Operational		
Location	A	B	Limit	A	B	Limit
a_x [m/s ²]	0.910	0.889	2.943	0.819	0.820	2.452
a_y [m/s ²]	0.910	0.889	2.943	0.819	0.820	2.452
a_z [m/s ²]	1.060	1.127	2.452	1.029	0.813	0.981
Inclination [deg]	4.06		13	3.31		7

All parameters are within the established limits, except for the vertical acceleration at location "A" during the operational condition, exceeding the limit by 4.6%. However, since no viscous effects are considered in the motions analysis performed, the accelerations found are higher than they would be in case this effect was included. That is because, in this case, the oscillation periods of the platform would be higher, leading to lower accelerations. Furthermore, these results refer to the SOL condition, in which the platform is naturally more compliant with the waves than it would be at the EOL, due to the higher weight of cables and mooring lines. Lastly, it should be highlighted that this environmental condition is expected to occur only once per year. Therefore, the acceleration levels found are considered acceptable.

10. CONCLUSION

The need for floating wind farm substations becomes more and more clear as floating wind farm projects move forward, such as the ones within the ScotWind project. Therefore, this thesis focuses on the preliminary design of a floating foundation for a 1232 MW AC substation.

In this work, the floater's main dimensions are defined based on a series of limitations that are managed by a genetic algorithm. These include dimensional, motions and stability restrictions. Furthermore, the floater's scantling is designed according to DNV standards to assure structural integrity under ultimate limit states. Following the structural design, a detailed stability analysis is performed so the floater can be verified against all the relevant intact and damaged large-angle stability criteria. The final design reaches 10000 tons and a length of 54.78 meters

Once the floater is defined, the mooring system is designed for a static condition based on the catenary equation. This provides an initial design to be verified in OrcaFlex, where the wave loads can be included and the line dynamic behaviour assessed. Using this software, two mooring configurations are tested and modified iteratively according to the challenges encountered. Finally, a 12-line configuration that complies with the ultimate, accidental and fatigue limit states is found. It consists of 150mm chains with 560 meters in length.

Next, the power cable arrangement is defined. Due to the high number of inter-array and export cables connected to the floater, this is a challenging task. The cables should not clash against other cables or mooring lines. Therefore, their total and buoyancy section lengths are designed in a way that each cable is in a different depth than the adjacent ones. Also, a pliant wave configuration is chosen to prevent touch-down point migration and cable clash.

Lastly, the OrcaFlex model composed of the floater, mooring lines and cables is used to assess the heeling and accelerations experienced in two points of interest in the substation. These are found to be within the established limits for the extreme and operational conditions.

The following step would be to work on the detailed design. This would include better characterization of the hull structure and the performance of tank tests to calibrate hydrodynamic models, for instance. Also, inputs from geotechnical and geophysical studies should be used to improve the mooring design and allow the choice of anchors. Regarding the cables, more investigation should be made towards the cable behaviour between buoyancy modules and near the hang-off and touch-down points.

The shift from fixed to floating substations comes with a series of challenges. These are not only related to naval architecture subjects such as motions and stability but also to various pieces of equipment that have been conceived for a static application and now will have to adapt to operate in a dynamic set-up. Therefore, there is still a significant maturing period for the industry to be ready for this transition. However, this thesis provides insight into how the floater, mooring system and cable arrangement can be thought to make floating substations a reality.

11. ACKNOWLEDGEMENTS

Participating in the EMship program was one of the most enriching experiences I have been through, not only professionally, but also personally. During these two years, I had the opportunity to learn from amazing professors at the Université de Liège and Universidad Politécnica de Madrid. I would like to thank Philippe Rigo for promoting this master's program and being a dedicated professor and mentor.

The EMship program was challenging for different reasons, such as leaving my home country, living in cities where the local language was new to me and having to face a heavy workload. To overcome these challenges, friendships played an important role in this journey. Therefore, I would like to thank Marianna Sipaupa, Marcos Vieira, Maria Tadea, Declan O'Connor, Neil Mertens, Papatsornpun Pangpun, Mapko Josipovicc, Abdulelah Al-Ghuwaidi, Ezio Mosciatti, Paco Yerkes and Mahmoud Reda for making this experience more pleasant.

Developing my master's thesis within Iberdrola was a great experience and I thank Simone for making this internship possible. Also, I am grateful to Antonio Medina, Ignacio Pantojo and Diego Palacin for assisting me throughout the development of this work with valuable input.

References

- COREWIND (n.d.). *DYNAMIC CABLE CONFIGURATIONS*. URL: <https://corewind.eu/>. (accessed: 03.07.2023).
- Council, Global Wind Energy (n.d.). *Offshore Wind Technical Potential in Spain*. URL: https://gwec.net/wp-content/uploads/2021/06/Spain_Offshore-Wind-Technical-Potential_GWEC-OREAC.pdf. (accessed: 18.04.2023).
- Data, Our World in (n.d.). *Modern renewable energy generation by source, World*. URL: <https://ourworldindata.org/grapher/modern-renewable-prod>. (accessed: 18.04.2023).
- DNV (2014). *DNV-RP-C205 Environmental Conditions and Environmental Loads*.
- (2018). *DNV-ST-0119 Floating wind turbine structures*.
 - (2020). *DNV-OS-C301 Stability and watertight integrity*.
 - (2021a). *DNV-OS-C101 Design of offshore steel structures, general - LRFD method*.
 - (2021b). *DNV-OS-E301 Position mooring*.
 - (2021c). *DNV-RP-C103 Column-stabilised units*.
 - (n.d.). *Floating Substations: the next challenge on the path to commercial scale floating windfarms*. URL: <https://www.dnv.com/article/floating-substations-the-next-challenge-on-the-path-to-commercial-scale-floating-windfarms-199213>. (accessed: 18.04.2023).
- Ellen Jump, Anthony Gray, David Thompson, Lewis Stevenson, and Charlotte Strang-Moran (n.d.). *OFFSHORE SUBSTATIONS: FIXED OR FLOATING? – TECHNOECONOMIC ANALYSIS*. URL: <https://offshorewindinnovationhub.com/wp-content/uploads/2021/09/OWIH-Report-Offshore-Substations.pdf>. (accessed: 18.04.2023).
- Energy, Siemens (n.d.). *Enabling higher voltage levels within offshore wind turbines*. URL: <https://www.siemens-energy.com/global/en/offerings/references/hv-products-for-offshore-wind-oems.html>. (accessed: 18.04.2023).
- Faltinsen, O. (1993). *Sea loads on ships and offshore structures (Vol. 1)*. Cambridge University Press.
- INNOSEA, COBRA, DTU, WIND EUROP, EQUINOR, IREC, UPC, and UL DEWI (2020). *D2.1 Review of the state of the art of mooring and anchoring designs, technical challenges and identification of relevant DLCs*. Core Wind.
- KIM, Hyungjun et al. (2013). “Study on mooring system design of floating offshore wind turbine in Jeju Offshore Area.” In: *International Journal of Ocean System Engineering* 3.4, pp. 209–217. DOI: <http://dx.doi.org/10.5574/IJOSE.2012.3.4.209>.
- Limited, BMT Fluid Mechanics (2006). *Review of issues associated with the stability of semi-submersibles*.
- Linxon (n.d.). *Linxon advances floating substation technology*. URL: <https://linxon.com/news/linxon-hitachi-abb-power-grids-and-atkins-advance-floating-substation-technology/>. (accessed: 21.04.2023).
-

-
- MALTA, Edgard B. et al. (2010). “Damping coefficient analyses for floating offshore structures.” In: *International Conference on Offshore Mechanics and Arctic Engineering*. 49095, pp. 83–89. DOI: 10.1115/OMAE2010-20093.
- Nevesbu (n.d.). *Floating offshore substation concept design*. URL: <https://www.nevesbu.com/projects/floating-offshore-substation-concept-design/>. (accessed: 21.04.2023).
- Rasmussen, Klaus Munck (n.d.). *Substations*. URL: <https://www.bladt.dk/solutions/substations/>. (accessed: 19.07.2023).
- Ritchie, Hannah and Max Roser (n.d.). *Sector by sector: where do global greenhouse gas emissions come from?* (accessed: 18.04.2023).
- Ruid, Madeline (n.d.). *Offshore Wind Power Industry Gaining Momentum*. URL: <https://www.globalxetfs.com/offshore-wind-power-industry-gaining-momentum/>. (accessed: 18.04.2023).
- RWE (n.d.). *Diving into the world of Floating Wind*. URL: <https://www.rwe.com/en/research-and-development/wind-power/floating-offshore-wind/floating-wind-education/>. (accessed: 30.05.2023).
- Subsea, CRP (n.d.). *Floating offshore wind*. URL: <https://www.crpsubsea.com/sectors/offshore-renewables/floating-offshore-wind/>. (accessed: 03.07.2023).
- Thomas, Christoffer Fjellstedt; Md Imran Ullah; Johan Forslund; Erik Jonasson; Irina Temiz; Karin (2022). “A Review of AC and DC Collection Grids for Offshore Renewable Energy with a Qualitative Evaluation for Marine Energy Resources.” In: *Energies* 15.16, p. 5816. DOI: <https://doi.org/10.3390/en15165816>.
- UNFCCC (n.d.). *The Paris Agreement*. URL: <https://unfccc.int/process-and-meetings/the-paris-agreement>. (accessed: 18.04.2023).
- WIND2GRID (n.d.). *VÍDEO DEL PROYECTO WIND2GRID*. URL: <https://www.wind2gridproject.com/en/news/video-del-proyecto-wind2grid/>. (accessed: 21.04.2023).
-

APPENDICES

A. STABILITY

Table 67. Ballast tanks

Name	Intact Perm.	Damaged Perm.	Specific gravity [kg/m ³]	Aft [m]	Fore [m]	F.Port [m]	F.Stbd. [m]	F.Top [m]	F.Bott. [m]
BTANS1	90	95	1025	0.001	6.695	14.000	20.695	8.400	0.000
BTANS2	90	95	1025	6.695	13.390	14.000	20.695	8.400	0.000
BTANS3	90	95	1025	0.001	6.695	20.695	28.000	8.400	0.000
BTANS4	90	95	1025	6.695	13.390	20.695	28.000	8.400	0.000
BTANP1	90	95	1025	0.001	6.695	-20.695	-14.000	8.400	0.000
BTANP2	90	95	1025	6.695	13.390	-20.695	-14.000	8.400	0.000
BTANP3	90	95	1025	0.001	6.695	-28.000	-20.695	8.400	0.000
BTANP4	90	95	1025	6.695	13.390	-28.000	-20.695	8.400	0.000
BTAPS1	90	95	1025	0.001	6.695	0.000	5.760	8.400	0.000
BTAPS2	90	95	1025	6.695	13.390	0.000	5.760	8.400	0.000
BTAPS3	90	95	1025	0.001	6.695	5.760	14.000	8.400	0.000
BTAPS4	90	95	1025	6.695	13.390	5.760	14.000	8.400	0.000
BTAPP1	90	95	1025	0.001	6.695	-5.760	0.000	8.400	0.000
BTAPP2	90	95	1025	6.695	13.390	-5.760	0.000	8.400	0.000
BTAPP3	90	95	1025	0.001	6.695	-14.000	-5.760	8.400	0.000
BTAPP4	90	95	1025	6.695	13.390	-14.000	-5.760	8.400	0.000
BTPS1	90	95	1025	13.390	21.630	14.000	20.695	8.400	0.000
BTPS2	90	95	1025	21.630	27.390	14.000	20.695	8.400	0.000
BTPS3	90	95	1025	27.390	33.150	14.000	20.695	8.400	0.000
BTPS4	90	95	1025	33.150	41.390	14.000	20.695	8.400	0.000
BTPS5	90	95	1025	13.390	21.630	20.695	27.390	8.400	0.000
BTPS6	90	95	1025	21.630	27.390	20.695	27.390	8.400	0.000
BTPS7	90	95	1025	27.390	33.150	20.695	27.390	8.400	0.000
BTPS8	90	95	1025	33.150	41.390	20.695	27.390	8.400	0.000
BTPP1	90	95	1025	13.390	21.630	-20.695	-14.000	8.400	0.000
BTPP2	90	95	1025	21.630	27.390	-20.695	-14.000	8.400	0.000
BTPP3	90	95	1025	27.390	33.150	-20.695	-14.000	8.400	0.000
BTPP4	90	95	1025	33.150	41.390	-20.695	-14.000	8.400	0.000
BTPP5	90	95	1025	13.390	21.630	-27.390	-20.695	8.400	0.000
BTPP6	90	95	1025	21.630	27.390	-27.390	-20.695	8.400	0.000
BTPP7	90	95	1025	27.390	33.150	-27.390	-20.695	8.400	0.000
BTPP8	90	95	1025	33.150	41.390	-27.390	-20.695	8.400	0.000
BTFNS1	90	95	1025	41.390	48.085	14.000	20.695	8.400	0.000
BTFNS2	90	95	1025	48.085	54.779	14.000	20.695	8.400	0.000
BTFNS3	90	95	1025	41.390	48.085	20.695	27.390	8.400	0.000
BTFNS4	90	95	1025	48.085	54.779	20.695	27.390	8.400	0.000
BTFNP1	90	95	1025	41.390	48.085	-20.695	-14.000	8.400	0.000
BTFNP2	90	95	1025	48.085	54.779	-20.695	-14.000	8.400	0.000

Table 67. Ballast tanks

Name	Intact Perm.	Damaged Perm.	Specific gravity [kg/m ³]	Aft [m]	Fore [m]	F.Port [m]	F.Stbd. [m]	F.Top [m]	F.Bott. [m]
BTFNP3	90	95	1025	41.390	48.085	-27.390	-20.695	8.400	0.000
BTFNP4	90	95	1025	48.085	54.779	-27.390	-20.695	8.400	0.000
BTFPS1	90	95	1025	40.960	48.085	0.000	5.760	8.400	0.000
BTFPS2	90	95	1025	48.085	54.779	0.000	5.760	8.400	0.000
BTFPS3	90	95	1025	41.390	48.085	5.760	14.000	8.400	0.000
BTFPS4	90	95	1025	48.085	54.779	5.760	14.000	8.400	0.000
BTFPP1	90	95	1025	41.390	48.085	-5.760	0.000	8.400	0.000
BTFPP2	90	95	1025	48.085	54.779	-5.760	0.000	8.400	0.000
BTFPP3	90	95	1025	41.390	48.085	-14.000	-5.760	8.400	0.000
BTFPP4	90	95	1025	48.085	54.779	-14.000	-5.760	8.400	0.000

Table 68. Watertight compartments

Name	Intact Perm.	Damaged Perm.	Aft [m]	Fore [m]	F.Port [m]	F.Stbd. [m]	F.Top [m]	F.Bott. [m]
BTFCS1	90	90	41.390	48.085	14.000	20.695	12.520	8.400
BTFCS2	90	90	48.085	54.779	14.000	20.695	12.520	8.400
BTFCS3	90	90	41.390	48.085	20.695	27.390	12.520	8.400
BTFCS4	90	90	48.085	54.779	20.695	27.390	12.520	8.400
BTFCS5	90	90	41.390	48.085	14.000	20.695	16.640	12.520
BTFCS6	90	90	48.085	54.779	14.000	20.695	16.640	12.520
BTFCS7	90	90	41.390	48.085	20.695	27.390	16.640	12.520
BTFCS8	90	90	48.085	54.779	20.695	27.390	16.640	12.520
BTFCS9	90	90	41.390	48.085	14.000	20.695	20.760	16.640
BTFCS10	90	90	48.085	54.779	14.000	20.695	20.760	16.640
BTFCS11	90	90	41.390	48.085	20.695	27.390	20.760	16.640
BTFCS12	90	90	48.085	54.779	20.695	27.390	20.760	16.640
BTFCS13	90	90	41.390	48.085	14.000	20.695	24.880	20.760
BTFCS14	90	90	48.085	54.779	14.000	20.695	24.880	20.760
BTFCS15	90	90	41.390	48.085	20.695	27.390	24.880	20.760
BTFCS16	90	90	48.085	54.779	20.695	27.390	24.880	20.760
BTFCS17	90	90	41.390	48.085	14.000	20.695	29.000	24.880
BTFCS18	90	90	48.085	54.779	14.000	20.695	29.000	24.880
BTFCS19	90	90	41.390	48.085	20.695	27.390	29.000	24.880
BTFCS20	90	90	48.085	54.779	20.695	27.390	29.000	24.880
BTFCS21	90	90	41.390	48.085	14.000	20.695	33.120	29.000
BTFCS22	90	90	48.085	54.779	14.000	20.695	33.120	29.000
BTFCS23	90	90	41.390	48.085	20.695	27.390	33.120	29.000
BTFCS24	90	90	48.085	54.779	20.695	27.390	33.120	29.000
BTFCS25	90	90	41.390	48.085	14.000	20.695	37.300	33.120
BTFCS26	90	90	48.085	54.779	14.000	20.695	37.300	33.120
BTFCS27	90	90	41.390	48.085	20.695	27.390	37.300	33.120
BTFCS28	90	90	48.085	54.779	20.695	27.390	37.300	33.120

Table 68. Watertight compartments

Name	Intact Perm.	Damaged Perm.	Aft [m]	Fore [m]	F.Port [m]	F.Stbd. [m]	F.Top [m]	F.Bott. [m]
BTFCP1	90	90	41.390	48.085	-20.695	-14.000	12.520	8.400
BTFCP2	90	90	48.085	54.779	-20.695	-14.000	12.520	8.400
BTFCP3	90	90	41.390	48.085	-27.390	-20.695	12.520	8.400
BTFCP4	90	90	48.085	54.779	-27.390	-20.695	12.520	8.400
BTFCP5	90	90	41.390	48.085	-20.695	-14.000	16.640	12.520
BTFCP6	90	90	48.085	54.779	-20.695	-14.000	16.640	12.520
BTFCP7	90	90	41.390	48.085	-27.390	-20.695	16.640	12.520
BTFCP8	90	90	48.085	54.779	-27.390	-20.695	16.640	12.520
BTFCP9	90	90	41.390	48.085	-20.695	-14.000	20.760	16.640
BTFCP10	90	90	48.085	54.779	-20.695	-14.000	20.760	16.640
BTFCP11	90	90	41.390	48.085	-27.390	-20.695	20.760	16.640
BTFCP12	90	90	48.085	54.779	-27.390	-20.695	20.760	16.640
BTFCP13	90	90	41.390	48.085	-20.695	-14.000	24.880	20.760
BTFCP14	90	90	48.085	54.779	-20.695	-14.000	24.880	20.760
BTFCP15	90	90	41.390	48.085	-27.390	-20.695	24.880	20.760
BTFCP16	90	90	48.085	54.779	-27.390	-20.695	24.880	20.760
BTFCP17	90	90	41.390	48.085	-20.695	-14.000	29.000	24.880
BTFCP18	90	90	48.085	54.779	-20.695	-14.000	29.000	24.880
BTFCP19	90	90	41.390	48.085	-27.390	-20.695	29.000	24.880
BTFCP20	90	90	48.085	54.779	-27.390	-20.695	29.000	24.880
BTFCP21	90	90	41.390	48.085	-20.695	-14.000	33.120	29.000
BTFCP22	90	90	48.085	54.779	-20.695	-14.000	33.120	29.000
BTFCP23	90	90	41.390	48.085	-27.390	-20.695	33.120	29.000
BTFCP24	90	90	48.085	54.779	-27.390	-20.695	33.120	29.000
BTFCP25	90	90	41.390	48.085	-20.695	-14.000	37.300	33.120
BTFCP26	90	90	48.085	54.779	-20.695	-14.000	37.300	33.120
BTFCP27	90	90	41.390	48.085	-27.390	-20.695	37.300	33.120
BTFCP28	90	90	48.085	54.779	-27.390	-20.695	37.300	33.120
BTACP1	90	90	0.001	6.695	-20.695	-14.000	12.520	8.400
BTACP2	90	90	6.695	13.390	-20.695	-14.000	12.520	8.400
BTACP3	90	90	0.001	6.695	-27.390	-20.695	12.520	8.400
BTACP4	90	90	6.695	13.390	-27.390	-20.695	12.520	8.400
BTACP5	90	90	0.001	6.695	-20.695	-14.000	16.640	12.520
BTACP6	90	90	6.695	13.390	-20.695	-14.000	16.640	12.520
BTACP7	90	90	0.001	6.695	-27.390	-20.695	16.640	12.520
BTACP8	90	90	6.695	13.390	-27.390	-20.695	16.640	12.520
BTACP9	90	90	0.001	6.695	-20.695	-14.000	20.760	16.640
BTACP10	90	90	6.695	13.390	-20.695	-14.000	20.760	16.640
BTACP11	90	90	0.001	6.695	-27.390	-20.695	20.760	16.640
BTACP12	90	90	6.695	13.390	-27.390	-20.695	20.760	16.640
BTACP13	90	90	0.001	6.695	-20.695	-14.000	24.880	20.760
BTACP14	90	90	6.695	13.390	-20.695	-14.000	24.880	20.760
BTACP15	90	90	0.001	6.695	-27.390	-20.695	24.880	20.760

Table 68. Watertight compartments

Name	Intact Perm.	Damaged Perm.	Aft [m]	Fore [m]	F.Port [m]	F.Stbd. [m]	F.Top [m]	F.Bott. [m]
BTACP16	90	90	6.695	13.390	-27.390	-20.695	24.880	20.760
BTACP17	90	90	0.001	6.695	-20.695	-14.000	29.000	24.880
BTACP18	90	90	6.695	13.390	-20.695	-14.000	29.000	24.880
BTACP19	90	90	0.001	6.695	-27.390	-20.695	29.000	24.880
BTACP20	90	90	6.695	13.390	-27.390	-20.695	29.000	24.880
BTACP21	90	90	0.001	6.695	-20.695	-14.000	33.120	29.000
BTACP22	90	90	6.695	13.390	-20.695	-14.000	33.120	29.000
BTACP23	90	90	0.001	6.695	-27.390	-20.695	33.120	29.000
BTACP24	90	90	6.695	13.390	-27.390	-20.695	33.120	29.000
BTACP25	90	90	0.001	6.695	-20.695	-14.000	37.300	33.120
BTACP26	90	90	6.695	13.390	-20.695	-14.000	37.300	33.120
BTACP27	90	90	0.001	6.695	-27.390	-20.695	37.300	33.120
BTACP28	90	90	6.695	13.390	-27.390	-20.695	37.300	33.120
BTACS1	90	90	0.001	6.695	14.000	20.695	12.520	8.400
BTACS2	90	90	6.695	13.390	14.000	20.695	12.520	8.400
BTACS3	90	90	0.001	6.695	20.695	27.390	12.520	8.400
BTACS4	90	90	6.695	13.390	20.695	27.390	12.520	8.400
BTACS5	90	90	0.001	6.695	14.000	20.695	16.640	12.520
BTACS6	90	90	6.695	13.390	14.000	20.695	16.640	12.520
BTACS7	90	90	0.001	6.695	20.695	27.390	16.640	12.520
BTACS8	90	90	6.695	13.390	20.695	27.390	16.640	12.520
BTACS9	90	90	0.001	6.695	14.000	20.695	20.760	16.640
BTACS10	90	90	6.695	13.390	14.000	20.695	20.760	16.640
BTACS11	90	90	0.001	6.695	20.695	27.390	20.760	16.640
BTACS12	90	90	6.695	13.390	20.695	27.390	20.760	16.640
BTACS13	90	90	0.001	6.695	14.000	20.695	24.880	20.760
BTACS14	90	90	6.695	13.390	14.000	20.695	24.880	20.760
BTACS15	90	90	0.001	6.695	20.695	27.390	24.880	20.760
BTACS16	90	90	6.695	13.390	20.695	27.390	24.880	20.760
BTACS17	90	90	0.001	6.695	14.000	20.695	29.000	24.880
BTACS18	90	90	6.695	13.390	14.000	20.695	29.000	24.880
BTACS19	90	90	0.001	6.695	20.695	27.390	29.000	24.880
BTACS20	90	90	6.695	13.390	20.695	27.390	29.000	24.880
BTACS21	90	90	0.001	6.695	14.000	20.695	33.120	29.000
BTACS22	90	90	6.695	13.390	14.000	20.695	33.120	29.000
BTACS23	90	90	0.001	6.695	20.695	27.390	33.120	29.000
BTACS24	90	90	6.695	13.390	20.695	27.390	33.120	29.000
BTACS25	90	90	0.001	6.695	14.000	20.695	37.300	33.120
BTACS26	90	90	6.695	13.390	14.000	20.695	37.300	33.120
BTACS27	90	90	0.001	6.695	20.695	27.390	37.300	33.120
BTACS28	90	90	6.695	13.390	20.695	27.390	37.300	33.120

Table 69. Operational load case details

Item	Quantity	Mass [tons]	Volume [m ³]	LCG [m]	TCG [m]	VCG [m]	FSM [tons.m]
Lightweight	1	10011	-	27.67	0.01	15.09	-
Substation	1	6960.9	-	27.39	0	42.83	-
Total Fixed Mass		16971.9	-	27.555	0.006	26.467	-
BTPS8	70.25%	300.31	292.985	37.401	24.132	2.966	219.666
BTPS7	70.25%	209.925	204.805	30.334	24.132	2.961	153.51
BTPS6	70.25%	209.925	204.805	24.574	24.132	2.961	153.51
BTPS5	70.25%	300.31	292.985	17.641	24.132	2.966	219.666
BTPS4	70.25%	300.31	292.985	37.401	17.437	2.966	219.666
BTPS3	70.25%	209.925	204.805	30.334	17.437	2.961	153.51
BTPS2	70.25%	209.925	204.805	24.574	17.437	2.961	153.51
BTPS1	70.25%	300.31	292.985	17.641	17.437	2.966	219.666
BTPP8	70.25%	300.31	292.985	37.401	-23.953	2.966	219.666
BTPP7	70.25%	209.925	204.805	30.334	-23.953	2.961	153.51
BTPP6	70.25%	209.925	204.805	24.574	-23.953	2.961	153.51
BTPP5	70.25%	300.31	292.985	17.641	-23.953	2.966	219.666
BTPP4	70.25%	300.31	292.985	37.401	-17.258	2.966	219.666
BTPP3	70.25%	209.925	204.805	30.334	-17.258	2.961	153.51
BTPP2	70.25%	209.925	204.805	24.574	-17.258	2.961	153.51
BTPP1	70.25%	300.31	292.985	17.641	-17.258	2.966	219.666
BTFPS4	63.25%	270.366	263.771	51.528	10.03	2.674	332.621
BTFPS3	70.25%	297.918	290.652	44.849	9.999	2.96	327.343
BTFPS2	70.25%	209.91	204.79	51.519	2.946	2.961	113.643
BTFPS1	70.25%	208.302	203.222	44.848	2.947	2.955	111.917
BTFPP4	63.25%	270.366	263.771	51.528	-9.73	2.674	332.621
BTFPP3	70.25%	297.918	290.652	44.849	-9.713	2.96	327.507
BTFPP2	70.25%	209.91	204.79	51.519	-2.814	2.961	113.643
BTFPP1	70.25%	208.253	203.174	44.849	-2.799	2.955	111.875
BTFNS4	70.25%	243.984	238.033	51.519	24.132	2.963	178.432
BTFNS3	70.25%	244.002	238.051	44.824	24.132	2.963	178.445
BTFNS2	70.25%	243.984	238.033	51.519	17.437	2.963	178.432
BTFNS1	70.25%	244.002	238.051	44.824	17.437	2.963	178.445
BTFNP4	70.25%	243.984	238.033	51.519	-23.953	2.963	178.432
BTFNP3	70.25%	244.002	238.051	44.824	-23.953	2.963	178.445
BTFNP2	70.25%	243.984	238.033	51.519	-17.258	2.963	178.432
BTFNP1	70.25%	244.002	238.051	44.824	-17.258	2.963	178.445
BTAPS4	70.25%	297.918	290.651	10.101	9.996	2.957	329.517
BTAPS3	77.25%	330.185	322.131	3.427	10.003	3.259	332.596
BTAPS2	70.25%	208.253	203.174	10.101	2.947	2.952	112.562
BTAPS1	70.25%	209.894	204.775	3.434	2.946	2.961	113.635
BTAPP4	70.25%	297.918	290.652	10.101	-9.707	2.957	329.353
BTAPP3	77.25%	330.185	322.131	3.427	-9.757	3.259	332.596
BTAPP2	70.25%	208.253	203.174	10.101	-2.796	2.952	112.546

Table 69. Operational load case details

Item	Quantity	Mass [tons]	Volume [m ³]	LCG [m]	TCG [m]	VCG [m]	FSM [tons.m]
BTAPP1	70.25%	209.894	204.775	3.434	-2.814	2.961	113.635
BTANS4	70.25%	244.002	238.051	10.129	24.132	2.963	178.445
BTANS3	70.25%	243.984	238.033	3.434	24.132	2.963	178.432
BTANS2	70.25%	244.002	238.051	10.129	17.437	2.963	178.445
BTANS1	70.25%	243.984	238.033	3.434	17.437	2.963	178.432
BTANP4	70.25%	244.002	238.051	10.129	-23.953	2.963	178.445
BTANP3	70.25%	243.965	238.015	3.434	-23.953	2.963	178.419
BTANP2	70.25%	244.002	238.051	10.129	-17.258	2.963	178.445
BTANP1	70.25%	243.965	238.015	3.434	-17.258	2.963	178.419
Total Ballast	70.25%	12051.171	11757.24	27.244	0.097	2.965	9388.008
Total Loadcase		29023.071	11757.24	27.426	0.044	16.709	9388.008
FS correction						0.323	
VCG fluid						17.032	

Table 70. Transit load case details

Item	Quantity	Mass [tons]	Volume [m ³]	LCG [m]	TCG [m]	VCG [m]	FSM [tons.m]
Lightweight	1	10011	-	27.67	0.01	15.09	-
Substation	1	6960.9	-	27.39	0	42.83	-
Total Fixed Mass		16971.9	-	27.555	0.006	26.467	-
BTAPS8	66%	282.142	275.26	37.409	24.138	2.788	219.666
BTAPS7	66%	197.225	192.415	30.338	24.138	2.783	153.51
BTAPS6	66%	197.225	192.415	24.578	24.138	2.783	153.51
BTAPS5	66%	282.142	275.26	17.649	24.138	2.788	219.666
BTAPS4	66%	282.142	275.26	37.409	17.443	2.788	219.666
BTAPS3	66%	197.225	192.415	30.338	17.443	2.783	153.51
BTAPS2	66%	197.225	192.415	24.578	17.443	2.783	153.51
BTAPS1	66%	282.142	275.26	17.649	17.443	2.788	219.666
BTPP8	66%	282.142	275.26	37.409	-23.947	2.788	219.666
BTPP7	66%	197.225	192.415	30.338	-23.947	2.783	153.51
BTPP6	66%	197.225	192.415	24.578	-23.947	2.783	153.51
BTPP5	66%	282.142	275.26	17.649	-23.947	2.788	219.666
BTPP4	66%	282.142	275.26	37.409	-17.252	2.788	219.666
BTPP3	66%	197.225	192.415	30.338	-17.252	2.783	153.51
BTPP2	66%	197.225	192.415	24.578	-17.252	2.783	153.51
BTPP1	66%	282.142	275.26	17.649	-17.252	2.788	219.666
BTFPS4	63.25%	270.366	263.771	51.528	10.03	2.674	332.621
BTFPS3	66%	279.894	273.068	44.855	10.007	2.783	327.322
BTFPS2	66%	197.211	192.401	51.524	2.95	2.783	113.643
BTFPS1	66%	195.7	190.927	44.854	2.951	2.777	111.91

B. FATIGUE LOAD CASES

Table 71. Fatigue load cases

LC	UC [m/s]	Current Heading [°]	Hs [m]	Tp [s]	UW [m/s]	Wave & Wind Heading [°]
1	0.25	0	0.75	3.50	10.67	0
2	0.25	0	0.25	4.50	10.67	0
3	0.25	0	0.75	4.50	10.67	0
4	0.25	0	1.25	4.50	10.67	0
5	0.25	0	0.75	5.50	10.67	0
6	0.25	0	1.25	5.50	10.67	0
7	0.25	0	1.75	5.50	10.67	0
8	0.25	0	0.75	6.50	10.67	0
9	0.25	0	1.25	6.50	10.67	0
10	0.25	0	1.75	6.50	10.67	0
11	0.25	0	2.25	6.50	10.67	0
12	0.25	0	2.75	6.50	10.67	0
13	0.25	0	0.75	7.50	10.67	0
14	0.25	0	1.25	7.50	10.67	0
15	0.25	0	1.75	7.50	10.67	0
16	0.25	0	2.25	7.50	10.67	0
17	0.25	0	2.75	7.50	10.67	0
18	0.25	0	3.25	7.50	10.67	0
19	0.25	0	0.75	8.5	10.67	0
20	0.25	0	1.25	8.5	10.67	0
21	0.25	0	1.75	8.5	10.67	0
22	0.25	0	2.25	8.5	10.67	0
23	0.25	0	2.75	8.5	10.67	0
24	0.25	0	3.25	8.5	10.67	0
25	0.25	0	3.75	8.5	10.67	0
26	0.25	0	4.25	8.5	10.67	0
27	0.25	0	0.75	9.5	10.67	0
28	0.25	0	1.25	9.5	10.67	0
29	0.25	0	1.75	9.5	10.67	0
30	0.25	0	2.25	9.5	10.67	0
31	0.25	0	2.75	9.5	10.67	0
32	0.25	0	3.25	9.5	10.67	0
33	0.25	0	3.75	9.5	10.67	0
34	0.25	0	4.25	9.5	10.67	0
35	0.25	0	4.75	9.5	10.67	0
36	0.25	0	1.25	10.5	10.67	0
37	0.25	0	1.75	10.5	10.67	0
38	0.25	0	2.25	10.5	10.67	0
39	0.25	0	2.75	10.5	10.67	0
40	0.25	0	3.25	10.5	10.67	0
41	0.25	0	3.75	10.5	10.67	0

Table 71. Fatigue load cases

LC	UC [m/s]	Current Heading [°]	Hs [m]	Tp [s]	UW [m/s]	Wave & Wind Heading [°]
42	0.25	0	4.25	10.5	10.67	0
43	0.25	0	4.75	10.5	10.67	0
44	0.25	0	1.25	11.5	10.67	0
45	0.25	0	1.75	11.5	10.67	0
46	0.25	0	2.25	11.5	10.67	0
47	0.25	0	2.75	11.5	10.67	0
48	0.25	0	0.75	3.50	10.67	180
49	0.25	0	0.25	4.50	10.67	180
50	0.25	0	0.75	4.50	10.67	180
51	0.25	0	1.25	4.50	10.67	180
52	0.25	0	0.75	5.50	10.67	180
53	0.25	0	1.25	5.50	10.67	180
54	0.25	0	1.75	5.50	10.67	180
55	0.25	0	0.75	6.50	10.67	180
56	0.25	0	1.25	6.50	10.67	180
57	0.25	0	1.75	6.50	10.67	180
58	0.25	0	2.25	6.50	10.67	180
59	0.25	0	2.75	6.50	10.67	180
60	0.25	0	0.75	7.50	10.67	180
61	0.25	0	1.25	7.50	10.67	180
62	0.25	0	1.75	7.50	10.67	180
63	0.25	0	2.25	7.50	10.67	180
64	0.25	0	2.75	7.50	10.67	180
65	0.25	0	3.25	7.50	10.67	180
66	0.25	0	0.75	8.5	10.67	180
67	0.25	0	1.25	8.5	10.67	180
68	0.25	0	1.75	8.5	10.67	180
69	0.25	0	2.25	8.5	10.67	180
70	0.25	0	2.75	8.5	10.67	180
71	0.25	0	3.25	8.5	10.67	180
72	0.25	0	3.75	8.5	10.67	180
73	0.25	0	4.25	8.5	10.67	180
74	0.25	0	0.75	9.5	10.67	180
75	0.25	0	1.25	9.5	10.67	180
76	0.25	0	1.75	9.5	10.67	180
77	0.25	0	2.25	9.5	10.67	180
78	0.25	0	2.75	9.5	10.67	180
79	0.25	0	3.25	9.5	10.67	180
80	0.25	0	3.75	9.5	10.67	180
81	0.25	0	4.25	9.5	10.67	180
82	0.25	0	4.75	9.5	10.67	180
83	0.25	0	1.25	10.5	10.67	180
84	0.25	0	1.75	10.5	10.67	180

Table 71. Fatigue load cases

LC	UC [m/s]	Current Heading [°]	Hs [m]	Tp [s]	UW [m/s]	Wave & Wind Heading [°]
85	0.25	0	2.25	10.5	10.67	180
86	0.25	0	2.75	10.5	10.67	180
87	0.25	0	3.25	10.5	10.67	180
88	0.25	0	3.75	10.5	10.67	180
89	0.25	0	4.25	10.5	10.67	180
90	0.25	0	4.75	10.5	10.67	180
91	0.25	0	1.25	11.5	10.67	180
92	0.25	0	1.75	11.5	10.67	180
93	0.25	0	2.25	11.5	10.67	180
94	0.25	0	2.75	11.5	10.67	180
95	0.25	0	0.75	3.50	10.67	112.5
96	0.25	0	0.25	4.50	10.67	112.5
97	0.25	0	0.75	4.50	10.67	112.5
98	0.25	0	1.25	4.50	10.67	112.5
99	0.25	0	0.75	5.50	10.67	112.5
100	0.25	0	1.25	5.50	10.67	112.5
101	0.25	0	1.75	5.50	10.67	112.5
102	0.25	0	0.75	6.50	10.67	112.5
103	0.25	0	1.25	6.50	10.67	112.5
104	0.25	0	1.75	6.50	10.67	112.5
105	0.25	0	2.25	6.50	10.67	112.5
106	0.25	0	2.75	6.50	10.67	112.5
107	0.25	0	0.75	7.50	10.67	112.5
108	0.25	0	1.25	7.50	10.67	112.5
109	0.25	0	1.75	7.50	10.67	112.5
110	0.25	0	2.25	7.50	10.67	112.5
111	0.25	0	2.75	7.50	10.67	112.5
112	0.25	0	3.25	7.50	10.67	112.5
113	0.25	0	0.75	8.5	10.67	112.5
114	0.25	0	1.25	8.5	10.67	112.5
115	0.25	0	1.75	8.5	10.67	112.5
116	0.25	0	2.25	8.5	10.67	112.5
117	0.25	0	2.75	8.5	10.67	112.5
118	0.25	0	3.25	8.5	10.67	112.5
119	0.25	0	3.75	8.5	10.67	112.5
120	0.25	0	4.25	8.5	10.67	112.5
121	0.25	0	0.75	9.5	10.67	112.5
122	0.25	0	1.25	9.5	10.67	112.5
123	0.25	0	1.75	9.5	10.67	112.5
124	0.25	0	2.25	9.5	10.67	112.5
125	0.25	0	2.75	9.5	10.67	112.5
126	0.25	0	3.25	9.5	10.67	112.5
127	0.25	0	3.75	9.5	10.67	112.5

Table 71. Fatigue load cases

LC	UC [m/s]	Current Heading [°]	Hs [m]	Tp [s]	UW [m/s]	Wave & Wind Heading [°]
128	0.25	0	4.25	9.5	10.67	112.5
129	0.25	0	4.75	9.5	10.67	112.5
130	0.25	0	1.25	10.5	10.67	112.5
131	0.25	0	1.75	10.5	10.67	112.5
132	0.25	0	2.25	10.5	10.67	112.5
133	0.25	0	2.75	10.5	10.67	112.5
134	0.25	0	3.25	10.5	10.67	112.5
135	0.25	0	3.75	10.5	10.67	112.5
136	0.25	0	4.25	10.5	10.67	112.5
137	0.25	0	4.75	10.5	10.67	112.5
138	0.25	0	1.25	11.5	10.67	112.5
139	0.25	0	1.75	11.5	10.67	112.5
140	0.25	0	2.25	11.5	10.67	112.5
141	0.25	0	2.75	11.5	10.67	112.5
142	0.25	180	0.75	3.50	10.67	0
143	0.25	180	0.25	4.50	10.67	0
144	0.25	180	0.75	4.50	10.67	0
145	0.25	180	1.25	4.50	10.67	0
146	0.25	180	0.75	5.50	10.67	0
147	0.25	180	1.25	5.50	10.67	0
148	0.25	180	1.75	5.50	10.67	0
149	0.25	180	0.75	6.50	10.67	0
150	0.25	180	1.25	6.50	10.67	0
151	0.25	180	1.75	6.50	10.67	0
152	0.25	180	2.25	6.50	10.67	0
153	0.25	180	2.75	6.50	10.67	0
154	0.25	180	0.75	7.50	10.67	0
155	0.25	180	1.25	7.50	10.67	0
156	0.25	180	1.75	7.50	10.67	0
157	0.25	180	2.25	7.50	10.67	0
158	0.25	180	2.75	7.50	10.67	0
159	0.25	180	3.25	7.50	10.67	0
160	0.25	180	0.75	8.5	10.67	0
161	0.25	180	1.25	8.5	10.67	0
162	0.25	180	1.75	8.5	10.67	0
163	0.25	180	2.25	8.5	10.67	0
164	0.25	180	2.75	8.5	10.67	0
165	0.25	180	3.25	8.5	10.67	0
166	0.25	180	3.75	8.5	10.67	0
167	0.25	180	4.25	8.5	10.67	0
168	0.25	180	0.75	9.5	10.67	0
169	0.25	180	1.25	9.5	10.67	0
170	0.25	180	1.75	9.5	10.67	0

Table 71. Fatigue load cases

LC	UC [m/s]	Current Heading [°]	Hs [m]	Tp [s]	UW [m/s]	Wave & Wind Heading [°]
171	0.25	180	2.25	9.5	10.67	0
172	0.25	180	2.75	9.5	10.67	0
173	0.25	180	3.25	9.5	10.67	0
174	0.25	180	3.75	9.5	10.67	0
175	0.25	180	4.25	9.5	10.67	0
176	0.25	180	4.75	9.5	10.67	0
177	0.25	180	1.25	10.5	10.67	0
178	0.25	180	1.75	10.5	10.67	0
179	0.25	180	2.25	10.5	10.67	0
180	0.25	180	2.75	10.5	10.67	0
181	0.25	180	3.25	10.5	10.67	0
182	0.25	180	3.75	10.5	10.67	0
183	0.25	180	4.25	10.5	10.67	0
184	0.25	180	4.75	10.5	10.67	0
185	0.25	180	1.25	11.5	10.67	0
186	0.25	180	1.75	11.5	10.67	0
187	0.25	180	2.25	11.5	10.67	0
188	0.25	180	2.75	11.5	10.67	0
189	0.25	180	0.75	3.50	10.67	180
190	0.25	180	0.25	4.50	10.67	180
191	0.25	180	0.75	4.50	10.67	180
192	0.25	180	1.25	4.50	10.67	180
193	0.25	180	0.75	5.50	10.67	180
194	0.25	180	1.25	5.50	10.67	180
195	0.25	180	1.75	5.50	10.67	180
196	0.25	180	0.75	6.50	10.67	180
197	0.25	180	1.25	6.50	10.67	180
198	0.25	180	1.75	6.50	10.67	180
199	0.25	180	2.25	6.50	10.67	180
200	0.25	180	2.75	6.50	10.67	180
201	0.25	180	0.75	7.50	10.67	180
202	0.25	180	1.25	7.50	10.67	180
203	0.25	180	1.75	7.50	10.67	180
204	0.25	180	2.25	7.50	10.67	180
205	0.25	180	2.75	7.50	10.67	180
206	0.25	180	3.25	7.50	10.67	180
207	0.25	180	0.75	8.5	10.67	180
208	0.25	180	1.25	8.5	10.67	180
209	0.25	180	1.75	8.5	10.67	180
210	0.25	180	2.25	8.5	10.67	180
211	0.25	180	2.75	8.5	10.67	180
212	0.25	180	3.25	8.5	10.67	180
213	0.25	180	3.75	8.5	10.67	180

Table 71. Fatigue load cases

LC	UC [m/s]	Current Heading [°]	Hs [m]	Tp [s]	UW [m/s]	Wave & Wind Heading [°]
214	0.25	180	4.25	8.5	10.67	180
215	0.25	180	0.75	9.5	10.67	180
216	0.25	180	1.25	9.5	10.67	180
217	0.25	180	1.75	9.5	10.67	180
218	0.25	180	2.25	9.5	10.67	180
219	0.25	180	2.75	9.5	10.67	180
220	0.25	180	3.25	9.5	10.67	180
221	0.25	180	3.75	9.5	10.67	180
222	0.25	180	4.25	9.5	10.67	180
223	0.25	180	4.75	9.5	10.67	180
224	0.25	180	1.25	10.5	10.67	180
225	0.25	180	1.75	10.5	10.67	180
226	0.25	180	2.25	10.5	10.67	180
227	0.25	180	2.75	10.5	10.67	180
228	0.25	180	3.25	10.5	10.67	180
229	0.25	180	3.75	10.5	10.67	180
230	0.25	180	4.25	10.5	10.67	180
231	0.25	180	4.75	10.5	10.67	180
232	0.25	180	1.25	11.5	10.67	180
233	0.25	180	1.75	11.5	10.67	180
234	0.25	180	2.25	11.5	10.67	180
235	0.25	180	2.75	11.5	10.67	180
236	0.25	180	0.75	3.50	10.67	112.5
237	0.25	180	0.25	4.50	10.67	112.5
238	0.25	180	0.75	4.50	10.67	112.5
239	0.25	180	1.25	4.50	10.67	112.5
240	0.25	180	0.75	5.50	10.67	112.5
241	0.25	180	1.25	5.50	10.67	112.5
242	0.25	180	1.75	5.50	10.67	112.5
243	0.25	180	0.75	6.50	10.67	112.5
244	0.25	180	1.25	6.50	10.67	112.5
245	0.25	180	1.75	6.50	10.67	112.5
246	0.25	180	2.25	6.50	10.67	112.5
247	0.25	180	2.75	6.50	10.67	112.5
248	0.25	180	0.75	7.50	10.67	112.5
249	0.25	180	1.25	7.50	10.67	112.5
250	0.25	180	1.75	7.50	10.67	112.5
251	0.25	180	2.25	7.50	10.67	112.5
252	0.25	180	2.75	7.50	10.67	112.5
253	0.25	180	3.25	7.50	10.67	112.5
254	0.25	180	0.75	8.5	10.67	112.5
255	0.25	180	1.25	8.5	10.67	112.5
256	0.25	180	1.75	8.5	10.67	112.5

Table 71. Fatigue load cases

LC	UC	Current	Hs	Tp	UW	Wave & Wind
	[m/s]	Heading [°]	[m]	[s]	[m/s]	Heading [°]
257	0.25	180	2.25	8.5	10.67	112.5
258	0.25	180	2.75	8.5	10.67	112.5
259	0.25	180	3.25	8.5	10.67	112.5
260	0.25	180	3.75	8.5	10.67	112.5
261	0.25	180	4.25	8.5	10.67	112.5
262	0.25	180	0.75	9.5	10.67	112.5
263	0.25	180	1.25	9.5	10.67	112.5
264	0.25	180	1.75	9.5	10.67	112.5
265	0.25	180	2.25	9.5	10.67	112.5
266	0.25	180	2.75	9.5	10.67	112.5
267	0.25	180	3.25	9.5	10.67	112.5
268	0.25	180	3.75	9.5	10.67	112.5
269	0.25	180	4.25	9.5	10.67	112.5
270	0.25	180	4.75	9.5	10.67	112.5
271	0.25	180	1.25	10.5	10.67	112.5
272	0.25	180	1.75	10.5	10.67	112.5
273	0.25	180	2.25	10.5	10.67	112.5
274	0.25	180	2.75	10.5	10.67	112.5
275	0.25	180	3.25	10.5	10.67	112.5
276	0.25	180	3.75	10.5	10.67	112.5
277	0.25	180	4.25	10.5	10.67	112.5
278	0.25	180	4.75	10.5	10.67	112.5
279	0.25	180	1.25	11.5	10.67	112.5
280	0.25	180	1.75	11.5	10.67	112.5
281	0.25	180	2.25	11.5	10.67	112.5
282	0.25	180	2.75	11.5	10.67	112.5

Table 72. Fatigue load cases probability

LC	UC	Current Heading	Wave	Wind	Wave & Wind Heading	Total
1	100%	50%	0.6%	100%	41%	0.1%
2	100%	50%	0.7%	100%	41%	0.1%
3	100%	50%	4.1%	100%	41%	0.8%
4	100%	50%	1.5%	100%	41%	0.3%
5	100%	50%	4.3%	100%	41%	0.9%
6	100%	50%	6.4%	100%	41%	1.3%
7	100%	50%	2.8%	100%	41%	0.6%
8	100%	50%	3.4%	100%	41%	0.7%
9	100%	50%	5%	100%	41%	1%
10	100%	50%	6%	100%	41%	1.2%
11	100%	50%	4.5%	100%	41%	0.9%
12	100%	50%	0.7%	100%	41%	0.1%
13	100%	50%	1.7%	100%	41%	0.4%
14	100%	50%	4%	100%	41%	0.8%
15	100%	50%	3.7%	100%	41%	0.7%
16	100%	50%	3.7%	100%	41%	0.7%
17	100%	50%	4.1%	100%	41%	0.8%
18	100%	50%	1.8%	100%	41%	0.4%
19	100%	50%	1.4%	100%	41%	0.3%
20	100%	50%	2.9%	100%	41%	0.6%
21	100%	50%	3.1%	100%	41%	0.6%
22	100%	50%	2.5%	100%	41%	0.5%
23	100%	50%	2.1%	100%	41%	0.4%
24	100%	50%	2.2%	100%	41%	0.5%
25	100%	50%	1.9%	100%	41%	0.4%
26	100%	50%	0.7%	100%	41%	0.1%
27	100%	50%	0.9%	100%	41%	0.2%
28	100%	50%	2.2%	100%	41%	0.5%
29	100%	50%	2%	100%	41%	0.4%
30	100%	50%	1.7%	100%	41%	0.4%
31	100%	50%	1.6%	100%	41%	0.3%
32	100%	50%	1.4%	100%	41%	0.3%
33	100%	50%	1.3%	100%	41%	0.3%
34	100%	50%	1.1%	100%	41%	0.2%
35	100%	50%	0.9%	100%	41%	0.2%
36	100%	50%	1.2%	100%	41%	0.3%
37	100%	50%	1.8%	100%	41%	0.4%
38	100%	50%	1.4%	100%	41%	0.3%
39	100%	50%	0.9%	100%	41%	0.2%
40	100%	50%	0.7%	100%	41%	0.2%
41	100%	50%	0.7%	100%	41%	0.1%
42	100%	50%	0.6%	100%	41%	0.1%
43	100%	50%	0.6%	100%	41%	0.1%

Table 72. Fatigue load cases probability

LC	UC	Current Heading	Wave	Wind	Wave & Wind Heading	Total
44	100%	50%	0.6%	100%	41%	0.1%
45	100%	50%	1.1%	100%	41%	0.2%
46	100%	50%	1.2%	100%	41%	0.2%
47	100%	50%	0.7%	100%	41%	0.1%
48	100%	50%	0.6%	100%	36%	0.1%
49	100%	50%	0.7%	100%	36%	0.1%
50	100%	50%	4.1%	100%	36%	0.7%
51	100%	50%	1.5%	100%	36%	0.3%
52	100%	50%	4.3%	100%	36%	0.8%
53	100%	50%	6.4%	100%	36%	1.1%
54	100%	50%	2.8%	100%	36%	0.5%
55	100%	50%	3.4%	100%	36%	0.6%
56	100%	50%	5%	100%	36%	0.9%
57	100%	50%	6%	100%	36%	1.1%
58	100%	50%	4.5%	100%	36%	0.8%
59	100%	50%	0.7%	100%	36%	0.1%
60	100%	50%	1.7%	100%	36%	0.3%
61	100%	50%	4%	100%	36%	0.7%
62	100%	50%	3.7%	100%	36%	0.7%
63	100%	50%	3.7%	100%	36%	0.7%
64	100%	50%	4.1%	100%	36%	0.7%
65	100%	50%	1.8%	100%	36%	0.3%
66	100%	50%	1.4%	100%	36%	0.3%
67	100%	50%	2.9%	100%	36%	0.5%
68	100%	50%	3.1%	100%	36%	0.6%
69	100%	50%	2.5%	100%	36%	0.4%
70	100%	50%	2.1%	100%	36%	0.4%
71	100%	50%	2.2%	100%	36%	0.4%
72	100%	50%	1.9%	100%	36%	0.3%
73	100%	50%	0.7%	100%	36%	0.1%
74	100%	50%	0.9%	100%	36%	0.2%
75	100%	50%	2.2%	100%	36%	0.4%
76	100%	50%	2%	100%	36%	0.4%
77	100%	50%	1.7%	100%	36%	0.3%
78	100%	50%	1.6%	100%	36%	0.3%
79	100%	50%	1.4%	100%	36%	0.2%
80	100%	50%	1.3%	100%	36%	0.2%
81	100%	50%	1.1%	100%	36%	0.2%
82	100%	50%	0.9%	100%	36%	0.2%
83	100%	50%	1.2%	100%	36%	0.2%
84	100%	50%	1.8%	100%	36%	0.3%
85	100%	50%	1.4%	100%	36%	0.2%
86	100%	50%	0.9%	100%	36%	0.2%

Table 72. Fatigue load cases probability

LC	UC	Current Heading	Wave	Wind	Wave & Wind Heading	Total
87	100%	50%	0.7%	100%	36%	0.1%
88	100%	50%	0.7%	100%	36%	0.1%
89	100%	50%	0.6%	100%	36%	0.1%
90	100%	50%	0.6%	100%	36%	0.1%
91	100%	50%	0.6%	100%	36%	0.1%
92	100%	50%	1.1%	100%	36%	0.2%
93	100%	50%	1.2%	100%	36%	0.2%
94	100%	50%	0.7%	100%	36%	0.1%
95	100%	50%	0.6%	100%	23%	0.1%
96	100%	50%	0.7%	100%	23%	0.1%
97	100%	50%	4.1%	100%	23%	0.5%
98	100%	50%	1.5%	100%	23%	0.2%
99	100%	50%	4.3%	100%	23%	0.5%
100	100%	50%	6.4%	100%	23%	0.7%
101	100%	50%	2.8%	100%	23%	0.3%
102	100%	50%	3.4%	100%	23%	0.4%
103	100%	50%	5%	100%	23%	0.6%
104	100%	50%	6%	100%	23%	0.7%
105	100%	50%	4.5%	100%	23%	0.5%
106	100%	50%	0.7%	100%	23%	0.1%
107	100%	50%	1.7%	100%	23%	0.2%
108	100%	50%	4%	100%	23%	0.5%
109	100%	50%	3.7%	100%	23%	0.4%
110	100%	50%	3.7%	100%	23%	0.4%
111	100%	50%	4.1%	100%	23%	0.5%
112	100%	50%	1.8%	100%	23%	0.2%
113	100%	50%	1.4%	100%	23%	0.2%
114	100%	50%	2.9%	100%	23%	0.3%
115	100%	50%	3.1%	100%	23%	0.4%
116	100%	50%	2.5%	100%	23%	0.3%
117	100%	50%	2.1%	100%	23%	0.2%
118	100%	50%	2.2%	100%	23%	0.3%
119	100%	50%	1.9%	100%	23%	0.2%
120	100%	50%	0.7%	100%	23%	0.1%
121	100%	50%	0.9%	100%	23%	0.1%
122	100%	50%	2.2%	100%	23%	0.3%
123	100%	50%	2%	100%	23%	0.2%
124	100%	50%	1.7%	100%	23%	0.2%
125	100%	50%	1.6%	100%	23%	0.2%
126	100%	50%	1.4%	100%	23%	0.2%
127	100%	50%	1.3%	100%	23%	0.1%
128	100%	50%	1.1%	100%	23%	0.1%
129	100%	50%	0.9%	100%	23%	0.1%

Table 72. Fatigue load cases probability

LC	UC	Current Heading	Wave	Wind	Wave & Wind Heading	Total
130	100%	50%	1.2%	100%	23%	0.1%
131	100%	50%	1.8%	100%	23%	0.2%
132	100%	50%	1.4%	100%	23%	0.2%
133	100%	50%	0.9%	100%	23%	0.1%
134	100%	50%	0.7%	100%	23%	0.1%
135	100%	50%	0.7%	100%	23%	0.1%
136	100%	50%	0.6%	100%	23%	0.1%
137	100%	50%	0.6%	100%	23%	0.1%
138	100%	50%	0.6%	100%	23%	0.1%
139	100%	50%	1.1%	100%	23%	0.1%
140	100%	50%	1.2%	100%	23%	0.1%
141	100%	50%	0.7%	100%	23%	0.1%
142	100%	50%	0.6%	100%	41%	0.1%
143	100%	50%	0.7%	100%	41%	0.1%
144	100%	50%	4.1%	100%	41%	0.8%
145	100%	50%	1.5%	100%	41%	0.3%
146	100%	50%	4.3%	100%	41%	0.9%
147	100%	50%	6.4%	100%	41%	1.3%
148	100%	50%	2.8%	100%	41%	0.6%
149	100%	50%	3.4%	100%	41%	0.7%
150	100%	50%	5%	100%	41%	1%
151	100%	50%	6%	100%	41%	1.2%
152	100%	50%	4.5%	100%	41%	0.9%
153	100%	50%	0.7%	100%	41%	0.1%
154	100%	50%	1.7%	100%	41%	0.4%
155	100%	50%	4%	100%	41%	0.8%
156	100%	50%	3.7%	100%	41%	0.7%
157	100%	50%	3.7%	100%	41%	0.7%
158	100%	50%	4.1%	100%	41%	0.8%
159	100%	50%	1.8%	100%	41%	0.4%
160	100%	50%	1.4%	100%	41%	0.3%
161	100%	50%	2.9%	100%	41%	0.6%
162	100%	50%	3.1%	100%	41%	0.6%
163	100%	50%	2.5%	100%	41%	0.5%
164	100%	50%	2.1%	100%	41%	0.4%
165	100%	50%	2.2%	100%	41%	0.5%
166	100%	50%	1.9%	100%	41%	0.4%
167	100%	50%	0.7%	100%	41%	0.1%
168	100%	50%	0.9%	100%	41%	0.2%
169	100%	50%	2.2%	100%	41%	0.5%
170	100%	50%	2%	100%	41%	0.4%
171	100%	50%	1.7%	100%	41%	0.4%
172	100%	50%	1.6%	100%	41%	0.3%

Table 72. Fatigue load cases probability

LC	UC	Current Heading	Wave	Wind	Wave & Wind Heading	Total
173	100%	50%	1.4%	100%	41%	0.3%
174	100%	50%	1.3%	100%	41%	0.3%
175	100%	50%	1.1%	100%	41%	0.2%
176	100%	50%	0.9%	100%	41%	0.2%
177	100%	50%	1.2%	100%	41%	0.3%
178	100%	50%	1.8%	100%	41%	0.4%
179	100%	50%	1.4%	100%	41%	0.3%
180	100%	50%	0.9%	100%	41%	0.2%
181	100%	50%	0.7%	100%	41%	0.2%
182	100%	50%	0.7%	100%	41%	0.1%
183	100%	50%	0.6%	100%	41%	0.1%
184	100%	50%	0.6%	100%	41%	0.1%
185	100%	50%	0.6%	100%	41%	0.1%
186	100%	50%	1.1%	100%	41%	0.2%
187	100%	50%	1.2%	100%	41%	0.2%
188	100%	50%	0.7%	100%	41%	0.1%
189	100%	50%	0.6%	100%	36%	0.1%
190	100%	50%	0.7%	100%	36%	0.1%
191	100%	50%	4.1%	100%	36%	0.7%
192	100%	50%	1.5%	100%	36%	0.3%
193	100%	50%	4.3%	100%	36%	0.8%
194	100%	50%	6.4%	100%	36%	1.1%
195	100%	50%	2.8%	100%	36%	0.5%
196	100%	50%	3.4%	100%	36%	0.6%
197	100%	50%	5%	100%	36%	0.9%
198	100%	50%	6%	100%	36%	1.1%
199	100%	50%	4.5%	100%	36%	0.8%
200	100%	50%	0.7%	100%	36%	0.1%
201	100%	50%	1.7%	100%	36%	0.3%
202	100%	50%	4%	100%	36%	0.7%
203	100%	50%	3.7%	100%	36%	0.7%
204	100%	50%	3.7%	100%	36%	0.7%
205	100%	50%	4.1%	100%	36%	0.7%
206	100%	50%	1.8%	100%	36%	0.3%
207	100%	50%	1.4%	100%	36%	0.3%
208	100%	50%	2.9%	100%	36%	0.5%
209	100%	50%	3.1%	100%	36%	0.6%
210	100%	50%	2.5%	100%	36%	0.4%
211	100%	50%	2.1%	100%	36%	0.4%
212	100%	50%	2.2%	100%	36%	0.4%
213	100%	50%	1.9%	100%	36%	0.3%
214	100%	50%	0.7%	100%	36%	0.1%
215	100%	50%	0.9%	100%	36%	0.2%

Table 72. Fatigue load cases probability

LC	UC	Current Heading	Wave	Wind	Wave & Wind Heading	Total
216	100%	50%	2.2%	100%	36%	0.4%
217	100%	50%	2%	100%	36%	0.4%
218	100%	50%	1.7%	100%	36%	0.3%
219	100%	50%	1.6%	100%	36%	0.3%
220	100%	50%	1.4%	100%	36%	0.2%
221	100%	50%	1.3%	100%	36%	0.2%
222	100%	50%	1.1%	100%	36%	0.2%
223	100%	50%	0.9%	100%	36%	0.2%
224	100%	50%	1.2%	100%	36%	0.2%
225	100%	50%	1.8%	100%	36%	0.3%
226	100%	50%	1.4%	100%	36%	0.2%
227	100%	50%	0.9%	100%	36%	0.2%
228	100%	50%	0.7%	100%	36%	0.1%
229	100%	50%	0.7%	100%	36%	0.1%
230	100%	50%	0.6%	100%	36%	0.1%
231	100%	50%	0.6%	100%	36%	0.1%
232	100%	50%	0.6%	100%	36%	0.1%
233	100%	50%	1.1%	100%	36%	0.2%
234	100%	50%	1.2%	100%	36%	0.2%
235	100%	50%	0.7%	100%	36%	0.1%
236	100%	50%	0.6%	100%	23%	0.1%
237	100%	50%	0.7%	100%	23%	0.1%
238	100%	50%	4.1%	100%	23%	0.5%
239	100%	50%	1.5%	100%	23%	0.2%
240	100%	50%	4.3%	100%	23%	0.5%
241	100%	50%	6.4%	100%	23%	0.7%
242	100%	50%	2.8%	100%	23%	0.3%
243	100%	50%	3.4%	100%	23%	0.4%
244	100%	50%	5%	100%	23%	0.6%
245	100%	50%	6%	100%	23%	0.7%
246	100%	50%	4.5%	100%	23%	0.5%
247	100%	50%	0.7%	100%	23%	0.1%
248	100%	50%	1.7%	100%	23%	0.2%
249	100%	50%	4%	100%	23%	0.5%
250	100%	50%	3.7%	100%	23%	0.4%
251	100%	50%	3.7%	100%	23%	0.4%
252	100%	50%	4.1%	100%	23%	0.5%
253	100%	50%	1.8%	100%	23%	0.2%
254	100%	50%	1.4%	100%	23%	0.2%
255	100%	50%	2.9%	100%	23%	0.3%
256	100%	50%	3.1%	100%	23%	0.4%
257	100%	50%	2.5%	100%	23%	0.3%
258	100%	50%	2.1%	100%	23%	0.2%

Table 72. Fatigue load cases probability

LC	UC	Current Heading	Wave	Wind	Wave & Wind Heading	Total
259	100%	50%	2.2%	100%	23%	0.3%
260	100%	50%	1.9%	100%	23%	0.2%
261	100%	50%	0.7%	100%	23%	0.1%
262	100%	50%	0.9%	100%	23%	0.1%
263	100%	50%	2.2%	100%	23%	0.3%
264	100%	50%	2%	100%	23%	0.2%
265	100%	50%	1.7%	100%	23%	0.2%
266	100%	50%	1.6%	100%	23%	0.2%
267	100%	50%	1.4%	100%	23%	0.2%
268	100%	50%	1.3%	100%	23%	0.1%
269	100%	50%	1.1%	100%	23%	0.1%
270	100%	50%	0.9%	100%	23%	0.1%
271	100%	50%	1.2%	100%	23%	0.1%
272	100%	50%	1.8%	100%	23%	0.2%
273	100%	50%	1.4%	100%	23%	0.2%
274	100%	50%	0.9%	100%	23%	0.1%
275	100%	50%	0.7%	100%	23%	0.1%
276	100%	50%	0.7%	100%	23%	0.1%
277	100%	50%	0.6%	100%	23%	0.1%
278	100%	50%	0.6%	100%	23%	0.1%
279	100%	50%	0.6%	100%	23%	0.1%
280	100%	50%	1.1%	100%	23%	0.1%
281	100%	50%	1.2%	100%	23%	0.1%
282	100%	50%	0.7%	100%	23%	0.1%

C. MATLAB CODE FOR LC FILE GENERATION

```
1
2 %% Read the input file
3
4 content = {}; % Creates an empty cell array
5 fileID = fopen('LC_Base.yml','r'); % Opens file
6 line = fgets(fileID); % Creates a blank first line
7
8 i = 1;
9 while i < 33151
10     line = fgets(fileID); % Gets line by line of the
11         file
12     [l,c] = size(line);
13     content{i,1} = line; % Includes each line in a
14         cell
15     i = i + 1;
16 end
17 fclose(fileID); % Closes file
18 clc
19
20 %% Change and write the code in a new file
21 L_c = [71, 76, 77, 95, 109]; % Index of lines do be
22     changed
23 original = [90, 3, 7, 175, 90]; % Original values to be
24     changed in each line
25 new = xlsread('LC_Table.xlsx','Sheet1','B3:F284'); % New values to be
26     introduced
27
28 for n = 1:282
29     fileName = strcat('LC',string(n),'.yml');
30     fileID = fopen(fileName,'w'); % Creates a LC file
31     fprintf(fileID, '%YAML 1.1'); % Prints the first line
32     fprintf(fileID, '\n'); % Skips a line
33
34 [row, cols] = size(content);
35
36 l = 1;
37
38 for i = 1:row
39     for j = 1:cols
40         cellContent = content{i,j};
```

```
41         if i == L_c(1,1)                % Replaces the indicated
           value (original) by the new one
42             new_cellContent = replace(cellContent,string(original(1,1
               )),string(new(n,1)));
43             fprintf(fileID, new_cellContent);
44             if l < 5
45                 l = l + 1;
46             end
47         else
48             fprintf(fileID, cellContent);
49         end
50     end
51 end
52
53 fclose(fileID);
54
55 end
```
